2009-11-30

Studies of Coal Nitrogen Release Chemistry for Oxyfuel Combustion and Chemical Additives

John M. Sowa
Brigham Young University - Provo

STUDIES OF COAL NITROGEN RELEASE CHEMISTRY FOR OXYFUEL COMBUSTION AND CHEMICAL ADDITIVES

by

John M. Sowa

A thesis submitted to the faculty of

Brigham Young University

in partial fulfillment of the requirements for the degree of

Master of Science

Department of Chemical Engineering

Brigham Young University

December 2009

ABSTRACT

STUDIES OF COAL NITROGEN RELEASE CHEMISTRY FOR OXYFUEL COMBUSTION AND CHEMICAL ADDITIVES

John M. Sowa

Department of Chemical Engineering

Master of Science

Pollution is one of the greatest concerns with pulverized coal combustion. With tightening standards on pollution emissions, more information is needed to create better design models. Burner modifications are the most efficient changes that can be made to assure sufficient carbon burnout and low NO_x emissions.

Experiments were performed in the BYU Flat Flame Burner (FFB) lab, operating under fuel rich conditions for pyrolysis experiments and fuel lean conditions for char oxidation experiments. Effects of temperature, coal rank, residence time, and post flame oxygen content on mass release, nitrogen release, and reactivity were examined. Elemental and Inductively coupled plasma (ICP) analyses were used to determine the mass and nitrogen release of coals and chars. FT-IR was used to determine gas phase nitrogen compositions on selected experiments. Results of char oxidation experiments

were fit to a first-order model to obtain an Arrhenius pre-exponential factor, while activation energies were approximated using a published correlation. CPD model calculations were used to find experimental residence times and particle diameters that obtained full pyrolysis yields.

Oxy-fuel experiments were performed by switching the burner diluent gas from N_2 to CO_2. Oxy-fuel experiments exhibited a rank effect in nitrogen release. Bituminous coal tests showed no statistically significant difference in mass or nitrogen release between the two conditions. A sub-bituminous coal exhibited a greater mass and nitrogen release for the same residence time under the CO_2 environment, which could be due to early gasification of the char.

Two samples of a chemically treated coal with different additive concentrations were tested against an untreated sample for combustion enhancement. The treated samples showed an increase on the order of 15% absolute in pyrolysis yield compared to the untreated sample. An increase in reactivity on the order of 35% was observed for the higher concentrated sample, but not for the lower treatment concentration.

Gas phase nitrogen measurements showed both HCN and NH_3 at the 1300 K gas temperature condition. HCN and NH_3 release during pyrolysis was largely rank dependent, with more HCN formed initially than NH_3 for 5 of the 6 samples. However, a bituminous coal was found to have more NH_3 than HCN. These nitrogen species data can be used to evaluate or refine nitrogen transformation mechanisms.

ACKNOWLEDGMENTS

I would like to thank my advisor Dr. Thomas Fletcher for the help and confidence given during this project.

I would also like to thank Kolbein Kolste for his work in the lab. Without his spirited vision and help attitude it would have been difficult to achieve what we did in the life of the projects. I would also like to thank Sam Goodrich who took the unenviable job of fixing the FT-IR system when he was the only one working in the lab. I would also like to thank John Walser, Aaron Lewis, Daniel Fenn, and Brady Burgener for their help at various stages of this project. I would like to thank Randy Shurtz for his technical experitise in both modeling and experiments. He was always there to bounce ideas off and to offer perspective to experimental results.

I would like to thank Siemens, the DOE and Oryxe for their funding and support of these projects.

Finally I would like to thank my family for their constant support of my choices and my research. Without good parents and siblings it would have been hard to work through all of the challenges that were faced on this project.

TABLE OF CONTENTS

LIST OF TABLES ..... **xi**

LIST OF FIGURES ..... **xiii**

1 Introduction **1**

2 Literature Review **3**

2.1 Nitrogen Transformations During Coal Devolatilization 3

2.1.1 Primary Pyrolysis Transformations 4

2.1.2 Secondary Pyrolysis Reactions 5

2.1.3 Light Gas Phase Pyrolysis Chemistry 5

2.1.4 Devolatilization Models 10

2.2 Nitrogen Transformations During Char Oxidation 11

2.3 Oxycombustion Technology 11

2.3.1 Nitrogen Transformations Observed In Oxy-fuel Processes 12

2.4 Fuel Additive Studies 14

2.5 Summary 15

3 Objective and Approach **17**

4 Description of Experiments **19**

4.1 Flat Flame Burner 19

4.1.1 Burner Clogging 20

4.2 Temperature Conditions 22

4.2.1 Thermcouple Coating and Evaluation 22

4.2.2 Burner Settings 24
4.3 Coal Selection, Preparation and Analysis 24
4.3.1 Ultimate Analysis 25
4.4 Tracer Analysis 27
4.4.1 Particle Density and Swelling 29
4.5 FT-IR Operating Procedures 30
4.5.1 Post Flame Oxygen Measurement 32
4.6 Devolatilization Modeling 32
4.6.1 N_2 Environment CPD Modeling 32
4.6.2 CO_2 Environment CPD Modeling 33
4.7 Char Combustion Model 34
5 Coal Nitrogen Release in Oxy-fuel vs. Air-Blown Environments 39
5.1 Gas Temperature Profiles 39
5.2 Experiments Performed 40
5.3 Mass and Nitrogen Release Data 40
5.4 Modeling 44
5.5 Density and Swelling 45
5.6 Discussion of Results 47
5.7 Summary 50
6 Combustion Enhancement Through a Chemical Additive 51
6.1 Coal Analysis 51
6.2 Pyrolysis Results 52
6.2.1 Pyrolysis Density and Swelling 56
6.2.2 Pyrolysis Conclusions 56
6.3 Char Oxidation Results 57

6.3.1 C To H and C To N Ratios 60
6.3.2 Char Oxidation Experimental Density and Swelling 61
6.4 Char Oxidation Abnormalities 62
6.5 Conclusions 63
7 Coal Nitrogen Release Data 65
7.1 Coal Analysis 65
7.2 Pyrolysis Results 65
7.2.1 Pyrolysis Density and Swelling 69
7.2.2 Coal Database Figures 70
7.2.3 Discussion of Pyrolysis Results 72
7.2.4 CPD Model Results 73
7.3 Char Oxidation Results 76
7.3.1 Char Combustion Model 77
7.3.2 C/H and C/N Ratios From Char Oxidation Experiments 79
7.3.3 Changes in Diameter and Density During Char Oxidation 80
7.3.4 Conclusions 82
8 Conclusions 83
8.1 Oxyfuel Combustion 83
8.2 Combustion Enhance Through a Chemical Additive 84
8.3 Coal Nitrogen Release Data 85
9 Recommendations 87
10 References 89
Appendix A. Gas Temperature Correction for Radiation 95
Appendix B. Gas Temperature Profiles 98
Appendix C. Oxyfuel Coal and Char Data 102

Appendix D. Chemical Additive Temperature Profiles 104

Appendix E. Chemical Additive Pyrolysis Results 108

Appendix F. Coal Additive Char Oxidation Results 110

Appendix G. Coal Nitrogen Release Data 112

G.1 Pyrolysis Results 112

G.2 Oxidation Results 114

G.3 C/H, C/N Ratios 122

G.4 Coal Density and Swelling 123

Appendix H. CPD Input Parameters 124

Appendix I. Raw FT-IR Data 126

Appendix J. Sample FT-IR Calculation 128

LIST OF TABLES

Table 2-1 Nitrogen gas species results at 1280 K from Zhang (2001) 7

Table 2-2 Table of findings during nitrogen release pyrolysis experiments 8

Table 4-1 Mass mean diameter for the suite of coals 25

Table 4-2 Table of experiments performed 26

Table 4-3 ASTM ash test results for Coal E coal and char samples 28

Table 4-4 ASTM ash test results for Kentucky char and soot samples 28

Table 4-5 Sample oxygen concentration profile for the FFB 31

Table 6-1 Proximate analysis of coals (as rec'd basis) 52

Table 6-2 Proximate analysis of coals (daf basis) 52

Table 6-3 CPD predicted mass and nitrogen partitioning* 53

Table 6-4 Swelling ratios of coals during pyrolysis 56

Table 6-5 Pre-exponential factors determined for the first-order model 60

Table 6-6 C/N and C/H ratios for Kentucky, CC2, and CF2 coal combustion experiments 61

Table 6-7 Density and diameter changes during combustion of Kentucky treated and untreated coals in FFB 61

Table 7-1 Proximate analysis of coals (as rec'd basis) 66

Table 7-2 Proximate analysis of coals (daf basis), coal rank, and mass mean diameter 66

Table 7-3 Gas phase results from the 1300 K pyrolysis experiments 67

Table 7-4 Swelling ratios of coals during pyrolysis 69

Table 7-5 Nitrogen gas species results from Zhang (2001) 73

Table 7-6 CPD calculations of coal pyrolysis in the 1300 K FFB condition 75

Table 7-7 Pre-exponential factors determined for the 1st-order model....77

Table C-1 Ultimate analysis for Ill #6 coal and chars in CO_2 at 1 inch on a dry ash-free (daf) basis....102

Table C-2 Mass release and nitrogen release data from Oxy-fuel experiments....103

Table E-1 Ultimate analysis for coal, tar/PAH, and char samples....108

Table E-2 Ash and elemental tracer analysis results....108

Table F-1 Ultimate analyses from char oxidation experiments....110

Table F-2 Sample analysis from 1500 K char oxidation experiments....111

Table G-1 CHNS analysis for coal, tar/PAH, and char....112

Table G-2 Ash and elemental tracer analysis results....114

Table G-3 Ultimate analyses from char oxidation experiments on Coals A, B & C....114

Table G-4 Sample analysis from 1700 K char oxidation experiments on Coals A, B & C...115

Table G-5 Sample analysis from char oxidation experiments on Coals D, E, & F....116

Table G-6 Mass and nitrogen release during char oxidation experiments on Coals D, E, & F....117

Table G-7 C/N and C/H ratios for coal combustion experiments....122

Table G-8 Density and diameter changes during combustion coals in FFB....123

Table H-1 Oxyfuel CPD input parameters....124

Table H-2 Chemical additive CPD input parameters....124

Table H-3 Coal nitrogen database CPD chemical structure input parameters....124

Table I-1 FTIR results from the 1300 K pyrolysis experiments....126

LIST OF FIGURES

Figure 2-1 Simplified mechanism for the formation of NO and N_2O from coal (Zhang, 2001) 4

Figure 2-2 Effect of temperature on nitrogen partitioning (Zhang, 2001)....7

Figure 2-3. HCN and NH_3 concentrations as a function of temperature measured by Zhang (Zhang and Fletcher, 2001)....9

Figure 2-4 Oxycombustion power plant schematic from (Mackrory, 2008) 12

Figure 4-1 Flat flame burner system schematic diagram....21

Figure 5-1 Mass release during pyrolysis of Illinois #6 coal as a function of peak temperature 42

Figure 5-2 Nitrogen release during pyrolysis of Illinois #6 coal as a function of peak temperature 42

Figure 5-3 Mass release of Pittsburgh #8 coal as a function of peak temperature 43

Figure 5-4 Nitrogen release of Pittsburgh #8 coal as a function of peak temperature....43

Figure 5-5 Mass release of Black Thunder coal as a function of peak temperature....44

Figure 5-6 Nitrogen release of Black Thunder coal as a function of peak temperature 44

Figure 5-7 Devolatilization yield from Mackrory, CPDCO_2, and CPD codes for 1600 K temperature conditions....46

Figure 5-8 Black Thunder coal experimental values versus CPD predicted mass release for the 1600 K temperature condition....46

Figure 5-9 Apparent density ratios measured for the coal chars as a function of temperature 48

Figure 5-10 Diameter ratios measured for the coal chars as a function of temperature 48

Figure 6-1 Partitioning of pyrolysis products (overall and nitrogen) for Kentucky coal, CC2, and CF2 treatments in the FFB at 1300 K....53

Figure 6-2 Experimental results and CPD model predictions of volatiles and nitrogen release during pyrolysis of the Kentucky, CC2, and CF2 coals in the 1300 K FFB condition 54

Figure 6-3 Char oxidation predictions and measurements for (a-b) Kentucky coal, (c-d) CC2 coal, and (e-f) CF2 coal in the 1500 K and 1700 K FFB conditions.....58

Figure 6-4 Char oxidation predictions and measurements for the (g, h) Kentucky coal in the 1500 and 1700 K FFB conditions when the pre-exponential factor is considered temperature dependant.....59

Figure 6-5 Calculated χ factors for the treated and untreated coals.....63

Figure 7-1 Mass partitioning of the pyrolysis product for all coals.....68

Figure 7-2 Partitioning of nitrogen pyrolysis products for all coals.....68

Figure 7-3 Nitrogen partitioning among coals studied in the second year 69

Figure 7-4 Database of mass release as a function of rank.....70

Figure 7-5 Database of tar yield as a function of rank.....71

Figure 7-6 Database of mass release as a function of O to C ratio.....71

Figure 7-7 Database of tar yield as a function of O to C ratio.....72

Figure 7-8 Nitrogen release as a function of time for the first year coals (A, B, C).....74

Figure 7-9 Nitrogen release as a function of time for the second year suite of coals (D, E, F).....74

Figure 7-10 Comparison of CPD model predictions with measured values of total volatiles, tar/soot formed, fraction of nitrogen remaining in the char, and fraction of nitrogen in the tar/soot for the three coals.....75

Figure 7-11 Comparison of CPD model predictions with measured values of total volatiles, tar/soot formed, fraction of nitrogen remaining in the char, and fraction of nitrogen in the tar/soot for the three coals.....76

Figure 7-12 Mass release during char oxidation experiments for the suite of coals.....78

Figure 7-13 Nitrogen release during char oxidation experiments for the suite of coals.....78

Figure 7-14 C/N ratios for char oxidation experiments.....80

Figure 7-15 C/H ratios for char oxidation experiments.....80

Figure 7-16 Char to coal density ratios for char oxidation experiments.....81

Figure 7-17 Char to coal diameter ratios for char oxidation experiments 81

Figure B-1 Vertical gas temperature profiles for the 1600 K Oxy-fuel conditions in the FFB 98

Figure B-2 Vertical gas temperature profiles for the 1700 K Oxy-fuel conditions in the FFB 98

Figure B-3 Vertical gas temperature profiles for the 1800 K Oxy-fuel pyrolysis condition in the FFB 99

Figure B-4 Vertical gas temperature profiles for the 1900 K Oxy-fuel pyrolysis condition in the FFB 99

Figure B-5 Vertical gas temperature profiles for the 1600 K air simulated pyrolysis condition in the FFB 100

Figure B-6 Vertical gas temperature profiles for the 1700 K air simulated pyrolysis condition in the FFB 100

Figure B-7 Vertical gas temperature profiles for the 1800 K air simulated pyrolysis condition in the FFB 101

Figure B-8 Vertical gas temperature profiles for the 1900 K air simulated pyrolysis condition in the FFB 101

Figure D-1 Vertical gas temperature profile of the 1300 K pyrolysis condition in the FFB 104

Figure D-2 Vertical gas temperature profile of the 1500 K char oxidation condition in the FFB.....104

Figure D-3 Vertical gas temperature profile of the 1700 K char oxidation condition in the FFB.....105

Figure D-4 Vertical gas temperature profiles for the 1300 K pyrolysis condition in the FFB 105

Figure D-5 Vertical gas temperature profile of the 1500 K char oxidation condition in the FFB.....106

Figure D-6 Vertical gas temperature profile of the 1700 K char oxidation condition in the FFB.....106

Figure G-1 CPD model predictions of volatiles release during pyrolysis of Coals D, E, & F in the 1300 K FFB condition 113

Figure G-2 Char oxidation predictions and measurements for Coals A, B, & C in the 1500 K FFB condition 118

Figure G-3 Char oxidation predictions and measurements for Coals D, E & F in the 1500 K FFB condition. These results are from curve fits of both the 1500 and 1700 K data 119

Figure G-4 Char oxidation predictions and measurements for Coals D, E, & F in the 1700 K FFB condition. These results are from curve fits of both the 1500 and 1700 K data 120

Figure G-5 Char oxidation predictions and measurements for Coals D & E in the 1500 and 1700 K FFB condition considered separately 121

Figure J-1 The spectra for each step in the quantification process. 129

Figure J-2 A comparison of the flame background and the gas sample is on the bottom and the result of the subtraction is on top. The subtraction factor can be seen in the top box of the window in the upper left corner 129

Figure J-3 A comparison of C_2H_2 calibration gas sample and the coal sample is on the bottom and the result of the subtraction is on top. The subtraction factor can be seen in the top box of the window in the upper left corner 130

1 Introduction

Pulverized coal (pc) fired power plants are one of the cheapest means of electricity generation. With increasing demand for electricity, desire for less dependence on imported energy and large coal reserves in the United States, pc power plants remain one of the best options for electric power generation in the short term. However, they emit comparatively high amounts of pollution which must be cleaned at an increasingly higher level due to tightening government standards. Among the pollutants, NO_x emissions from coal are usually harmful and expensive to control. NO_x can contribute to cardiovascular problems, increased production of ozone in the troposphere while destroying it in the stratosphere, and acid rain. Pulverized coal boilers emit more NO_x per unit energy than most other major power technologies (2001). Post combustion carbon content in the fly ash is also a concern, since plants can sell fly ash to use for concrete rather than have it disposed of in a landfill.

Most NO_x pollution in pc boilers comes from nitrogen contained in the coal as heteroatoms. Nitrogen is released from coal in three stages. In the first stage tar and light gases are released. Light gases are defined as those that do not condense at room temperature. The majority of the nitrogen remains in the tar. This stage is called primary pyrolysis. The second stage is called secondary pyrolysis where the tar and light gases react in the gas phase. Here nitrogen in the tar can either move into the combining tar to

form soot or it can react into the light gas phase as NH_3 or HCN. After pyrolysis reactions are completed, the third stage occurs that is called char oxidation. During char oxidation, oxygen attacks the char and oxidizes the remaining nitrogen to form NO. If the NO passes through a fuel rich burner zone it can be reduced to form N_2.

General abatement strategies include combustion process modifications, post process treatment (e.g. SCR) or pre-process denitrification. Of these options, boiler modifications are the most cost effective, however they currently only reduce up to 65% of the NO_x emitted from a pulverized coal boiler (source). If more of the nitrogen could be released earlier in the process or the process better understood, then more effective ways could be developed to curtail pollution. Possible solutions to reduce NO_x pollution from coal nitrogen have included gaining a better understanding of the chemistry, inventing new technology that combusts the coal in different environments, and creating fuel additives which catalyze faster release, reactivity or reduction reactions.

Currently, these boiler modifications are designed using comprehensive numerical combustion simulations. However, these models are not yet capable of predicting NO_x emissions and must be tuned for a given boiler. Inside of these models are subroutines for both pyrolysis and char oxidation. To improve the subroutines the nitrogen split between the phases must be better understood. This project intends to gain a better understanding of nitrogen chemistry and overall combustion in a variety of areas (traditional combustion, Oxy-fuel combustion, and chemically treated coals). Although this work is not deep in any of the areas, the results add greater understanding and insight about these important processes.

2 Literature Review

This chapter presents a brief literature review of nitrogen transformations in (a) coal devolatilization, (b) char oxidation and (c) Oxycombustion conditions. Specific emphasis will be given to work done on flat flame burner systems.

2.1 Nitrogen Transformations During Coal Devolatilization

Nitrogen occurs in coal as heteroatoms in pyrrolic (five-membered) and pyridinic (six-membered) rings. Approximately 60% of the nitrogen occurs in the pyrrolic form, 30% in the pyridinic form, and the remaining 10% in other forms (mostly quaternary N) (Kelemen et al., 1994).

As the particle heats up, devolatilization occurs in two stages (primary and secondary pyrolysis), as shown in Figure 2-1. The amount of pyrolitic nitrogen release from the initial coal structure will affect NO_x formation. Four major factors influence pyrolysis nitrogen yield at atmospheric pressure: temperature, residence time, heating rate and coal rank (Zhang, 2001). Pyrolysis is rank-dependent due to the different chemical structures present with different degrees of coalification (Smith et al., 1994). The general temperature range of primary pyrolysis is 900 to 1100 K, with secondary pyrolysis at 1200 to 1500 K. Particle heating rate is important because it can change temperatures at

which reactions occur and the physical characteristics of the resulting char. Experiments have been performed with heating rates varying from 10 to 10^5 K/s (Gale et al., 1995).

2.1.1 Primary Pyrolysis Transformations

Primary pyrolysis involves thermal decomposition of the weakest aliphatic bonds within the coal, liberating finite clusters which may evaporate as tar for a given temperature and pressure. Those clusters that do not vaporize eventually crosslink back into the remaining char matrix. Most of the nitrogen evolved remains in aromatic rings in the tar (Blair et al., 1976; Zhang and Fletcher, 2001). A substantial amount of the nitrogen (often greater than 50%) remains in the char, depending on the coal and the temperature conditions.

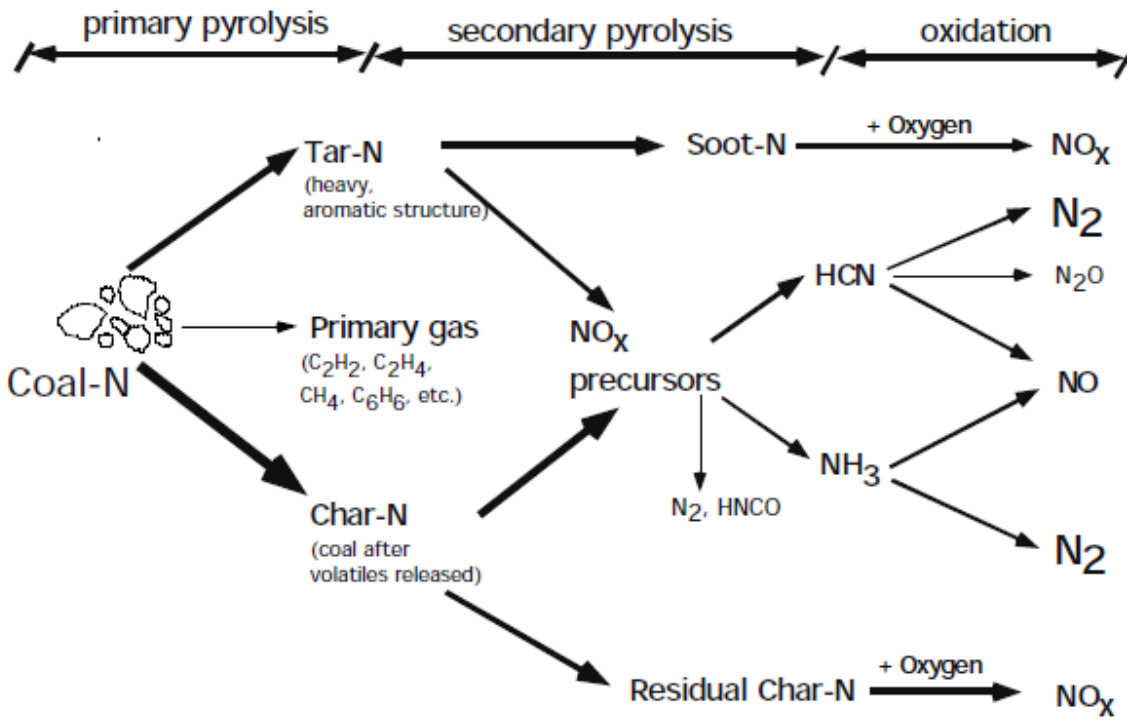

Figure 2-1 Simplified mechanism for the formation of NO and N_2O from coal (Zhang, 2001)

2.1.2 Secondary Pyrolysis Reactions

Secondary pyrolysis involves soot forming reactions from tar and light gas phase reactions with participants from the tar, soot, char and gas phases. These reactions have complex gas phase chemistry and have been studied by many investigators (Blair et al., 1976; Pohl and Sarofim, 1976; Zhang, 2001; Tsubouchi and Ohtsuka, 2008). Zhang, et al (2001) concluded that the release rate of nitrogen from the tar is greater than the char during secondary pyrolysis, with the nitrogen retaining a similar structure in both tar and the char. Glarborg and coworkers published a review of coal nitrogen studies, reporting that the majority of nitrogen release was due to tars and oils(Glarborg et al., 2003). Figure 2-1 shows the nitrogen pathways identified by Zhang during secondary pyrolysis. Figure 2-2 shows the nitrogen balance measured by Zhang which is typical of his findings (Zhang, 2001). The unlabeled portion of the nitrogen balance is unclosed and could be N_2 (Zhang, 2001). More research is needed to clarify understanding of secondary pyrolysis and its pathways.

Overall, as temperature increases, the amount of volatile nitrogen also increases. Eventually, all of the coal nitrogen will be released at high temperatures and long residence times (Pohl and Sarofim, 1976). It has also been shown that nitrogen in the tar remains relatively constant while the content in the light gases increases for increasing temperature (Solomon and Colket, 1978)

2.1.3 Light Gas Phase Pyrolysis Chemistry

Secondary reactions of tar and thermal decomposition of char will lead to the release of nitrogen species into the gas phase. N_2, HCN, HCNO, and NH_3 have been

identified as major nitrogen gas phase pyrolysis products(Zhang and Fletcher, 2001). N_2 is difficult to measure in pyrolysis and combustion experiments and HCNO has only been identified in fluidized bed experiments(Ledesma et al., 1998; Glarborg et al., 2003), therefore only HCN and NH_3 yield will be considered in this review.

Table 2-1 shows a summary of experiments performed to measure HCN and NH_3 concentrations adapted from (Zhang and Fletcher, 2001), including experimental apparatus and conditions as well pertinent conclusions pertaining to observed HCN and NH_3 yields. The concentration of both gases has a substantial impact on the final fuel-N conversion to NO (Zhang and Fletcher, 2001).

Entrained flow experiments performed on a flat flame burner (FFB) by Zhang and Fletcher used an FT-IR with a 10 m path length to detect volatile nitrogen concentrations down 10 ppb. Four coals were examined with rank ranging from lignite to low volatile bituminous. Table 2-2 shows concentrations of HCN and NH_3 at 1 and 3 inch probe heights with a peak gas temperature of 1280 K. HCN and NH_3 concentrations were measured as a percentage of the total coal nitrogen. Both nitrogen species were detected, with more HCN for higher rank coal and more NH_3 for lower rank coals.

Nitrogen release from lower rank coals differs from that in higher rank coal. Figure 2-3 shows the concentrations measured by Zhang as a function of temperature for the Illinois 6 and Utah Bituminous coals at a 1 inch probe height above the flat flame burner. Gaseous nitrogen release and transformation is a strong function of temperature. Above 1400 K, HCN yield increases from 5 to 25-30 % of the initial coal nitrogen. NH_3 yield shows a less pronounced increased.

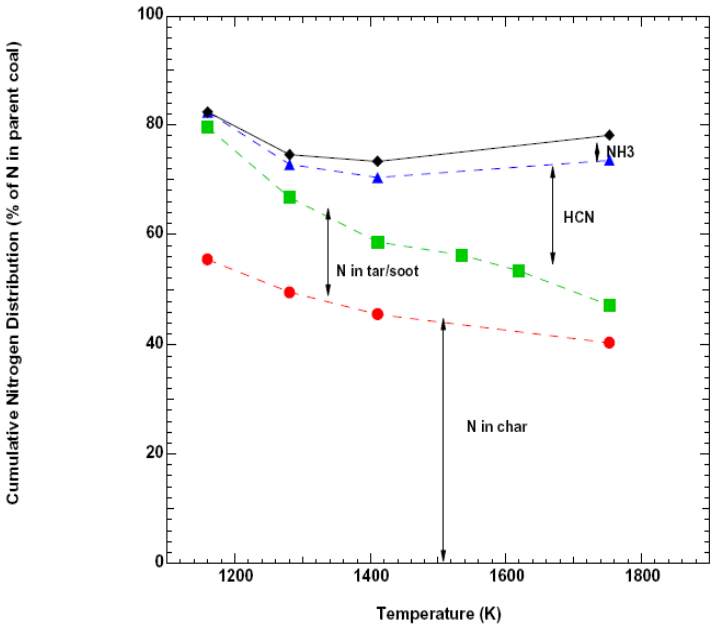

Figure 2-2 Effect of temperature on nitrogen partitioning (Zhang, 2001)

Table 2-1 Nitrogen gas species results at 1280 K from Zhang (2001)

	% conversion (N in coal basis)			
Sampling Height	1 inch		3 inches	
Coal	HCN	NH_3	HCN	NH_3
Ill #6	2.14	1.90	7.69	3.91
Utah	2.73	3.71	7.18	5.51
BT	2.14	3.84	9.11	6.28
Knife River	0.00	5.09	7.89	11.34

Table 2-2 Table of findings during nitrogen release pyrolysis experiments

Finding	Authors	Reactor	Heating Rate (K/s)	Temperature Range	Conditions
HCN is the dominant product	(Haussmann, 1989)	arc-jet fired entrained flow re	$5*10^4$ - $2*10^5$	1200-1700 K	900 ppm O2, bit. and subbit. Coal
	(Freihaut, et al. 1989)	heated grid	10^3 K s^{-1}	600-1200 °C	in N2, 14 coals
	(Chen, 1991)	radiant flow reactor	n/a	n/a	inert atmosphere, 6 coals
	(Freihaut, et al. 1993)	entrained flow reactor	10^3 K s^{-1}	600-1200 °C	inert atmosphere, 14 coals
	(Bassilakis, et al. 1993)	entrained flow reactor	10^4 K s^{-1}	900-1200 °C	inert atmosphere, Argonne Premium coals
	(Liu, et.al. 2004)	Radiant flow reactor	10^4 K s^{-1}	1850 K	Inert atmosphere 1850 K, 5 coals
both HCN and NH3	(Blair, et al. 1976)	pyroprobe	20 °C/msec	800-1400 °C	inert atmosphere, 20 coals
detected; HCN is the	(Rees, et al. 1981)	laboratory-scale combustor	n/a	n/a	substoichiometric; bit. coals
primary components with	(Phong-Anant, et al. 1985)	drop-tube reactor	10^4 - 10^5 K s^{-1}	800-1873 K	in argon, subbit. and lignite
small amount of NH3 for	(Nelson, et al. 1992)	fluidized bed	n/a	n/a	inert atmosphere; 3 coals
lower rank coals	(Niksa,1996)	radiant flow reactor	10^4 K s^{-1}	1700 K	slightly oxidizing atmosphere, bit. and subbit. Coals
	(Ledesma, et al. 1998)	fluidized bed	10^4 K s^{-1}	600-1000 °C	inert atmosphere, bit. coal
more NH3 is formed than HCN	(Kremer,1986)	electrically heated furnace	n/a	1000-1500 °C	oxidizing atmosphere; mv bit. Coal
	(Peck, et al. 1984)	flat-flame burner	10^5 K s^{-1}	1200-2100 K	Ar/O2 flame, subbit. coal
	(Leppalahti, 1995)	fixed bed	10 °C min^{-1}	600-1000 °C	inert atmosphere; slow heating rate; Russian coal
	(Bassilakis, et al. 1993)	TG-FTIR	10	900 °C	inert atmosphere; Argonne Premium coals
more HCN is found in high	(Chen, et al. 1988)	laboratory-scale combustor	225 °C/s	600-900 °C	Ar/O2/CO2; 48 coals; various stoichiometry
rank coals, while the	(Friebel, 1999)	fixed bed	.25, 5 K s^{-1}	673-1173 K	inert atmosphere, low rank coals
distribution of NH3	(Tan, 2000)	Modified entrained flow	10^3 -10^4 K s^{-1}	600-1000 °C	3 coals; 1 biomass
increases towards lower rank coals, and can become larger than HCN	(Zhang, 2001)	Entrained flow reactor	10^5 K s^{-1}	1150-1858 K	4 coals from 1150 to 1900 K

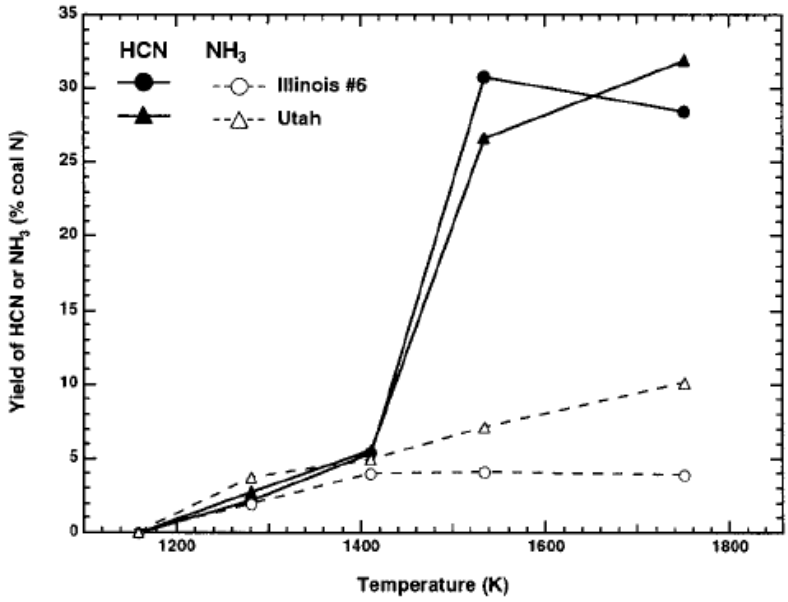

Figure 2-3. HCN and NH_3 concentrations as a function of temperature measured by Zhang (Zhang and Fletcher, 2001)

The pathway for NH_3 formation is currently not well understood. Previous studies have indicated that ratio of HCN to NH_3 appears to be rank dependent. HCN is considered to be the primary product while NH_3 is considered to be a product of HCN reactions for entrained flow coal pyrolysis (Glarborg et al., 2003).

In contrast to most entrained flow experiments, studies performed in TGAs and fluidized bed reactors have shown more NH_3 than HCN (Tsubouchi and Ohtsuka, 2002, 2008). However, Zhang observed NH_3 release before and subsequent to HCN release across the spectrum of coal rank, especially for low rank coal (Zhang and Fletcher, 2001). More data is needed to understand these conclusions and prove repeatability of the results.

2.1.4 Devolatilization Models

To model devolatilization behavior various engineering codes have been employed. The most complex network devolatilization models are the FG-DVC, FLASHCHAIN and CPD models (Niksa and Kerstein, 1991; Solomon et al., 1993). All three models are based on the assumptions that nitrogen only occurs in the aromatic rings the rate nitrogen release during devolatilization can be described as a first order process, and that HCN is the dominant product formed by ring rupture reactions(Smith et al., 1994). The FG-DVC and FLASHCHAIN models were tuned by matching light gas and nitrogen predictions with experimentally measured values in a range of experiments.

The chemical percolation devolatilization (CPD) code (Fletcher et al., 1990; Fletcher, 1992) treats devolatilization behavior using the chemical structure of the parent coals combined with percolation lattice statistics. The CPD model has no tunable parameters to predict both the volatiles and nitrogen release using the measured gas temperature history (Perry, 1999). The chemical structure parameters required by the CPD model for these coals were obtained from the correlation developed from the ultimate and proximate analysis of the parent coal (Genetti, 1999). The particle energy equation was solved to calculate particle temperature as a function of time (and hence distance with an assumed velocity profile). Model predictions obviously depend heavily on the particle temperature history, which is dependent in the FFB on the initial particle diameter. This model has been quite successful in predicting coal devolatilization behavior over a large range of coal types, heating rates, temperatures, and pressures. Currently the code is employed in simulation programs such as Fluent (Smith et al., 1994).

2.2 Nitrogen Transformations During Char Oxidation

Nitrogen release in char oxidation is a major contributor to post combustion NO_x (Glarborg et al., 2003). After devolatilization is complete, O_2 diffuses to the char surface and reacts with both carbon and heteroatoms such as N. Many studies conducted on char nitrogen conversion to NO are hard to compare because data were collected at different heating rates and temperatures (Glarborg et al., 2003; Spinti and Pershing, 2003). This is especially true for studies of char in pulverized coal conditions. Spinti et al. (2003) showed that NO_x formation is dependent on the initial local NO_x concentrations (Spinti and Pershing, 2003). Temperature has a stronger effect on the char- NO surface reactions than the oxidation reactions of char N (Aarna and Suuberg, 1997).

Various models have been proposed to predict oxidation and burnout. First-order models are computationally simple but not rigorous. The Carbon Burnout Kinetic (CBK) model has been proposed for char oxidation to predict carbon burnout and fly ash carbon content (Hurt et al., 1998). To improve previous versions during late burnout the CBK-8 version includes models for low carbon reactivity, thermal annealing, and ash inhibition. However, the CBK-8 model does not account for nitrogen release since it considers coal as carbon.

2.3 Oxycombustion Technology

One of the emerging technologies for NO_x control is Oxycombustion or Oxy-fuel combustion. In this method, a pure oxygen stream, coming from an air separation unit, is the oxidizer. The flame temperature of pure O_2 and coal would be much higher than in conventional systems. Since current boiler materials cannot withstand the high

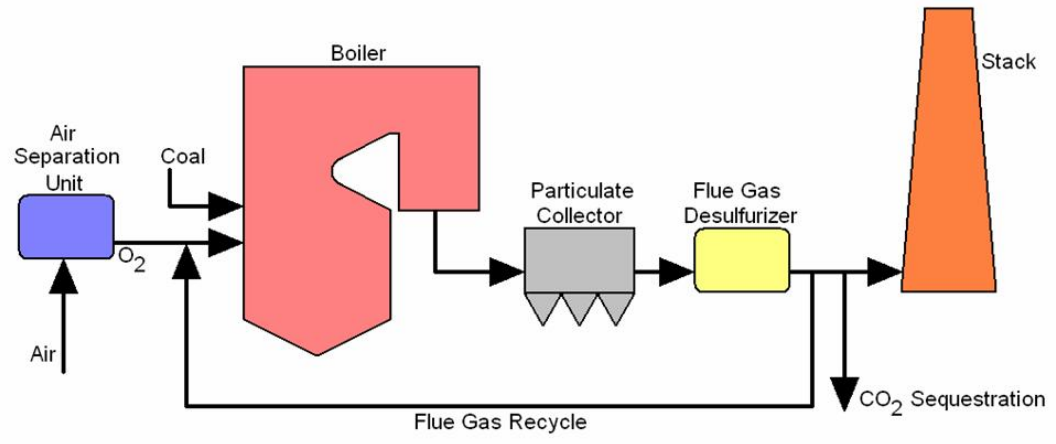

Figure 2-4 Oxycombustion power plant schematic from (Mackrory, 2008)

temperatures, some of the exit flue gas is recycled and fed into the reactor with the O_2. The recycled CO_2 becomes the primary diluent, replacing the N_2 in air-fired units. Figure 2-4 shows a simplified flow diagram of an Oxy-combustion power plant. Two important facts can be noted from the diagram.

First, there is no NO_x reduction unit, for reasons that will be discussed later. Second, there is an arrow for CO_2 sequestration. Only with CO_2 sequestration would the process be financially viable. After pollution controls the exit stream is mainly CO_2 and water, which can be easily separated. Therefore, Oxycombustion coupled with CO_2 sequestration, provides a cost competitive method to others with sequestration that uses existing technology and feasible retrofits.

2.3.1 Nitrogen Transformations Observed In Oxy-fuel Processes

Although the principal purpose of Oxycombustion is to provide a method for CO_2 sequestration, there are additional operational benefits. Since pure O_2 is the oxidizer, the flow rate of flue gas is greatly reduced, meaning smaller pollution control units (Châtel-

Pélage et al., 2004; Buhre et al., 2005). Another observed consequence of Oxycombustion is a reduction in NO_x emissions. One study showed a 70% reduction from the baseline NO_x emissions (Châtel-Pélage et al., 2004). A government study showed that a selective catalytic reduction unit (SCR) could be removed from the power plant when Oxycombustion was utilized. SCR units can reduce around 90% of flue gas NO to N_2; but have high capital and operational costs. An additional benefit is that the CO_2 is more reactive at the higher temperatures caused by increased O_2 in the primary mixing zone. Char reaction with CO_2 can contribute to the overall char conversion through gasification(Châtel-Pélage et al., 2004).

Experiments were conducted at BYU to confirm some of the previous conclusions using a multi-fuel reactor (Mackrory, 2008). This reactor had multiple sampling locations which allowed gas to be measured in the fuel rich regions. It was found that at the same stoichiometric ratio, there were higher levels of CO, hydrocarbons, NH_3, and HCN in oxy-fuel conditions than in air-fired conditions. High CO levels were attributed to dissociation of CO_2 above 1500 K, with minor influence of char gasification. It was concluded that oxy-fuel conditions may result in lower NO_x levels than traditional air-fired combustion (Mackrory, 2008).

On a laboratory scale, few Oxycombustion studies have focused on devolatilization. Molina and Shaddix (Molina and Shaddix, 2007) studied devolatilization of a Pittsburgh bituminous coal in a laminar flow entrained flow reactor using two different Oxy-fuel conditions and one simulated air-fired condition. Particles in the size fraction between 106 and 125 μm were studied, with a peak temperature of 1300 K. Entrained particle ignition and devolatilization was measured using high speed

cameras that tracked CH* radical luminescence. It was concluded that CO_2 retards particle ignition due to differences in specific molar heat between CO_2 and N_2. However, there was no difference in devolatilization time. No devolatilization yields were measured or nitrogen distributions were measured.

Several oxy-fuel char combustion studies have been conducted. Borrego and Alvarez (2007) concluded that the presence of a limited amount of O_2 had an effect of volatile inhibition on high volatile bituminous coal. Lower volatile yields reported for the chars prepared in a CO_2 environment were attributed to cross-linking surface reactions between the CO_2 and coal surface species. Other studies have shown that as O_2 concentration increases, coal particles burn under increasing kinetic control (Murphy and Shaddix, 2006). Relatively few published studies further document effects of Oxycombustion on char reaction behavior.

2.4 Fuel Additive Studies

A number of studies have been conducted to explore the effects of chemical additives on the combustion of raw coal. Desired effects of these experiments have been to increase volatile nitrogen release, reduce sulfur pollution, increase carbon burnout and increase the value of fly ash content or to reduce the amount of particulate matter. A recent study used Ca- and Mg- based additives to control the amount of $PM_{2.5}$ particles. Drop tube experiments found that an additive could change the mineral transformation process and thus control the $PM_{2.5}$ output, though the effect was rank dependent (Ninomiya et al., 2009). Other studies have investigated the properties of CaO- and Fe- as catalysts to transform coal-bound nitrogen to N_2. Fluidized bed experiments showed that

an increase in these elements could promote N_2 formation through solid-solid interactions in the char matrix (Tsubouchi and Ohtsuka, 2008). Other studies have reported mixed results with a variety of additives (Ohtsuka et al., 1998; Oehr and Yao, 2000; Put, 2000; Tsubouchi et al., 2000; Wu et al., 2001; Tsubouchi and Ohtsuka, 2002; Weijuan et al., 2007; Tsubouchi and Ohtsuka, 2008; Ninomiya et al., 2009). Studies of new additives could find new ways to combust coal more efficiently with less pollution.

2.5 Summary

Nitrogen release during pyrolysis and char oxidation have been studied in detail. Secondary pyrolysis gas phase reactions have yet to be understood and modeled at a detailed level. Devolatilization and oxidation subroutines in CFD models are important to predicting boiler behavior. In spite of the many findings about nitrogen evolution, more data are needed to refine the CPD and CBK models so they may be used with more confidence in industry. New technologies such as Oxycombustion or chemical additives could reduce pollution levels by mechanisms such as gasification or catalysis of fuel decomposition that also need to be studied and understood.

3 Objective and Approach

The primary objective of this project is to improve the understanding of nitrogen release from coal. Research was performed in three different areas. First the effect of an oxy-fuel environment on devolatilization and char reaction behavior was quantified for three coals of two ranks (bituminous and sub-bituminous). Second a fuel additive was studied to see if there was any effect on either the pyrolysis or oxidation process. Finally, a new suite of six coals was studied under both fuel rich and oxidizer rich conditions to determine nitrogen evolution pathways, particularly to determine HCN and NH_3 concentrations. These data were used to evaluate the capabilities of the CPD and CBK models, and to identify areas needing further improvement. The areas needing improvement are summarized within the chapters that follow.

This work is presented as follows. Chapter 4 describes the experimental procedure and models used in this project. Chapter 5 describes results from nitrogen release experiments in Oxycombustion environments compared with traditional combustion environments. Chapter 6 discusses the effects of an iron-based coal additive on both coal pyrolysis and char oxidation. Chapter 7 presents the results of coal pyrolysis and char oxidation experiments on a suite of six coals, specifically including measurements of gas phase nitrogen species during pyrolysis. Chapters 8 and 9 provide important conclusions from the research and recommendations for future work.

4 Description of Experiments

This section describes the apparatus and experiments performed in these studies as well as the modifications that were made during this project. These procedures were common to all experiments, and are cited in future sections of this thesis.

4.1 Flat Flame Burner

The Flat Flame Burner (FFB) facility at BYU is capable of gas temperatures from 1100 K to 2000 K and particle heating rates of 10^5 K/s, which is close to conditions in pulverized coal burners. Heating rates in a typical drop tube reactor are on the order of 10^4 K/s, while other experimental apparatus such as fluidized bed and TGA have lower heating rates. Since, coal char particles have drastically different physical properties under these conditions, samples generated from a drop tube do not compare well to behavior in pulverized coal boilers which have heating rates on the order of 10^6 K/s (Gale et al., 1995). The FFB was described in greater detail by Zhang and Ma (Ma, 1996; Zhang, 2001). Before the present study, the system had not been used for graduate coal studies since Zhang left in 2001. In late 2006, the lab was moved due to repairs on the building ventilation system. In 2007, the lab was reassembled in its original location. During the time when the system was moved, numerous small changes and updates were

made, though the core remained intact. Some of these modifications are explained in the paragraphs that follow.

Figure 4-1 is a schematic of the current Flat Flame Burner (FFB) system. The burner itself and the quartz tower are largely intact from previous experiments. There were some troubles with tubes clogging which will be explained in the next section. The collection probe was replaced with a new probe of similar design made by the BYU Precision Machine Shop. The collection system also remained the same as in previous studies. Flow meters for the vacuum pumps were cleaned, and standard operating settings were established for the flow rates for each experiment. The water traps were removed because they reduced the vacuum and were no longer needed with a CO flame. The FT-IR spectrometer, used by Zhang, was sent in for repairs then repositioned after its return. The gas stream is now drawn off of the soot leg, with a valve controlling flow to the FT-IR. The particle feeding system operates as explained by previous investigators (Ma, 1996; Zhang, 2001).

4.1.1 Burner Clogging

Major problems occurred with burner tubes clogging during the course of this study. Periodic cleaning of the burner tubes was necessary during previous studies using the FFB. However, during this research, the fuel tubes began clogging more frequently after the wrong size of activated carbon was placed in the iron carbonyl trap. The trap was meant to keep iron oxide from forming in the flame due the iron pentacarbonyl impurities in the carbon monoxide cylinders propagated with the gas (Williams and Shaddix, 2007). After a significant amount of work, an e-mail was sent to the designer of

the burner. He said that switching the fuel and oxidizer lines would be permissible if the O_2 content in the fuel tubes did not rise above 30%. These reverse settings ran the fuel through the oxidizer honeycomb and the oxidizer through the fuel tubes.

Although a solution was eventually reached, tube clogging continued to be an issue. The solution was to introduce high temperature reverse settings during the 45 minute warm-up period in place of the traditional warm up settings. Any clogged tubes were cleaned out during this period. It was discovered that running the burner with these

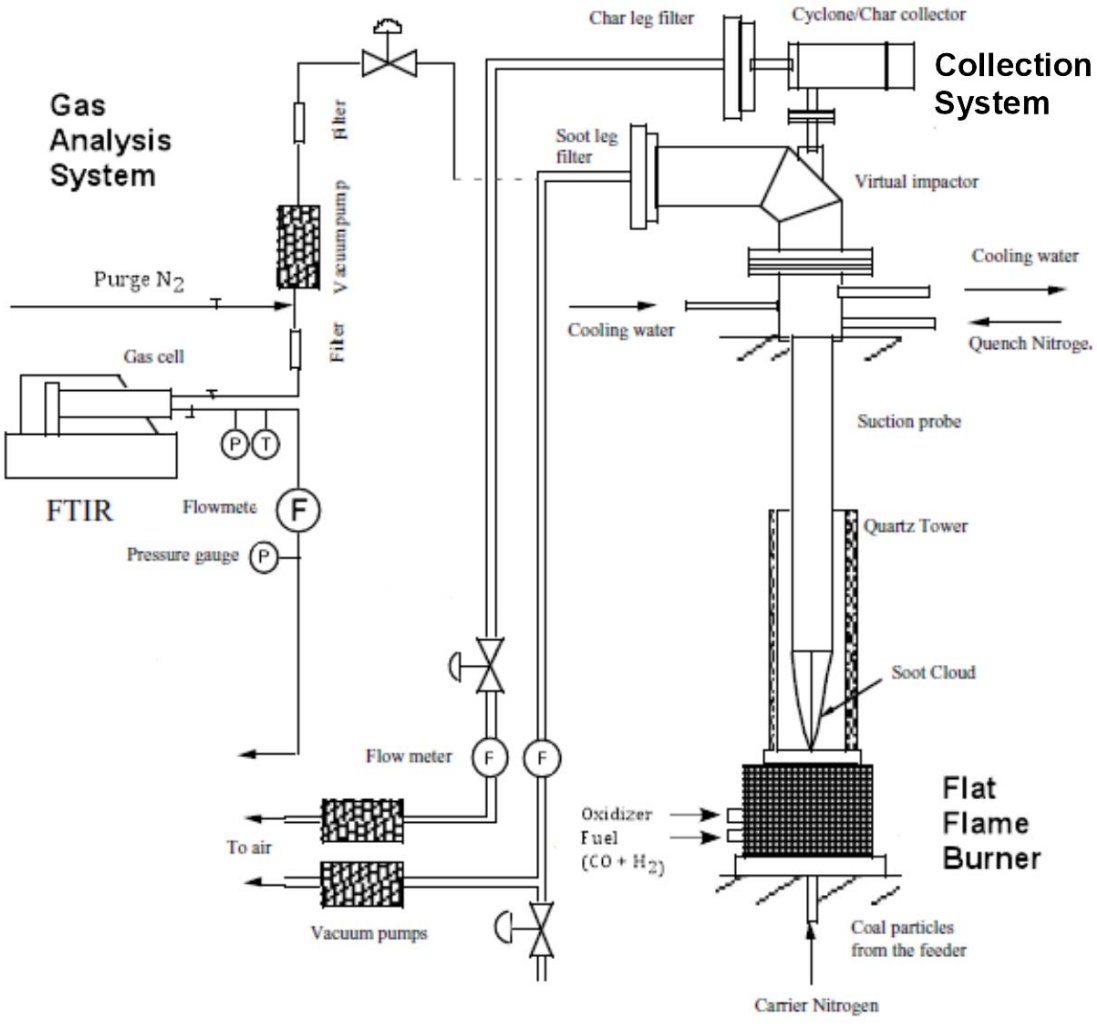

Figure 4-1 Flat flame burner system schematic diagram

inverted settings at a high temperature (about 2000 K) for at least 45 minutes would allow the system to run unclogged.

4.2 Temperature Conditions

This section describes specifics in obtaining gas temperature conditions for the FFB experiments. Measured gas temperature conditions are presented in each of the individual chapters. A complete set of gas temperature profiles are given in Appendices A and C.

4.2.1 Thermcouple Coating and Evaluation

The temperature was measured using a 600 μm diameter B type thermocouple (Omega), coated with silicon dioxide to prevent catalytic reactions. The thermocouple was first placed at the surface of the FFB just above the feed tube entrance (i.e., the centerline). The centerline gas temperature profile was measured by placing the thermocouple bead over the coolest point in the center of the burner, then lowering the burner to change vertical distance. The north, south, east and west readings were obtained by moving the thermocouple in a straight line from each of these directions and finding the peak temperature for that side. Gas temperature measurements were taken at the burner surface and at vertical heights above the burner surface ranging from 0.5 to 6.0 inches. Peak gas temperatures sometimes occurred closer to the burner surface when using inverted settings, so measurements were taken at 0.25 inches for these profiles. Measured thermocouple temperatures were corrected for radiation losses to obtain the gas temperature at each location as explained in Appendix A.

Type B thermocouples are composed of platinum rhodium alloy wires. Since these elements are strong catalysts, unwanted reactions must be prevented to obtain correct readings. Though various types of coatings exist, it was decided to coat the thermocouple with SiO_2 due to its ease of application and relative procedural safety (Wakai, 1979; Madsen, 1984; Fristrom, 1995; Bahlawane, 2007). However, this coating wears quickly when exposed to hot temperatures, so the thermocouples must be recoated frequently (Madsen, 1984; Fristrom, 1995). Instructions from the Wakai website and the Fristrom textbook were followed to coat and test the thermocouples (Wakai, 1979; Fristrom, 1995). The thermocouple coating was accomplished as follows. Dimethylsilohexane was poured into an open syringe. A tube was connected to the needle and laced through the center hole of a Mekker burner. The thermocouple was placed on a stand directly above the burner. A natural gas flame was lit and allowed to equilibrate so the thermocouple read a temperature around 1300-1400 K. The well of silicon liquid was released and the silicon flame was allowed to equilibrate. When the silicon flame had near constant intensity and height, the thermocouple bead was passed back and forth slowly just outside the luminous zone of the silicon flame for two minutes. An electrolysis test was performed to test the quality of the coating. An acidic solution was prepared and the coated bead was placed in the solution. The number and intensity of the bubbles was used as an indication of a complete thermocouple coating. If there were little or no bubbles, it was assumed to be well coated. If there were larger or more frequent bubbles the process was repeated. Specific coating lifetimes were not measured. The thermocouples in this study were re-coated when the temperature did not hold stable in a known condition.

4.2.2 Burner Settings

Burner flow rates were found using a two step process: (1) calculating adiabatic flame temperatures and (2) measuring the settings in the burner. Five gas flow settings could be changed in the FFB (fuel diluent, oxidizer diluent, H_2, CO, and O_2). Flow controller settings were input into a spreadsheet which calculated the mole fraction input of each gas. These mole fractions were used as inputs in the NASA-CEA code to calculate an adiabatic flame temperature(Claus, 2008). A fuel-rich post-flame condition was desired for the pyrolysis experiments and a post-flame O_2 concentration of approximately 6 mol% was desired for the char oxidation experiments.

The settings were dialed into the FFB and the centerline peak temperature was measured. Settings were identified to assure flame stability and to assure that the burner surface did not clog. Due to heat losses, the measured peak temperature was 100-300 K lower than the predicted adiabatic temperature for a given setting

4.3 Coal Selection, Preparation and Analysis

Ten coals were selected for the three projects. The Ill 6, Pitt 8 and Black Thunder, Kentucky, CC2, CF2, and coal B samples were received pre-ground and sieved to obtain the 45-75 μm fraction. Other coals were ground using a wheat grinder (The Wheat Mill, Blentec), then sieved to the 45-75 μm fraction. Mass mean diameter of all sieved coal samples were obtained using a Coulter Counter LS series machine and are displayed in Table 4-1. Proximate analyses (moisture test, ash test, and volatiles test) were performed at BYU according to ASTM standards as described by Zeng (Zeng, 2005). The experimental test matrix is displayed in Table 4-2.

Table 4-1 Mass mean diameter for the suite of coals

Coal	Mass Mean Diameter (μm)
Oxyfuel	
Ill 6	70
Pitt 8	50
BT	80
Chemical Additive Combustion	
KY	64
CC2	66
CF2	65
Air Pyrolysis/Combustion	
Coal A	70
Coal B	50
Coal C	80
Coal D	77
Coal E	71
Coal F	68

4.3.1 Ultimate Analysis

Ultimate analyses were performed on collected char and tar samples and on parent coal samples. These analyses were performed by Huffman Laboratories in Golden, CO until a LECO TruSpec Micro was obtained at BYU in August 2008. Results from Huffman Laboratories were reported on an as-received basis with loss on drying reported. Results obtained at BYU were reported on a dry basis. All results were converted to a dry, ash-free basis. Oxygen wt% was determined by difference from the other four elements (C, H, N, S). Chlorine content was not considered in this study. Some parallel results were obtained to check the correctness of the LECO machine. For samples analyzed at BYU the oxygen wt% often was negative. Two explanations were postulated: (1) an inaccurate carbon reading by the LECO machine, or (2) an inaccurate ash percentage.

Table 4-2 Table of experiments performed

Coal	Peak Temperature (K)					
	1300	1500	1600	1700	1800	1900
Oxyfuel						
Pitt 8			Py (CO_2)	Py (CO_2)	Py (CO_2)	Py (CO_2)
Ill 6			Py (CO_2)	PY (CO_2)	Py (CO_2)	Py (CO_2)
Black Thunder***			Py (CO_2/N_2)	Py (CO_2/N_2)	Py (CO_2/N_2)	Py (CO_2/N_2)
Chemical Additive						
Kentucky	Py	Ox*		Ox*		
CF 2	Py	Ox~		Ox~		
CC 2	Py	Ox~		Ox~		
Air Combustion						
Coal A	Py**	Ox*		Ox*		
Coal B	Py**	Ox*		Ox*		
Coal C	Py**	Ox*		Ox*		
Coal D	Py**	Ox*		Ox*		
Coal E	Py**	Ox*		Ox*		
Coal F	Py**	Ox*		Ox*		

Py = Pyrolysis
Ox = Char Oxidation
CO_2/N_2 = Diluent Gas
*Experiments performed at probe heights of 1, 2, 4 and 6 inches
~ Experiments performed at probe heights of 2, 4 and 6 inches
** FT-IR scans performed for these tests
*** Experiments performed at 1 inch and 2 inch probe heights; FT-IR scans taken for 2 inch 2 CO_2 experiments

Replicate ash tests were performed in the LECO machine for selected Coal E and Kentucky coals, tar/soots and chars. Both sample size and furnace time were tested.

Samples were placed in the furnace for two cycles as opposed to the one that was normally run for the ASTM ash test. The only sample that showed a significant change was the Kentucky tar/soot sample which has low ash content, and was therefore subject to greater relative change. Since the ash tests did not indicate variability, a series of ashing tests in a furnace were conducted to examine the effect of sample size. Coal ash tests were run with a sample size of 1 gram, while char samples were ashed with 100 mg due to scarcity of collected sample. A 100 mg coal sample was also ashed. The results are summarized in Table 4-3 and Table 4-4. From the results it was concluded that ash content was measured correctly, and therefore the carbon content was in error. Duplicate elemental analyses of char samples were not possible due to time and monetary constraints, so the oxygen content was set to 0 in cases where the balance did not close.

4.4 Tracer Analysis

Mass release data were obtained in three ways: (1) a mass balance of collected sample, with gas calculated by difference, (2) an ash tracer, and (3) elemental tracers. The mass balance was the least accurate because char and tar get caught in the collection system. The mass balance used only for rough estimates of the char/tar/gas split. The ash tracer method is based on the assumption that all of the ash remains in the particle during pyrolysis. Equation 4-1 shows how mass release is calculated using the ash tracer method:

$$\textbf{MR (wt\% daf)} = \frac{m_{coal} - m_{char}}{m_{coal} - m_{ash}} = \frac{1 - \frac{x_a^0}{x_a}}{1 - x_a^0} \qquad (4\text{-}1)$$

Table 4-3 ASTM ash test results for Coal E coal and char samples

Sample	% ash run 1	% ash run 2	Absolute Difference	% Rel error
1700 K (1")	23.7%	23.6%	0.1%	0.1%
1700 K (2")	22.4%	23.0%	0.6%	2.5%
1700 K (4")	25.8%	24.9%	0.9%	3.2%
1700 K (6")	30.1%	30.2%	0.1%	0.3%
Coal	14.7%	14.7%	0%	0.5%

Table 4-4 ASTM ash test results for Kentucky char and soot samples

Sample	% ash run 1	% ash run 2	Absolute Difference	% error
1300 K	18.4%	18.1%	0.3%	1.9%
1500 K (1")	23.2%	23.2%	0%	0.0%
1500 K (2")	27.4%	27.0%	0.4%	1.5%
1500 K (4")	34.1%	34.0%	0.1%	0.3%
1500 K (6")	37.0%	36.6%	0.4%	1.1%
1700 K (1")	21.8%	20.6%	1.2%	5.6%
1700 K (2")	20.7%	19.5%	1.2%	6.1%
1700 K (4")	23.1%	22.2%	.9%	3.9%
1700 K (6")	25.6%	24.2%	1.2%	5.3%
1300 K Soot	1.6%	1.2%	0.4%	25.0%

where x_a^0 and x_a are the mass fractions of ash in the coal and char, respectively. Researchers have shown this is generally not a valid assumption (Borrego and Alvarez, 2007). The ash tracer was calculated and recorded, but not used in obtaining mass or nitrogen release data.

Elemental tracer analysis is based on the assumption that during pyrolysis some inorganic elements are not released. The equation to calculate mass release from the titanium tracer is shown in equation 4-3:

$$\textbf{\% mass release (daf)} = \frac{1-\frac{x_{Ti,coal}}{x_{Ti,char}}}{1-\frac{x_{Ti,coal}}{x_{Ti,ash}}} = \left(\frac{x_{Ti,char}-x_{Ti,coal}}{x_{Ti,ash}-x_{Ti,coal}}\right)\left(\frac{x_{Ti,ash}}{x_{Ti,char}}\right) \qquad \textbf{(4-2)}$$

where $x_{Ti,coal}$ is the titanium fraction in the parent coal, $x_{Ti,\ char}$ is the titanium fraction in the char, and $x_{Ti,\ ash}$ is the titanium fraction remaining in the ash. In this study the silicon, aluminum and titanium tracers were used because each of these elements is considered stable in the ash (Zhang, 2001). Occasionally one of these 3 tracers gave spurious mass release values, as mentioned in the results section.

Once the mass release was calculated the nitrogen release could be found using equation 4-3:

$$\textbf{\% N release (daf)} = 1 - \left(1 - MR_{daf}\right)\left(\frac{x_{N,daf\ char}}{x_{N,daf\ coal}}\right) \tag{4-3}$$

where $x_{N,daf\ \mathrm{char}}$ is the mass fraction of nitrogen in the char, $x_{N,daf\ \mathrm{coal}}$ is the mass fraction of nitrogen in the coal and MR_{daf} is the mass release calculated on a dry ash free basis averaged among the three tracers.

4.4.1 Particle Density and Swelling

The average amount of particle swelling was determined from a combination of the apparent density and the particle mass ratios, as follows:

$$\frac{m}{m_o} = \frac{\rho}{\rho_0}\left(\frac{d}{d_0}\right)^3 \tag{4-4}$$

The apparent density (ρ) is the mass per particle divided by the volume of the particle based on the diameter. Therefore, the value of m/m_0 in Eq. 4-1 must be on an as received basis to match the density ratio. The apparent density is measured by pouring a known mass of particles into a graduated cylinder and tapping the sides of the cylinder until the particles settle. The mass of particles divided by the volume of the bed is the

bulk density, and a packing factor of 0.5 was used to determine the apparent density. The density ratio is independent of the packing factor chosen, as long as the size and shape of the particles do not change drastically from those of the parent coal particles. The value of d/d_0 calculated from Eq. 4-1 using data from pyrolysis experiments in the FFB is the swelling ratio.

4.5 FT-IR Operating Procedures

A Bomem MB-155 FTIR with a 10-meter path length was used to measure the amounts of HCN and NH_3 in the FFB. Before coal was fed to the FFB system, nitrogen background scans were taken as a zero point reference. Afterwards flame background scans were taken to eliminate post flame combustion background gases. The light gas stream was pulled through the bottom leg and filter of the separation system for the Flat Flame Burner (FFB) system, passed through additional filters, and fed to the gas cell (see Figure 4-1). To assure a high enough flow of product gases, the carrier nitrogen flow to feed the coal was increased from 0.0367 standard liters per minute (splm) to 0.06 slpm. Once enough gas sample was collected, the inlet and outlet to the gas cell were closed. Thirty-two scans were taken of the pyrolysis gas sample at a resolution of 1 cm^{-1} to assure sufficient spectral detail. Once the sample scans were performed, the flame background was subtracted, leaving only the spectra from the coal pyrolysis gases.

To quantify the amount of HCN and NH_3, measurements were performed with calibrated gas samples (10 ppm for HCN and 50 ppm for NH_3). Using the spectral subtract function of Grams AI version 6 software with the QASoft analytical tool,

Table 4-5 Sample oxygen concentration profile for the FFB

Height (in)	% O_2
Surface	6.9
0.5	6.5
1.0	6.7
2.0	6.9
3.0	7.0
4.0	7.1
5.0	7.2
6.0	7.1

acetylene and ethylene spectra were eliminated from the sample. The remaining signal from the FTIR was then identified as either HCN (between 3200-3400 cm^{-1}) or NH_3 (between 850 – 1250 cm^{-1}), and then the range was lessened to include only major product peaks. The HCN and NH_3 areas were then compared linearly with the calibration sample to obtain a concentration in parts per million (ppm) or parts per billion (ppb).

Concentrations of HCN and NH_3 were used to calculate the fraction of coal nitrogen converted to HCN or NH_3 using equation 4-5 (see Appendix J for sample calculation), where y_{HCN} is the gas phase mole fraction of HCN, $\dot{n}_{gas}$ is the molar flow rate of gas entering the probe, MW_N is the molecular weight of elemental nitrogen, $\dot{m}_{coal}$ is the mass flow rate of coal fed to the burner, and x_N is the mass fraction of nitrogen in the coal determined by ultimate analysis. This equation uses the fact that one mole of HCN is formed from one mole of N in the coal. A similar equation can be used when calculating NH_3 conversion.

$$\%Conversion\ of\ \ fuel\ N = \frac{y_{HCN}\dot{n}_{gas}MW_N}{\dot{m}_{coal}x_N} \qquad (4\text{-}5)$$

4.5.1 Post Flame Oxygen Measurement

To simulate industrial pulverized coal conditions it was desired to have 6 mol% O_2 in the post combustion gases. An oxygen sensor, as described Pickett (2008), was used to measure the centerline O_2 profiles for this study. The 1500 K profile, displayed in Table 4-5, was within 1% absolute of the desired 6% while the 1700 K cases measured between 3.5 and 4.5 mol% O_2.

4.6 Devolatilization Modeling

The CPD code was chosen to model pyrolysis for these experiments. This section reviews major points of CPD modeling.

4.6.1 N_2 Environment CPD Modeling

CPD code version cpdcpnlg was chosen as a stand alone program to model experiments on the flat flame burner system since it solves the particle energy equation. For this study the input parameters required were the coal ultimate and proximate analyses, a gas temperature profile, a particle velocity profile, the mass mean diameter of the parent coal, the coal apparent density, and coal NMR parameters obtained from a correlation (Genetti, 1999). The measured gas temperature profile was used, which included measurements at one inch intervals from 1 mm to 152 mm. The gas temperature at the burner inlet was assigned a value of 300 K. A particle velocity profile measured in the BYU FFB facility then fitted by Ma and cited by Perry was used (Fletcher, 1988; Ma, 1996; Perry, 1999). Swelling and density were measured as a function of location, but

not used as code inputs. Input structural parameters for all experiments are found in Appendix H.

When the measured apparent density was placed into the CPD code the outputs did not match the experimental results. Empirical adjustments to the characteristic heating time were previously made by changing the density to 0.7 gm/cm^3 in order to match measured particle temperatures (Fletcher, 1989; Perry, 1999; Zeng, 2005; Mackrory, 2008). This may indicate that reported heat capacities are too high, that there are radial temperature gradients in the FFB, or that particle heating occurs in the feed tube. This artificial value of the apparent density was used here to calculate particle temperature.

4.6.2 CO_2 Environment CPD Modeling

As mentioned in section 2.3.1, Shaddix and Molina studied the ignition and devolatilization of coal in an oxy-combustion environment (Molina and Shaddix, 2007). They noted that some of the gas property differences between CO_2 and N_2 could be responsible for observed differences in ignition times. In particular, they reported a difference factor of 1.7 times for the combined density - heat capacity term at 1200 K. The CPD code subroutine called PROPS provides gas temperature properties for calculations. Ideal gas is a good approximation for high temperatures found in this system. Heat capacity is found based on a correlation from Himmelblau (2004). Gas viscosity and thermal conductivity are interpolated from data between 300 and 1200 K (Holman, 1976). Above 1200 K, the data is found using equation 5-1:

$$\theta = \theta_0 \cdot \left(\frac{T}{T_0} \right)^n \tag{4-6}$$

where θ is the gas transport property, T is temperature in K, subscript 0 denotes the transport property or temperature at the highest interpolation point and n is a property dependent growth factor, which is 0.68 for viscosity and 0.57 for thermal conductivity.

The stand alone CPD code was modified for CO_2 by reprogramming the PROPS subroutine and will be referred to as CPDCO$_2$. The upper temperature limit was increased from 1200 to 1400 K. The properties changed were gas density, viscosity, thermal conductivity and heat capacity. These changes simulated the atmosphere as CO_2.

Mackrory also modified the CPD code as a MATLAB program using Cantera, a free open source program for calculating chemical equilibrium data, to calculate chemical properties for CO_2 (Mackrory, 2008). This version can switch between N_2, CO_2, and user input properties. It will be referred to as CPDCO$_2$-Mackrory.

4.7 Char Combustion Model

The char mass release (i.e., burnout) data were modeled using a simplistic first-order reaction rate. More sophisticated models exist (e.g., Hurt et al., 1998), but this model was used to illustrate differences in reaction behavior. The mass release rate per unit external area (A_p) is calculated as follows:

$$\frac{1}{A_p}\frac{dm}{dt} = k_r P_{O_2,s} \tag{4-7}$$

where m is the mass of the char (assumed to be carbon), k_r is the reaction rate constant ($Ae^{-E/RT}$), and $P_{O2,s}$ is the partial pressure of O_2 at the particle surface. The mass transfer through the particle boundary layer must be calculated in order to obtain $P_{O2,s}$, as follows:

$$\frac{1}{A_p}\frac{dn_{O_2}}{dt} = k_m\left(C_{O_2,g} - C_{O_2,s}\right) \tag{4-8}$$

where k_m is the mass transfer coefficient. The molar concentration is calculated from the partial pressure using the ideal gas law. The surface reaction rate and the mass transfer rate must be equal at steady-state, as follows:

$$\frac{dm}{dt} = \frac{dn_{O_2}}{dt}\left(\frac{moles\ O_2}{s}\right)\left(\frac{mole\ C}{0.5\ moles\ O_2}\right)\left(\frac{12\ g\ C}{mole\ C}\right) \tag{4-9}$$

assuming that the surface reaction is:

$$C + 0.5\ O_2 \rightarrow CO$$

Combining eqs. 4-7 through 4-9, the equality becomes:

$$k_r P_{O_2,s} = 24k_m\left(\frac{P_{O_2,g}}{RT_g} - \frac{P_{O_2,s}}{RT_s}\right) \tag{4-10}$$

Solving for $P_{O2,s}$,

$$P_{O_2,s} = \frac{\frac{24k_m}{RT_g}}{k_r + \frac{24k_m}{RT_p}} P_{O_2,g} \tag{4-11}$$

Substituting Equation 4-11 into Equation 4-7, the reaction rate becomes:

$$\frac{dm}{dt} = \frac{P_{O_2,g}}{\frac{T_g}{k_r T_p} + \frac{RT_g}{24k_m}} \tag{4-12}$$

The mass transfer coefficient is calculated assuming a Sherwood number of 2.0:

$$Sh = \frac{k_m d_p}{D_{O_2}} = 2 \tag{4-13}$$

where d_p is the particle diameter and D_{O2} is the diffusivity of O_2 in the boundary layer, evaluated at the film temperature ($T_f = [T_p + T_g]/2$).

The particle energy balance must be solved to determine the particle temperature from the gas temperature, as follows:

$$mC_p \frac{dT_p}{dt} = hA\left(T_g - T_p\right) + \varepsilon\sigma A\left(T_w^4 - T_p^4\right) + \dot{r}_c \Delta H_{rxn} \tag{4-14}$$

where h is the convective heat transfer coefficient, ε is the particle emissivity, $\dot{r}_c$ is the char mass reaction rate (negative value), and ΔH_{rxn} is the heat of reaction for reaction R1 (negative value for exothermic reaction). The transient term is neglected in this analysis. A Nusselt number of 2.0 was assumed, so h was calculated as follows:

$$Nu = \frac{h d_p}{k_g} = 2 \tag{4-15}$$

where k_g is the thermal conductivity of the gas, evaluated at the film temperature.

Equation 4-14 is an iterative equation in T_p. Equations 4-12 and 4-14 were solved simultaneously in Excel to fit the char oxidation data from the FFB. The constants A and E were adjusted to fit the mass release data.

During the course of experiments, it was found that the range of experiments conducted did not permit resolution of the apparent activation energy. Hurt and Mitchell (1992) proposed a correlation of global activation energy as a function of the carbon

content of the parent coal on a dry, ash-free basis, albeit for a half-order model instead of a first-order model. This correlation is:

$$E\ (\text{kcal/mol}) = -5.94 + 0.355\ x_C \qquad (4\text{-}16)$$

where x_C is the wt% carbon (daf) in the parent coal. This correlation yielded values of 25.3, 25, and 24.6 kcal/mol (105.9, 104.7 and 103 kJ/mol) for the Kentucky, CC2 and CF2 coals, respectively. A value of 100 kJ/mol was therefore chosen as a representative global activation energy for comparative purposes in this project.

The first-order model described above was programmed into an Excel™ spreadsheet, using small time steps and a simple Euler's method for integration. The gas temperature profile was curve-fit as a function of distance from the burner, so the analysis was non-isothermal. The steady-state particle energy equation was solved at each time step. The initial particle diameter was set to 50 μm, and was not adjusted for swelling or changes during char oxidation (although this can be changed in later analysis). The diffusivity of O_2 in N_2 was used, according to the following equation reported by Mitchell (1990):

$$D_{O_2} = \frac{1.523 \times 10^{-5}\, T^{1.67}}{P} \qquad (4\text{-}17)$$

where T is in Kelvin, P is in atm and D_{O2} is in cm^2/s. Mitchell's thermal conductivity correlation for N_2 was used as well:

$$k_g = 7.6893 \times 10^{-7}\, T^{0.7722} \qquad (4\text{-}18)$$

where T is in Kelvin and k_g is in cal cm^{-1} s^{-1} K^{-1}. The gas velocity was computed from the total volumetric flow rate of gases into the burner, adjusted for the temperature of the gases. A better analysis of the gas and particle velocities for these experiments could be conducted in the future.

5 Coal Nitrogen Release in Oxy-fuel vs. Air-Blown Environments

The objective of this task was to compare the coal pyrolysis products obtained in oxyfuel versus air-blown environments. Of particular interest are the effects of temperature, residence time, diluent gas properties, and coal rank on the products.

5.1 Gas Temperature Profiles

As mentioned previously, Oxy-Fuel combustion results have shown significant NO_x reduction. One possible reason is the occurrence of local hotspots, due to combustion in eddies of high O_2 concentrations. It was therefore desired to understand the behavior of mass and nitrogen release versus temperature. Coal pyrolysis experiments, were performed at peak gas temperatures of approximately 1600, 1700, 1800 and 1900 K. Oxycombustion settings used CO_2 as the diluent gas for both the CO/H_2 fuel stream and the O_2 oxidizer stream, while N_2 was the diluent gas for the traditional combustion setting. Both settings used N_2 as the carrier gas to entrain the coal. Since the flow of carrier gas was 0.0367 standard liters per minute, it was considered negligible compared to the 30 slpm gas flow to the burner.

Gas temperature profiles were measured, with corrected centerline peak temperatures of 1580, 1699, 1789 and 1896 K. The 1896 K setting caused the burner tubes to clog in part of the burner after a short period of running. To remedy this

problem, a profile with a corrected peak of 1909 K was obtained by operating the burner with inverted settings. Gas temperatures were also measured using N_2 as diluent, with peak corrected gas temperatures of 1546, 1628, 1712, 1886 K respectively. While the peak temperatures for the N_2 cases were not exact matches to the CO_2 conditions, these experiments allow comparison at similar positions. The complete set of gas temperature profiles are shown in Appendix B and Appendix D.

5.2 Experiments Performed

Coal pyrolysis experiments were conducted at each of the four CO_2 diluted temperature conditions with each of the three coals, collecting approximately 600 mg of char from each coal at each condition. Initially the emphasis was on the CO_2 atmosphere experiments, causing the N_2 experiments to be neglected until funding was almost gone. Therefore, experiments were not performed with the Pitt 8 and Ill 6 coals under air-blown conditions. Most of the char samples were sent to Huffman labs in Golden, CO for ultimate and ICP analysis. Analysis of the experiments using the Black Thunder coal showed potential differences from the model and the results for bituminous coals, therefore FFB conditions were developed in an air-blown environment to compare with the data from CO_2-blown conditions. Replicates of the air-blown tests were performed at sample probe heights of 1 and 2 inches as will be discussed later in this thesis.

5.3 Mass and Nitrogen Release Data

The coal mass release and nitrogen release data for both the CO_2 and the N_2 experiments are compared in Figure 5-1 through Figure 5-6. Data from previous

experiments, conducted on the FFB system by Zhang (2001) are also shown. Zhang's experiments were performed at gas temperatures between 1534 K and 1850 K for the Black Thunder and Illinois #6 coals. A mass mean diameter of 60 μm was reported for the Illinois #6 coal, however no mass mean diameter was reported for the Black Thunder coal. No Pitt #8 coal experiments were conducted by Zhang. Data from Zhang are represented below by the unfilled green diamonds and labeled "Air (2001)." CPD predictions are displayed in the charts with the blue lines.

The mass release for the Illinois #6 coal had the same trend for the both the Oxy-fuel and air-blown cases between 1530 and 1900 K. In addition, the CPD predictions matched the measured mass release. The nitrogen release for the Illinois #6 coal exhibited a slight upward trend with temperature for the Oxy-fuel cases and was predicted by the CPD model. The air-blown cases did not have the same upward trend, but the difference from the Oxy-fuel case was not very significant. The mass and nitrogen release for the Pitt #8 coal showed a flat trend over the temperature range for both the model and the Oxy-fuel experiments. There was some separation between the data and the model, but the trend was accurately modeled and hence the model was not tuned to fit these data.

Figure 5-5 and Figure 5-6 show the results for the Black Thunder coal experiments, labeled as explained above. Further simulated air experiments were conducted at 1 and 2 inches at 100 K intervals between 1600 K and 1900 K to assure complete pyrolysis, labeled as "Air - 2 inch" and "Air - 1 inch," represented by unfilled black and orange squares, respectively. These data will be discussed in the next section after the corresponding modeling is described.

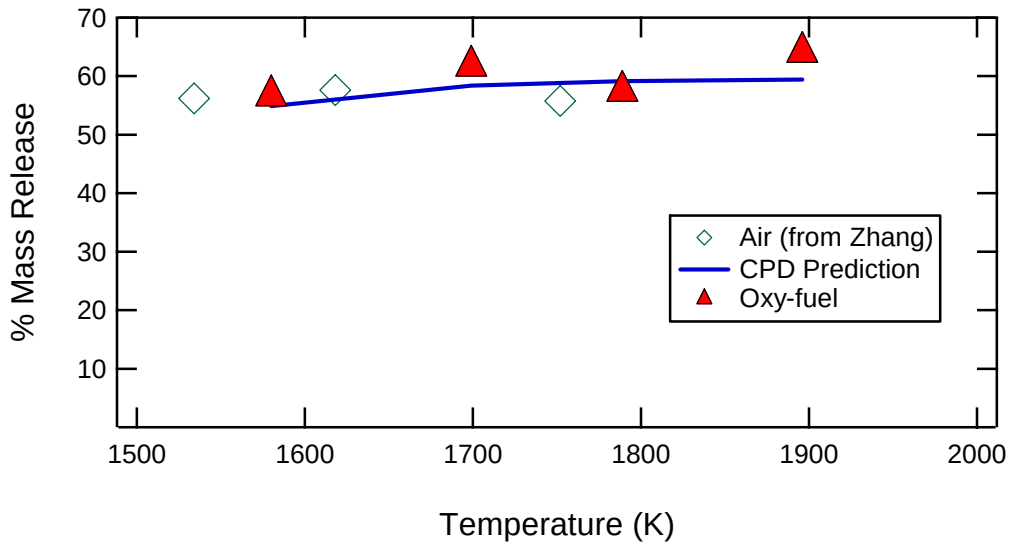

Figure 5-1 Mass release during pyrolysis of Illinois #6 coal as a function of peak temperature

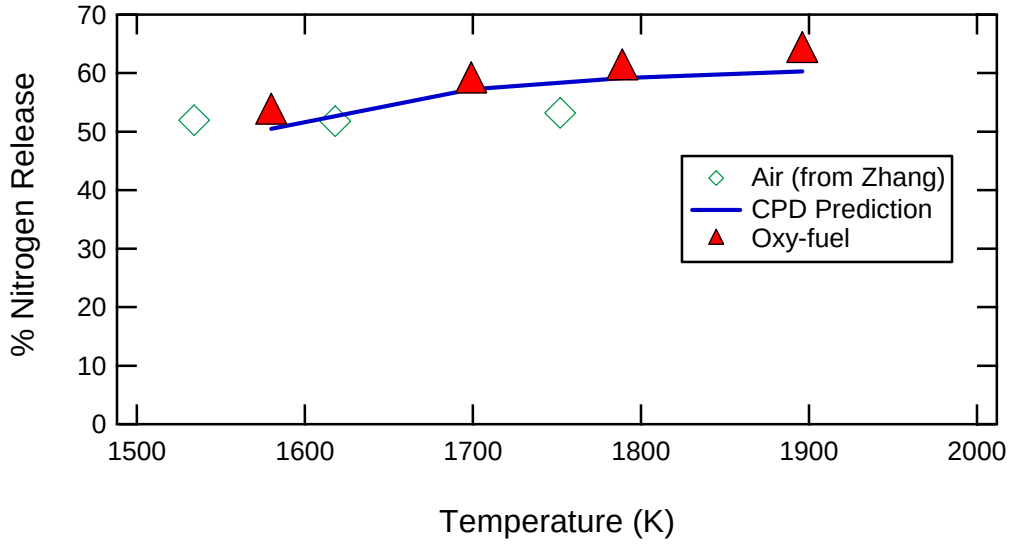

Figure 5-2 Nitrogen release during pyrolysis of Illinois #6 coal as a function of peak temperature

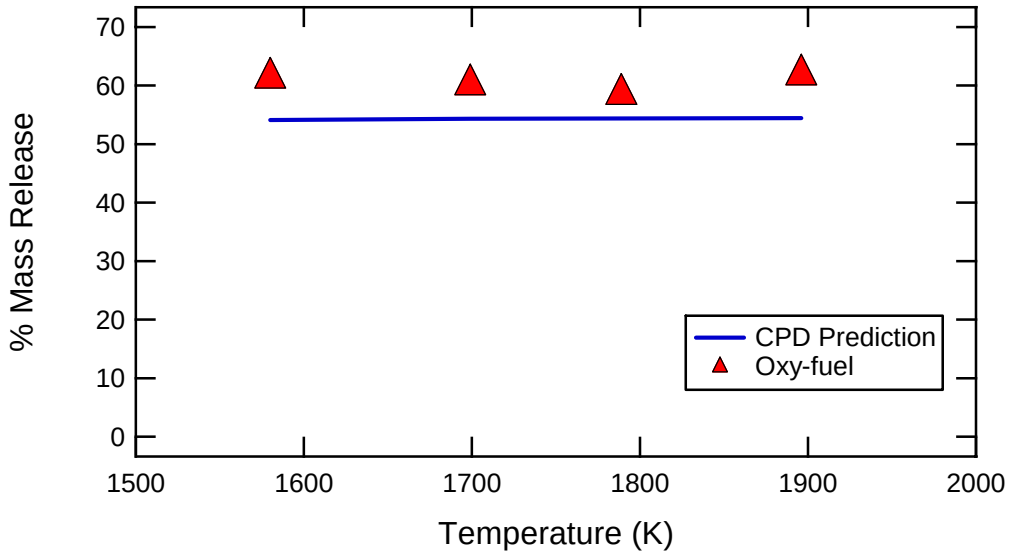

Figure 5-3 Mass release of Pittsburgh #8 coal as a function of peak temperature

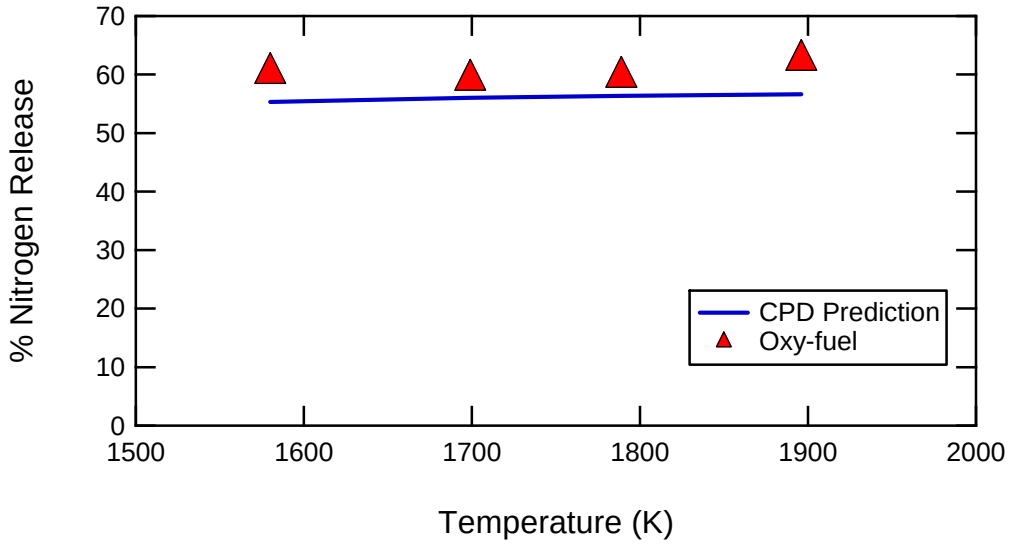

Figure 5-4 Nitrogen release of Pittsburgh #8 coal as a function of peak temperature

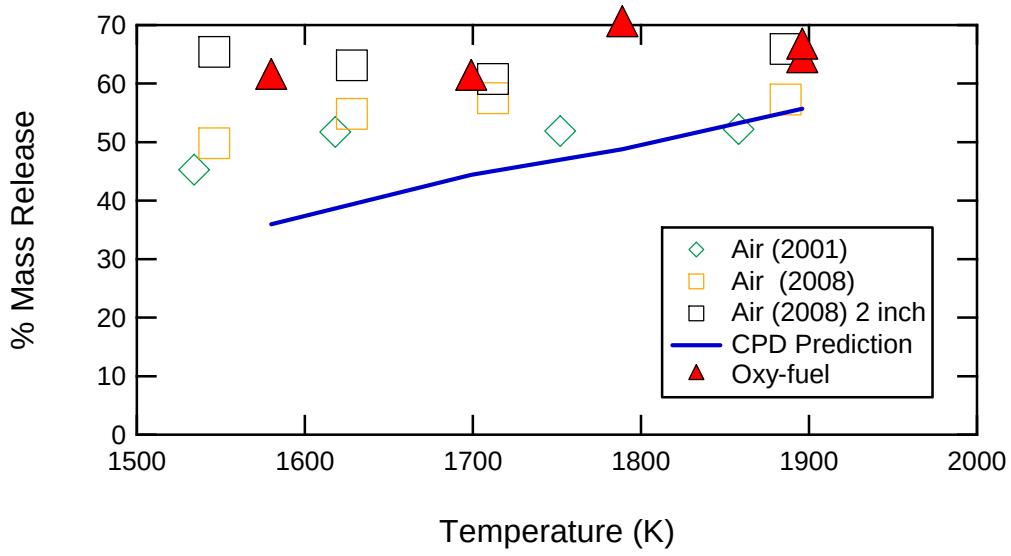

Figure 5-5 Mass release of Black Thunder coal as a function of peak temperature

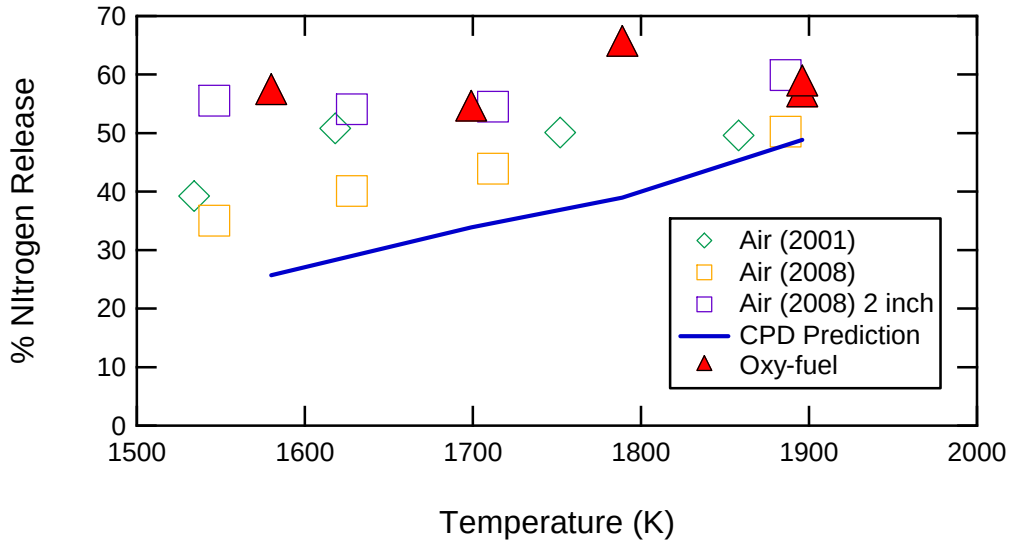

Figure 5-6 Nitrogen release of Black Thunder coal as a function of peak temperature

5.4 Modeling

Coal specific data, gas temperature and particle velocity profiles were input in the N_2 environment version of the CPD code at each burner condition. Figure 5-8

shows a plot of % mass release versus probe height (or distance from the burner) for 1600 K Black Thunder condition. The solid line represents the CPD predictions while the open triangles represent experimental results. The model suggests that the coals were not fully pyrolyzed at the 1 inch probe height, where being fully pyrolyzed is defined as being at or above the leveling point of the pyrolysis yield. Since complete pyrolysis was necessary to obtain a total volatile yield for a given coal and condition, further experiments were conducted at a two-inch probe height. After analyzing the Black Thunder coal using the methods above, it was decided that the coal was not fully pyrolyzed in Zhang's experiments.

The $CPDCO_2$ and $CPDCO_2$-Mackrory models were used to describe coal pyrolysis in Oxy-fuel conditions. The two modified codes had comparable final volatiles and volatile nitrogen yields. However, $CPDCO_2$ predicted a slightly slower rate of mass release than did $CPDCO_2$-Mackrory as illustrated for the 1600 K case in Figure 5-7, which also includes the CPD model predictions in N_2. All versions of the code are included in the CD accompanying this thesis.

5.5 Density and Swelling

The bulk densities of the coal and char were measured using a tap density technique, yielding the mass of particles per volume of graduated cylinder. Assuming a packing factor of 0.5, the ratio of the char density to the coal density was determined. The result is the ratio of the apparent density of the char to that of the coal. These data are shown in Figure 5-9 and Figure 5-10. These data show no real trend with temperature, as expected, and are consistent with the volatiles release data shown in Figure 5-5.

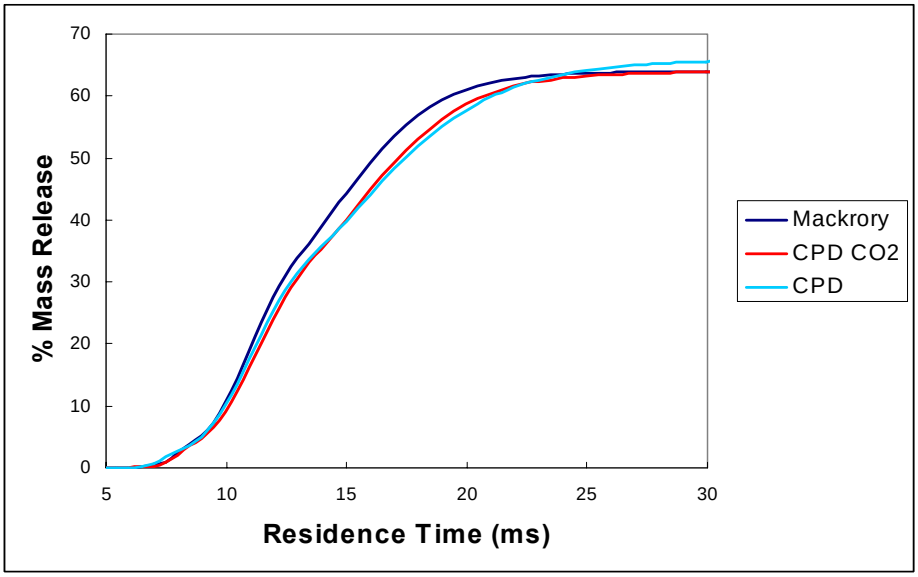

Figure 5-7 Devolatilization yield from Mackrory, CPDCO$_2$, and CPD codes for 1600 K temperature conditions

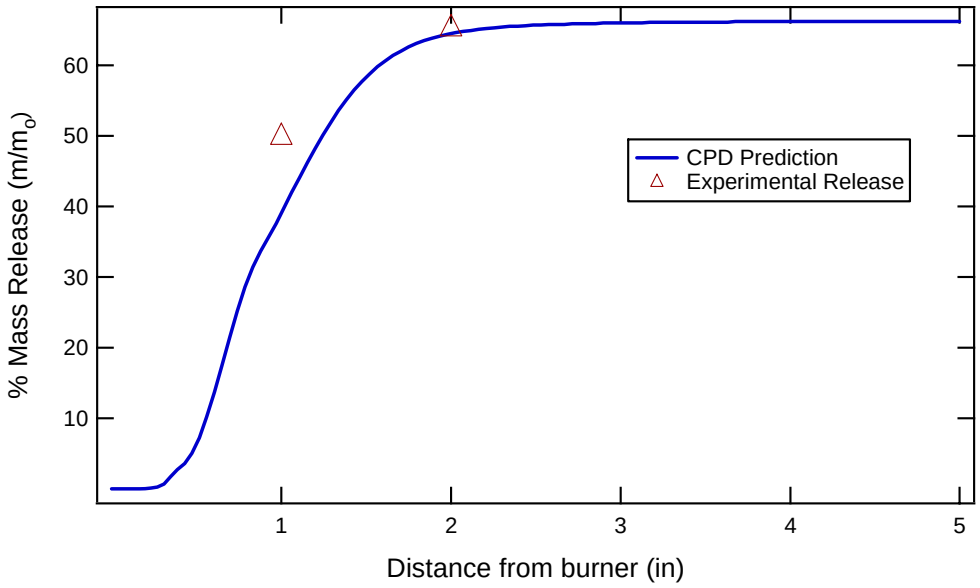

Figure 5-8 Black Thunder coal experimental values versus CPD predicted mass release for the 1600 K temperature condition

The density ratio and the mass release ratio are related by Equation 5-1:

$$\frac{m}{m_0} = \left(\frac{\rho}{\rho_0}\right)\left(\frac{d}{d_0}\right)^3 = 1 - f_{vol} \qquad (5\text{-}1)$$

The diameter ratios are shown in Figure 5-6, indicating a slight degree of shrinkage (rather than swelling) for all coal chars collected under these conditions.

5.6 Discussion of Results

The mass release for the Illinois #6 coal during pyrolysis remained relatively constant after 1700 K, while the nitrogen release increased slightly with temperature throughout the temperature range. Little difference in pyrolysis yield was seen between the data in either the N_2 or oxyfuel environment. The CPD model predictions for the Illinois #6 coal were in great agreement with both the mass release and the nitrogen release data. The mass release and nitrogen release for the Pittsburgh #8 coal did not show much change with temperature in these experiments; the slight trend seems to be within the scatter of the data. The lack of change in mass and nitrogen release at these temperatures was computed accurately by the CPD model. However, the CPD model predictions of both mass release and nitrogen release were slightly below the experimental values for this Pittsburgh #8 coal.

The data for the Black Thunder coal appear to have more scatter. At a 1 inch probe height, the Black Thunder coal mass release was greater in the oxy-fuel case than in Zhang's experiments or in the simulated air-blown conditions for this study. However, the mass release data in the 2-inch air-blown conditions matched the oxy-fuel case data at the 1-inch location. The CPD model seems to match the mass

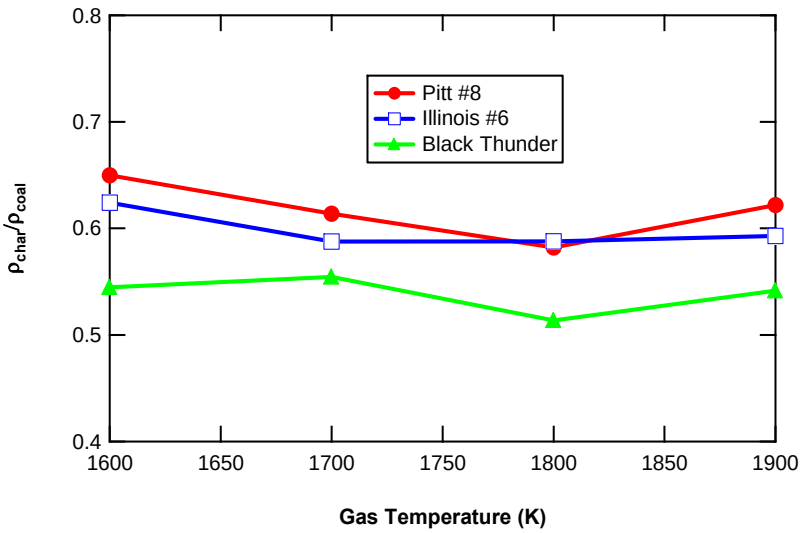

Figure 5-9 Apparent density ratios measured for the coal chars as a function of temperature

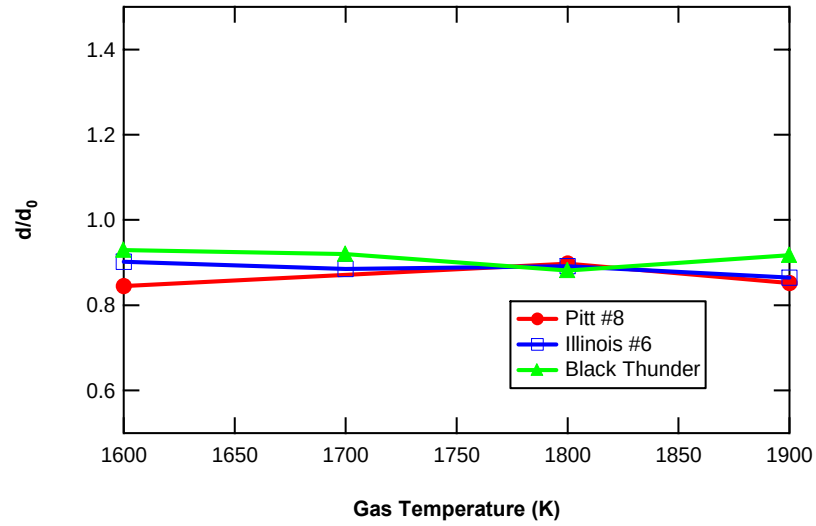

Figure 5-10 Diameter ratios measured for the coal chars as a function of temperature

release data in the 1-inch N_2 environment at higher temperatures but not in the oxy-fuel environment This may be due the reaction of CO_2 with the char at these temperatures when the CO_2 concentration is high, which has been suggested in the literature. This may also be due to the difference in gas properties of N_2 and CO_2 causing the coal to

lose its mass faster in the CO2 environment. Molina and Shaddix (2007) asserted that the different gas properties change the rates of ignition and devolatilization. Since data were not collected at the 2-inch location in the CO_2 environment, it is unknown whether volatile and nitrogen yield would show a similar increase to the N_2 environment or remain the same.

During the CPD model predictions of the Black Thunder coal, the computer code reported an error when predicting the species distribution of the light volatile gases. This error was due to an unfamiliar coal composition for interpolating from known pyrolysis data. It is likely that the ultimate analysis performed at the Huffman lab might be suspect, due to the high oxygen content (which is obtained by difference). A second ultimate analysis showed the O_2 content to vary by 13%.

The nitrogen release data for the Black Thunder coal in the oxy-fuel environment were scattered, but higher on average than in Zhang's data and the 1 inch N_2 environment. The 2 inch N_2 environment data showed good agreement with the 1 inch oxy-fuel numbers. The nitrogen release data obtained in this study in the 1-inch N_2 environment appeared lower than the other data. Upon further investigation, the measured amount of N in char was higher for these samples than the other cases, which accounted for the lower nitrogen release rates. The data from Zhang in the N_2 environment seem to indicate a plateau in nitrogen release after 1600 K, while the CPD model predicts increasing mass release. The cause for this discrepancy is not known. As with the mass release, no nitrogen release data from the CO_2 environment were available to see if a greater nitrogen release occurred at longer residence times. However, it seems reasonable that the nitrogen release reaches a plateau for this coal at roughly 55%.

5.7 Summary

Oxycombustion experiments were conducted on two bituminous coals (Pitt 8 and Ill 6) and one sub-bituminous coal (Black Thunder) at 100 K intervals between 1600 and 1900 K. Measured final volatile yields and nitrogen release showed little or no difference between the Oxycombustion and traditional air fired conditions for the bituminous coals. Model predictions agreed well with these data. However, for the sub-bituminous coal, higher mass release and nitrogen release were observed at the 1-inch sampling location in the oxyfuel condition compared to the air-fired condition. Model agreement with these data was not as good as for the bituminous coals. Further experiments were conducted in air pyrolysis conditions to quantify the difference. Mass release from the 2-inch air experiments roughly equaled that of the 1-inch oxy-fuel experiments. Unfortunately, 2-inch oxy-fuel experiments were not conducted. The difference between the mass release observed in the oxy-fuel condition and the air-fired condition is thought to be caused by early coal gasification in the CO_2-rich environment. Gas property differences between CO_2 and N_2 that affect the heating rate of the coal particle are likely not responsible since the predicted devolatilization is higher in the N_2 model.

6 Combustion Enhancement Through a Chemical Additive

The objective of this research was to quantify the effect of an iron-based coal additive on both coal pyrolysis and oxidation. The exact nature of chemical treatment, performed by personnel at Oryxe Energy International, is proprietary. Three samples of Kentucky bituminous coal were used in the experiments: untreated, moderately treated (CC2), and heavily treated (CF2).

6.1 Coal Analysis

Proximate analyses were performed at BYU on the base coal and the two treated samples as shown in Table 6-1 and Table 6-2 Ultimate analyses are shown in Appendix E. The dry ash-free (daf) carbon contents for the three coals were 87.93 wt% for the Kentucky coal, 87.12 wt% for the CC2 treated Kentucky coal, and 85.91% for the CF2 treated Kentucky coal. It is possible that the chemical treatment could have affected the measured carbon content though not likely. Mass mean diameters were measured on a Coulter Counter LS100 were 64 μm for the Kentucky, 65.8 μm for the CC2 treatment, and ~65 μm for the CF2 treatment. Thus, the coal was roughly uniform in mass mean diameter, volatile content (see Table 6-1) and carbon content for all three coal samples.

Table 6-1 Proximate analysis of coals (as rec'd basis)

	Moisture	Ash	Volatiles	Fixed Carbon*
Kentucky	2.67%	11.68%	40.02%	45.62%
CC2	2.24%	11.15%	40.87%	45.75%
CF2	1.80%	11.45%	40.44%	46.32%

*by difference

Table 6-2 Proximate analysis of coals (daf basis)

	Volatiles	Fixed Carbon
Kentucky	46.73%	53.27%
CC2	47.18%	52.82%
CF2	46.61%	53.39%

6.2 Pyrolysis Results

Char and tar/polyaromatic hydrocarbons (PAH) samples were collected from each coal at a vertical location of 2 inches above the burner surface in the 1300 K pyrolysis condition in the FFB to ensure complete pyrolysis. Elemental tracer results, as explained in chapter 4, and ultimate analysis of chars are listed in Appendix E. Figure 6-1 and Table 6-3 show the partitioning of pyrolysis of both mass and nitrogen products, calculating the gas by difference (i.e., light gas yields were not measured). When an "N" follows a name the column refers to the nitrogen balance. The daf mass release values for the CC2 (49%) and CF2 (53%) treatments were both greater than for the untreated Kentucky coal (35%). This increase in volatile yield was reflected both in the light gas yield (increasing from 21% for the untreated coal to 27% for the CC2 coal and 32% for the CF2 coal) and in the tar/soot yield (increasing from 14% for the untreated coal to 22% for the CC2 coal and 21% for the CF2 coal). The nitrogen release for the CC2 coal

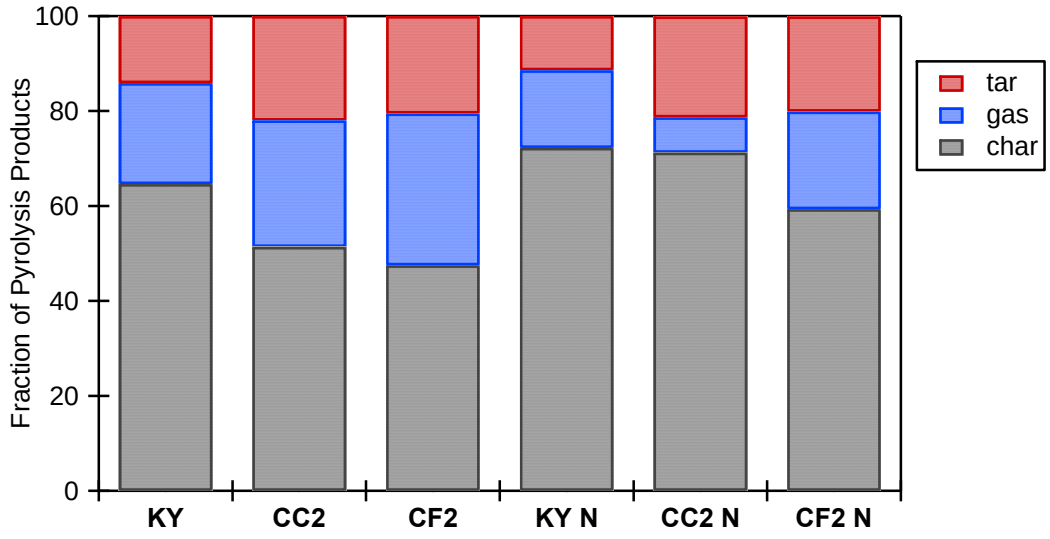

Figure 6-1 Partitioning of pyrolysis products (overall and nitrogen) for Kentucky coal, CC2, and CF2 treatments in the FFB at 1300 K

Table 6-3 CPD predicted mass and nitrogen partitioning*

	% Vol	% char	% tar	% gas	% char N	% tar N	% gas N
KY	35.4	64.6	14.1	21.3	72.2	11.4	16.4
KY CPD	33.2	66.8	17	16.5	70.4	16.2	13.4
CC2	48.6	51.4	22	26.6	71.2	21.2	7.5
CC2 CPD	37.7	62.3	23	15.1	65	23.4	11.6
CF2	52.5	47.5	20.5	32	59.3	20	20.6
CF2 CPD	44.6	55.4	32	12.6	58.2	33.5	8.3

* Yields are on a weight % daf basis. The "N" in the last three columns refers to the nitrogen partitioning

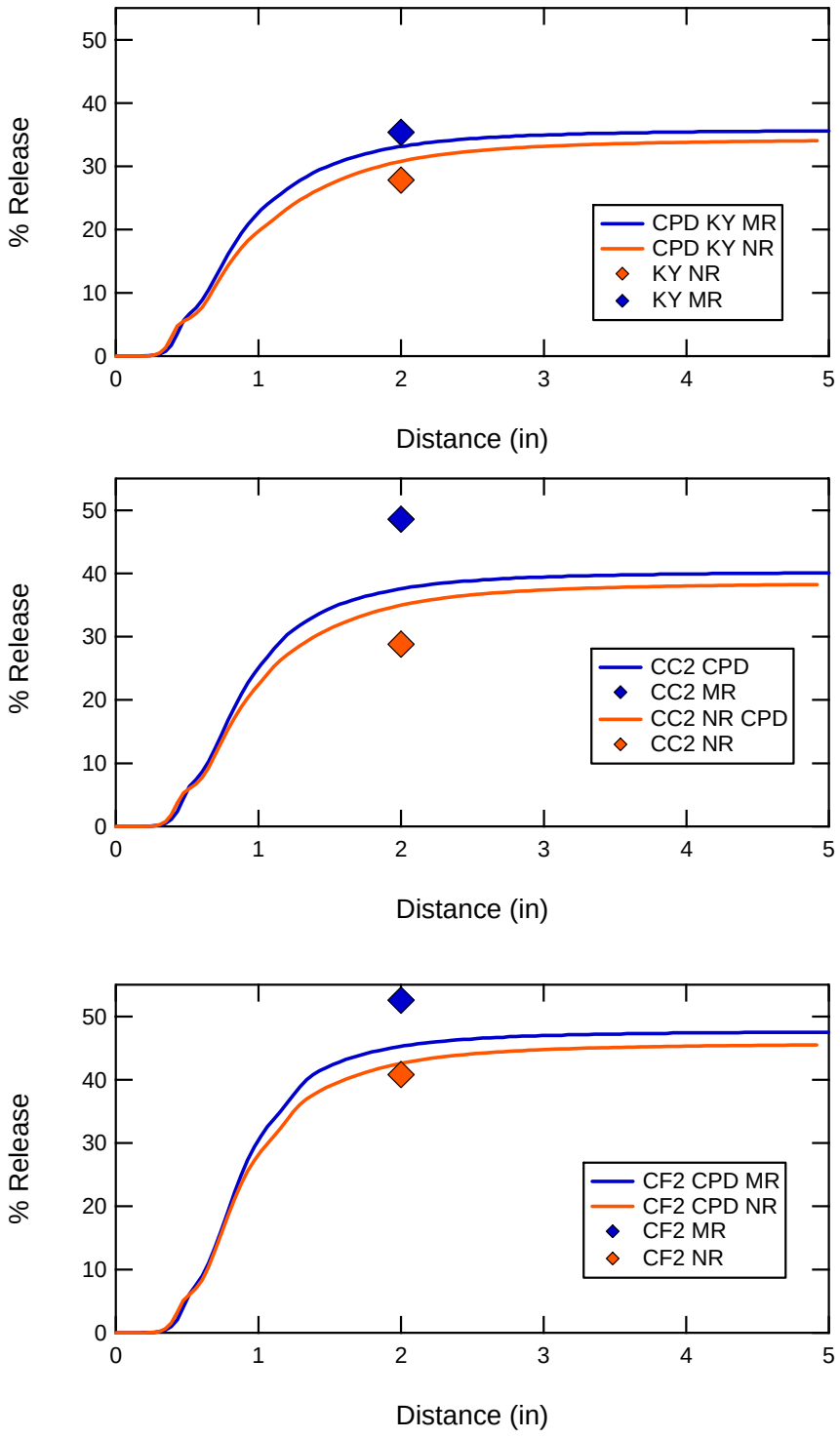

Figure 6-2 Experimental results and CPD model predictions of volatiles and nitrogen release during pyrolysis of the Kentucky, CC2, and CF2 coals in the 1300 K FFB condition

(29%) was about the same as the untreated coal (28%), but exhibited a much higher tar yield. The nitrogen release increased for the CF2 coal (41%).

Table 6-3 shows the predicted amounts of volatiles (tar and light gas) as well as char, and also the predicted nitrogen partitioning. The agreement between the model predictions and the measured overall volatiles yield is very good for the untreated Kentucky coal, with the volatile content different by 2% absolute. The predicted tar and light gas yields had a greater difference due to secondary reactions that are currently not modeled in the CPD. For the treated coal samples, the small change in elemental composition caused the CPD model to predict an increase in the volatile yield. The CF2 has a higher tar yield, while in contrast the CC2 has a higher light gas yield.

Figure 6-2 shows a plot of predicted and measured mass and nitrogen release versus distance from the burner surface. The predictions indicate that the experiments were performed in a location close to where the coal was fully pyrolyzed. Model agreement of the untreated coal is within 3% which is considered good, missing perhaps the location by only 0.25 inches. It is interesting that the small change in the coal dry-ash-free composition caused the CPD model to predict an increase in the volatiles yield. However, the measured increase in volatile yield was higher than the predicted increase, supporting the evidence that the chemical additive increases true volatile yield (note: the additive is considered to have a catalytic effect, thus the words are used interchangeably.)

Table 6-4 Swelling ratios of coals during pyrolysis

	Kentucky	CC2	CF2
m/m_0 (as rec'd)	0.682	0.535	0.520
ρ/ρ_0	0.35	0.39	0.35
d/d_0	1.25	1.11	1.14

Pyrolysis Density and Swelling

Table 6-4 shows the swelling ratios obtained in these experiments, with 25% swelling for the untreated Kentucky coal and ~ 13% swelling for the treated coals. The 25% swelling observed in this experiments is more than seen for most coals in the FFB (Gale et al., 1995; Ma, 1996; Zhang, 2001).

6.2.1 Pyrolysis Conclusions

The experiments performed in the FFB showed that the two treated samples exhibited a greater volatiles release than the untreated coal. A small increase in volatiles yield was predicted by the CPD model based on the differences in the dry ash-free carbon content, but not enough to match the measured volatile yield. Both the tar and light gas yields increased for the treated coals. The effect was only partially captured by the CPD model predictions that were due to small changes in elemental composition. The treated samples exhibited less swelling than the untreated sample, which is surprising, since more volatiles would generally correspond to higher swelling. The overall conclusion is that there seems to be a measurable catalytic effect on the pyrolysis behavior of this coal.

6.3 Char Oxidation Results

The purpose of the char oxidation experiments was to see if the char reactivity changed for the treated samples. Char samples were collected from each coal at four vertical locations (1, 2, 4 and 6 inches) above the burner surface in the two different oxidizing conditions in the FFB (1500 K with 7% O_2, 1700 K with 4% O_2). The char samples were sent to Huffman laboratories in Golden, Colorado, for inorganic tracer analysis (i.e., Al, Si, and Ti) by inductively coupled plasma (ICP) atomic absorption (AA). The remaining char and tar samples were retained for ultimate (i.e., CHNS) analysis performed at BYU on a LECO TruSpec Micro. Sample analyses are summarized in Appendix F. The 1 inch experiment was omitted for the treated samples because insufficient sample was sent.

One puzzling result was that in the char oxidation experiments, the mass release at the first measurement point was the same for treated and untreated coals. This means that perhaps at 1500 or 1700 K the pyrolysis yields were the same as at 1300 K, which does not seem consistent with the measured volatile yields for treated versus untreated coals at 1300 K. The volatiles combustion near the particle surface raised the particle temperature faster than in the pyrolysis experiment, which have influenced the volatiles yield in these combustion experiments.

As mentioned in Chapter 5, a first-order char oxidation model was used to analyze the data, with a constant apparent activation energy of 100 kJ/mol. The resulting curve fits for the pre-exponential factor (A) are shown in Figure 6-4, with values of A shown in Table 6-5 (the detailed spreadsheet is included on the accompanying CD). It was assumed that the activation energy and reactivity were independent of temperature. This

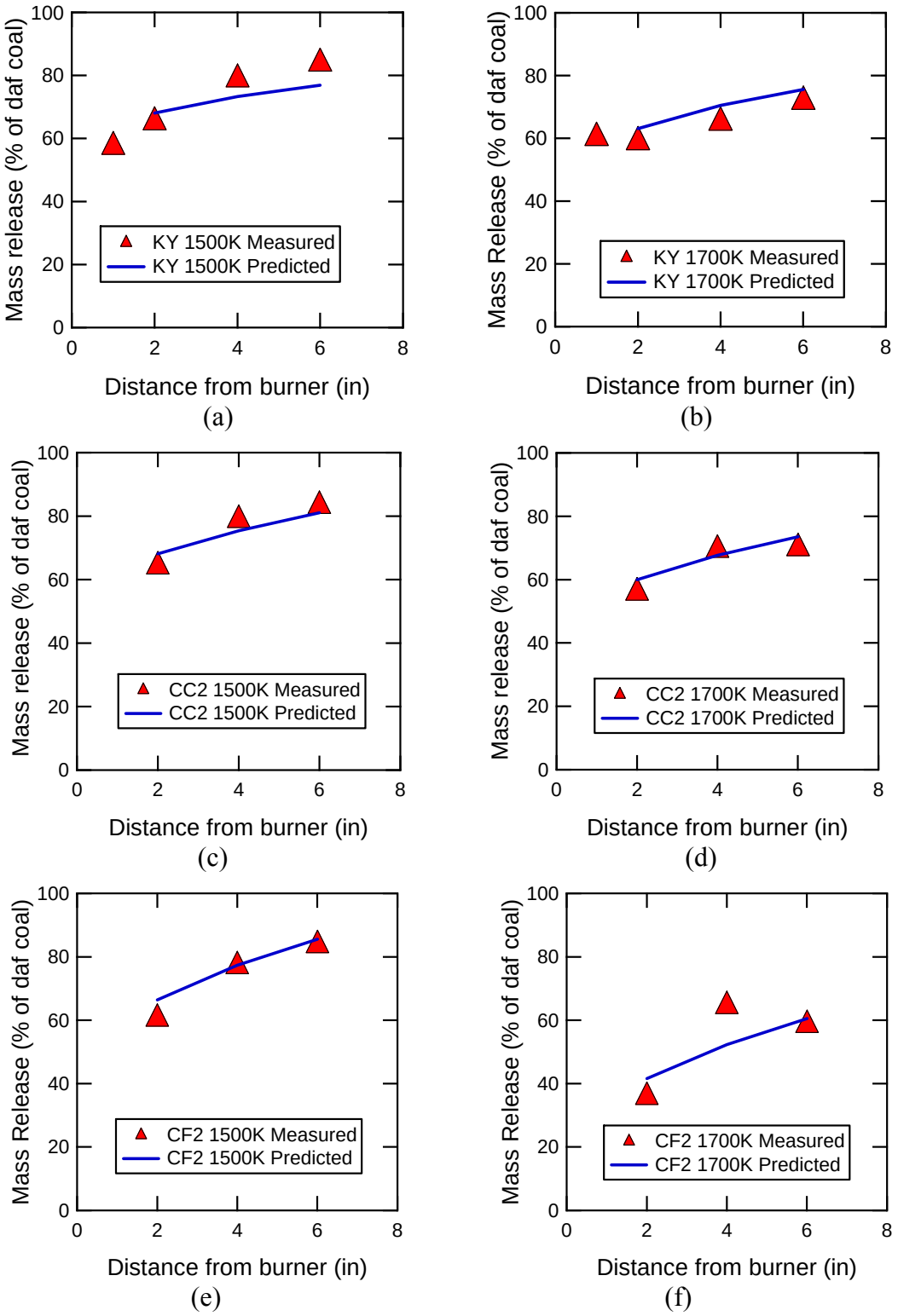

Figure 6-3 Char oxidation predictions and measurements for (a-b) Kentucky coal, (c-d) CC2 coal, and (e-f) CF2 coal in the 1500 K and 1700 K FFB conditions

procedure yielded good curve fits of each treated Kentucky coal (CC2 and CF2) for the two temperature/oxygen conditions. However, the untreated coal could not be fit well using that assumption. The untreated Kentucky coal was also fit assuming temperature dependence of the pre-exponential factor. Those graphs are shown in Figure 6-4. The reactivities for the untreated coal seem much different between the two conditions, based on the first-order model used here. It is possible that a more sophisticated model (such as an n^{th} order model) could better explain why a higher temperature but lower O_2 content causes less char oxidation. Fitted reactivities of the treated coals show a relative drop of 5% for the CC2, but a relative increase of 34% in reactivity in the CF2 from the untreated coal when fitted to one activation energy. This suggests that the additive has a positive effect on burning for higher treatment levels.

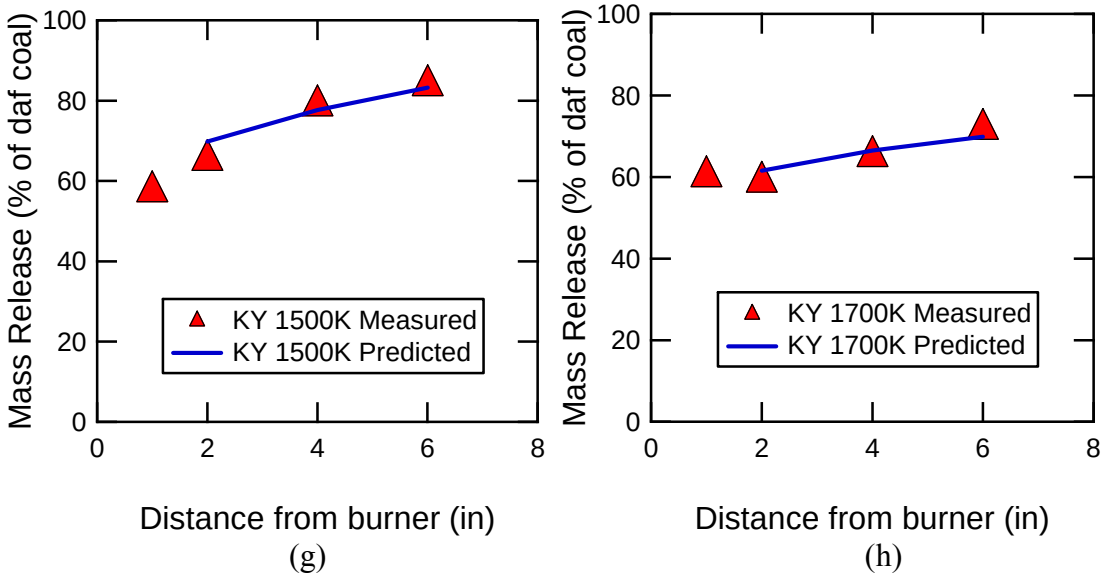

Figure 6-4 Char oxidation predictions and measurements for the (g, h) Kentucky coal in the 1500 and 1700 K FFB conditions when the pre-exponential factor is considered temperature dependant

Table 6-5 Pre-exponential factors determined for the first-order model

Coal	E* (kJ/mol)	A (g cm^{-2} s^{-1} atm$_{O2}^{-1}$) (2 conditions)	A (g cm^{-2} s^{-1} atm$_{O2}^{-1}$) (1500 K data)	A (g cm^{-2} s^{-1} atm$_{O2}^{-1}$) (1700 K data)
Kentucky	100	100	144	66
CC2	100	95	105	83
CF2	100	134	121	151

*Assumed from correlation by Hurt and Mitchell (1992)
n/a = data not available for this case

6.3.1 C To H and C To N Ratios

The carbon to nitrogen and carbon to hydrogen ratios for the coal combustion experiments are shown in Table 6-6. The values are normalized by the C/N or C/H ratios in the parent coal. These data clearly show that the C/N ratios stay roughly constant during char oxidation in the FFB, while the C/H ratio increases steadily. This means that the hydrogen is preferentially burned during char oxidation, leaving the more unreactive carbon in the char. Another way of thinking of this is that the char is becoming more graphitic as it burns, with less peripheral hydrogen (but the same ratio of nitrogen in the aromatic ring structures). The fact that the C/H data in the 1700 K condition show increased hydrogen release than in the 1500 K case seems to confirm that the gas temperature was indeed higher in the 1700 K condition. This seems to rule out errors in gas temperature measurement as an explanation of why the char burnout is less in the 1700 K condition than in the 1500 K condition.

Table 6-6 C/N and C/H ratios for Kentucky, CC2, and CF2 coal combustion experiments

Coal	Distance (inches)	$(C/N)/(C/N)_0$		$(C/H)/(C/H)_0$	
		1500 K	1700 K	1500 K	1700 K
KY	1	0.89	0.87	5.80	2.71
	2	1.26	1.06	6.27	3.09
	4	1.42	1.25	20.95	13.34
	6	1.20	1.30	4.63	10.96
CC2	2	1.18	1.16	9.69	9.79
	4	1.29	1.21	6.28	14.14
	6	1.42	1.35	19.38	13.26
CF2	2	1.32	1.03	12.58	11.63
	4	1.21	1.17	15.08	12.66
	6	1.42	1.22	15.28	18.13

6.3.2 Char Oxidation Experimental Density and Swelling

The density ratios and resulting diameter ratios for the char oxidation experiments are shown in Table 6-7. The diameter and density ratios decreased during combustion for both bituminous coals, as expected. This means that the char is burning in neither constant diameter nor constant density mode, but a combination mode where both diameter and density are changing.

Table 6-7 Density and diameter changes during combustion of Kentucky treated and untreated coals in FFB

		1500 K			1700 K		
	Distance (in)	m/m_0*	ρ/ρ_o*	d/d_o	m/m_0*	ρ/ρ_o*	d/d_o
KY	1	0.487	0.41	1.06	0.435	0.41	1.02
	2	0.413	0.31	1.10	0.443	0.27	1.18
	4	0.279	0.25	1.03	0.387	0.21	1.22
	6	0.221	0.24	0.97	0.324	0.21	1.15
CC2	2	0.406	0.25	1.18	0.454	0.24	1.24
	4	0.268	0.24	1.04	0.414	0.24	1.21
	6	0.229	0.24	0.99	0.345	0.22	1.16
CF2	2	0.417	0.28	1.15	0.450	0.27	1.19
	4	0.293	0.26	1.05	0.420	0.25	1.18
	6	0.268	0.24	1.04	0.319	0.21	1.15

6.4 Char Oxidation Abnormalities

One perplexing issue in the results is that the mass release percentage for the 1500 K cases is greater than for the corresponding 1700 K cases. The O_2 content for the 1700 K case was only 4.2 mol% for chapter 7 studies and 3.6% in the chapter 6 studies, which is lower than the 7.5 mol% O_2 in the 1500 K case. These O_2 concentration measurements matched the values predicted by the NASA CEA code, which were 7.87 mol% and 4.27% for the 1500 and 1700 K conditions, respectively. The great agreement between the predicted and measured O_2 concentrations adds confidence to the experimental procedure.

Sources for experimental error were examined in conjunction with the 1700 K experiments. All three coals exhibited lower burnout in the 1700 K case, so the situation is repeatable. Gas temperature measurements, were repeated, as were the O_2 content measurements in the post-flame gases. The only explanation that seems to make sense is the possible fact that there is some kind of low O_2 ignition limit, below which the char particles exhibit a smoldering combustion rather than a fully-ignited combustion. Other authors (Hurt and Mitchell, 1992) have put a lower limit on the partial pressure of O_2 over which their rate expressions are valid ($P_{O2} > 0.03$ atm in their case). Since atmospheric pressure in Utah is about 0.85 atm, $P_{O2} = 0.035$ atm in the 1700 K condition. This low partial pressure of O_2 may therefore be below some ignition limit.

Figure 6-5 shows the χ factors calculated by the first order model. The χ factor is the ratio of the observed burning rate to the maximum burning rate. These χ values are much less than 1.0, meaning that the char is burning at a rate much smaller than its maximum limit.

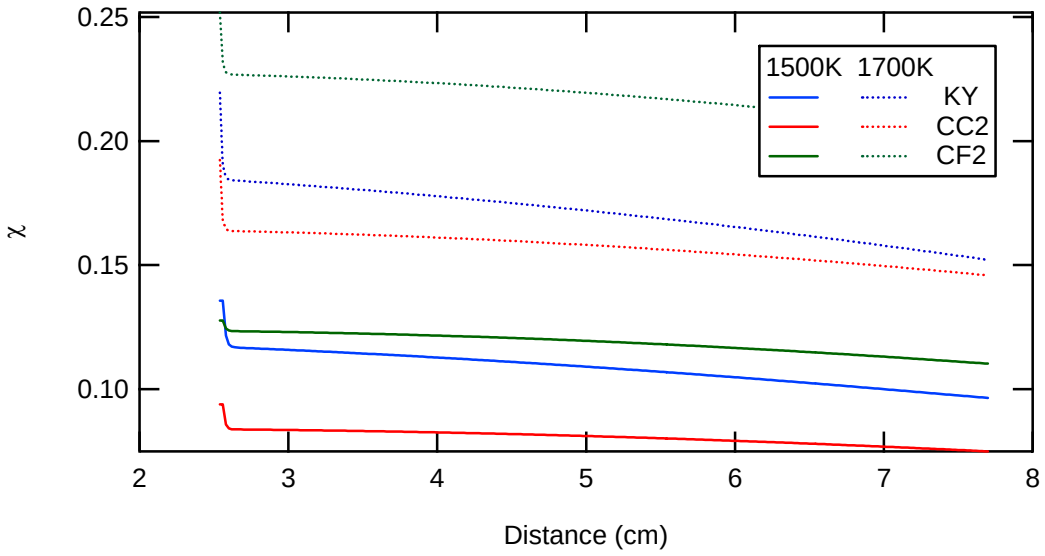

Figure 6-5 Calculated χ factors for the treated and untreated coals

6.5 Conclusions

The FFB pyrolysis experiments indicated that the treated coals exhibited higher total volatile yields in the 1300 K environment than the untreated coal. The CC2 had a 37% relative increase and the CF2 had a 49% relative increase in volatiles release. Both the tar and light gas yields were higher for the treated coals in this set of experiments. The nitrogen release followed the same trend with treatment severity as the volatiles release. Only a small portion of the increased yield in volatiles was modeled by the CPD model based on the changes in the composition of the parent treated coals. There was evidence for decreased particle swelling during pyrolysis of the treated coals as well.

The CC2 char oxidation experiments showed a decrease in reactivity of 5% based on a simplistic first-order model, which is close to being within experimental error. The

CF2 coal treatment had 34% increase in reactivity, which is a significant increase in reactivity. One puzzling result was that in the char oxidation experiments, the mass release at the first measurement point was the same for treated and untreated coals. This means that perhaps at this higher temperature the pyrolysis yields were the same, which does not seem consistent with the measured volatile yields for treated versus untreated coals at 1300 K. These results show that the additive has an effect on the char oxidation increasing the reactivity for higher treatment levels by about 35%.

7 Coal Nitrogen Release Data

This project's objective was to expand the database of coal pyrolysis and char oxidation experiments to worldwide coals. The expanded database assists in creating and reinforcing pyrolysis and oxidation modeling. Especially important was obtaining gas phase information about nitrogen containing species of HCN and NH_3. To this end, six coals were tested over a two-year period in both pyrolysis and oxidation conditions.

7.1 Coal Analysis

Proximate analysis was performed at BYU on each coal using the ASTM moisture, ash and volatiles tests, with results presented in Table 7-1 and Table 7-2. Complete ultimate analysis data are shown in Appendix G. All coals examined except for the Coal C were bituminous coals, though no coal is from the same seam. Coal rank and the mass mean diameter of each of the coals as measured in a Coulter Counter LS are provided in Table 7-2. All sizes were around 70 μm except the Coal Bl which was 50 μm and the Coal C which was 80 μm.

7.2 Pyrolysis Results

Char and tar/polyaromatic hydrocarbons (PAH) samples were collected at a vertical location of either 1 inch (Coals A, B, C) or 2 inches (Coals D, E, F) above the

burner surface in the 1300 K pyrolysis condition in the flat flame burner (FFB) system (see Table 4-2). Gas phase HCN and NH_3 concentrations were measured only at the 2 inch height under the same temperature conditions for all coals (after FT-IR repair). Figure 7-1 and Figure 7-2 show the fraction of mass and nitrogen in the char, tar, and light gas phases, with the gas yields calculated by difference. On average the coals examined at the 2-inch location exhibited a higher mass and nitrogen release than the 1-inch experiments, which was expected due to longer pyrolysis time. The fraction of nitrogen remaining in the tar/soot was equal to the mass fraction of tar for the Coals A & E, but not for the remaining coals. For coals A, B, D, and E, the fraction of nitrogen in the light gases was less than or equal to the mass fraction of light gases, while in coal F the fraction of nitrogen in the light gases was greater.

Table 7-1 Proximate analysis of coals (as rec'd basis)

	Moisture	Ash	Volatiles	Fixed Carbon*
Coal A	1.00%	10.61%	36.20%	52.19%
Coal B	0.87%	17.80%	31.80%	49.53%
Coal C	16.0%	8.40%	41.80%	33.80%
Coal D	5.42%	9.15%	37.54%	47.90%
Coal E	2.43%	14.74%	32.86%	49.98%
Coal F	1.71%	8.37%	38.69%	51.22%

*by difference

Table 7-2 Proximate analysis of coals (daf basis), coal rank, and mass mean diameter

	Volatiles	Fixed Carbon	Coal Rank	d_p*
Coal A	40.95%	59.05%	High volatile b bituminous	70
Coal B	39.10%	60.90%	High volatile b bituminous	50
Coal C	55.29%	44.71%	Subbituminous	80
Coal D	43.93%	56.07%	High volatile a bituminous	77
Coal E	39.66%	60.34%	High volatile a bituminous	71
Coal F	43.03%	56.97%	High volatile b bituminous	68

*mass mean diameter from Coulter Counter analysis

A more specific nitrogen balance was obtained by measuring the amount of HCN and NH_3. Table 7-3 shows the results from the FT-IR experiments to collect gas phase data on HCN and NH_3 concentrations and the ratio of HCN to NH_3. Coals C, D, & F had a HCN/NH_3 ratio much greater than 1; the ratios for the Coals A & E were closer to 1, while coal B had a ratio less than 1. It is not immediately apparent why the behavior of coal B is so different from the others. No NH_3 was detected from coal D experiments. The nitrogen balance did not close for any of the coals, but is considered pretty good for an entrained flow experiment. In previous studies, only around 80% of the nitrogen was balanced (Zhang, 2001). Unfortunately, the solid samples for the year one suite were collected at a 1 inch probe sampling height, therefore a similar balance was not possible for the first year coals. Figure 7-3 shows the nitrogen balance of the second year coals using the light gas distribution calculated by the FT-IR, showing balances of 85% or higher.

Table 7-3 Gas phase results from the 1300 K pyrolysis experiments

	% conversion of coal fuel N		
Coal	HCN	NH_3	HCN/ NH_3
Coal F	20.98	1.35	15.50
Coal C	18.53	1.30	14.26
Coal B	3.11	22.04	0.14
Coal A	10.51	2.06	5.11
Coal D	12.05	0.00	n/a
Coal E	11.73	3.27	3.58

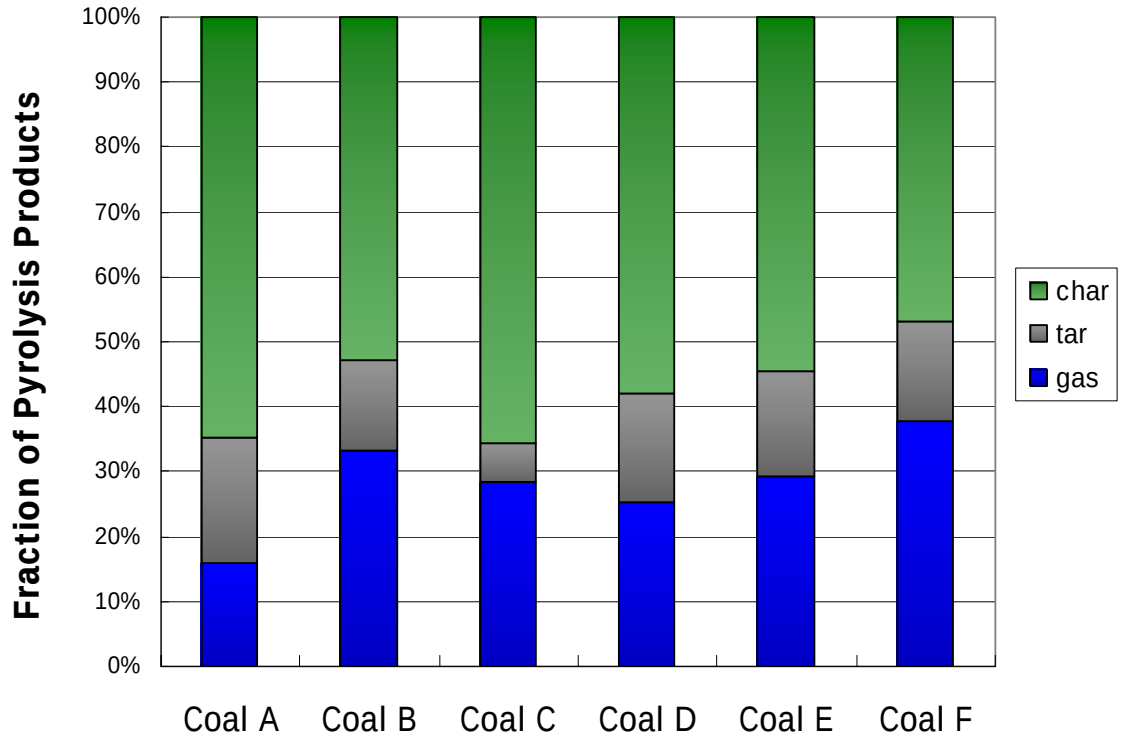

Figure 7-1 Mass partitioning of the pyrolysis product for all coals

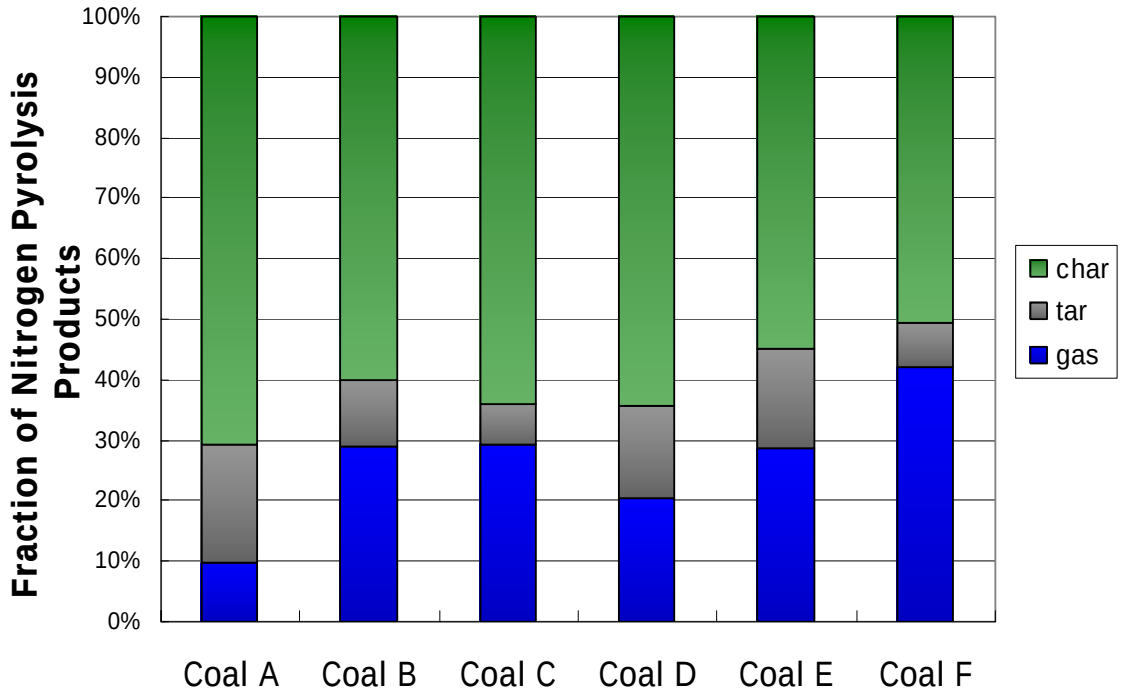

Figure 7-2 Partitioning of nitrogen pyrolysis products for all coals

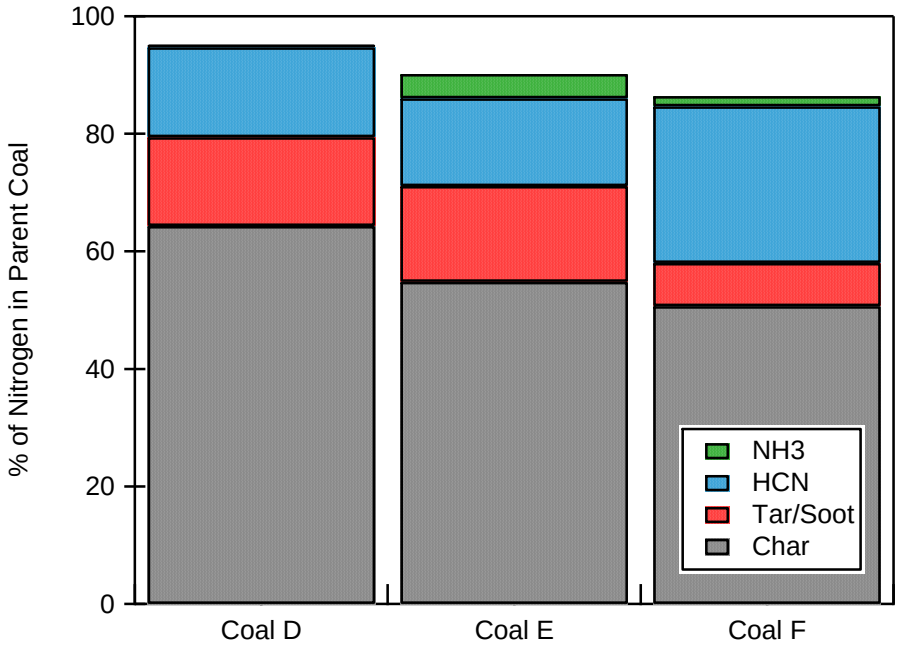

Figure 7-3 Nitrogen partitioning among coals studied in the second year

7.2.1 Pyrolysis Density and Swelling

Coal density and swelling for the six coals tested are recorded in Table 7-4. No swelling was observed for coals B, C, E, & F. However, 21% swelling was observed for coal A and 13% swelling for coal D; this is more swelling than seen for most coals in the FFB.

Table 7-4 Swelling ratios of coals during pyrolysis

	ρ/ρ_0	m/m_0 (as rec'd)	d/d_0
Coal A	0.37	0.65	1.21
Coal B	0.58	0.6	1.01
Coal C	0.72	0.69	0.99
Coal D	0.41	0.585	1.13
Coal E	0.57	0.615	1.03
Coal F	0.5	0.503	1

7.2.2 Coal Database Figures

Figure 7-4 through Figure 7-7 show a compilation of coal pyrolysis experiments performed at BYU (this study, (Zhang, 2001), Sandia National Laboratories (Fletcher and Hardesty, 1992), and in Japan (Xu and Tomita, 1987). The ratio of H to C and O to C are used as indicators of coal rank. These were compared to the total volatile yield and maximum tar yield. Each set of data reflects experiments performed between 1200 and 1300 K. Both total volatile graphs trend upwards from anthracite to lignite as expected. The maximum tar yield graphs reveal scatter in the data as there is not a defined maximum. The new data obtained in this study fits the data that has been previously obtained by different researchers.

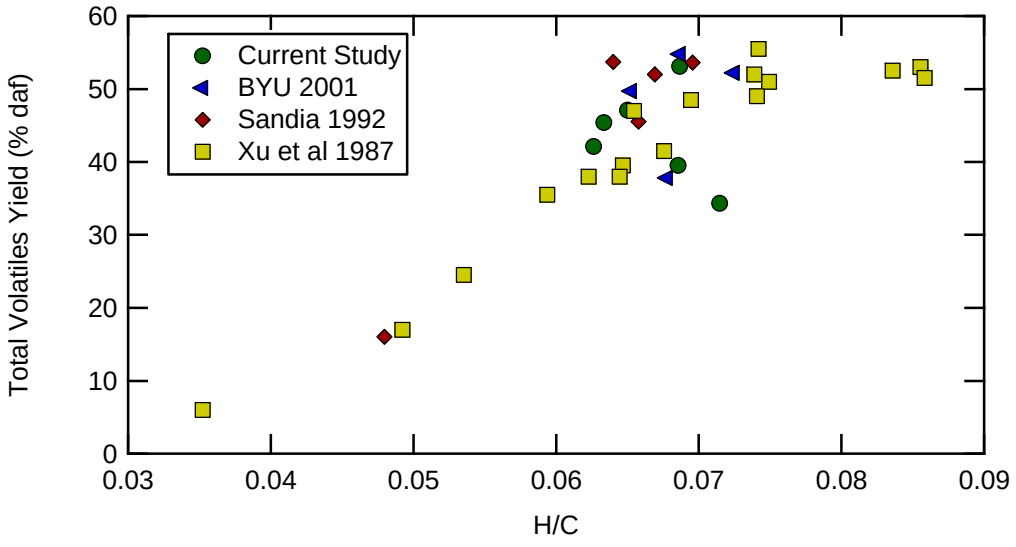

Figure 7-4 Database of mass release as a function of rank

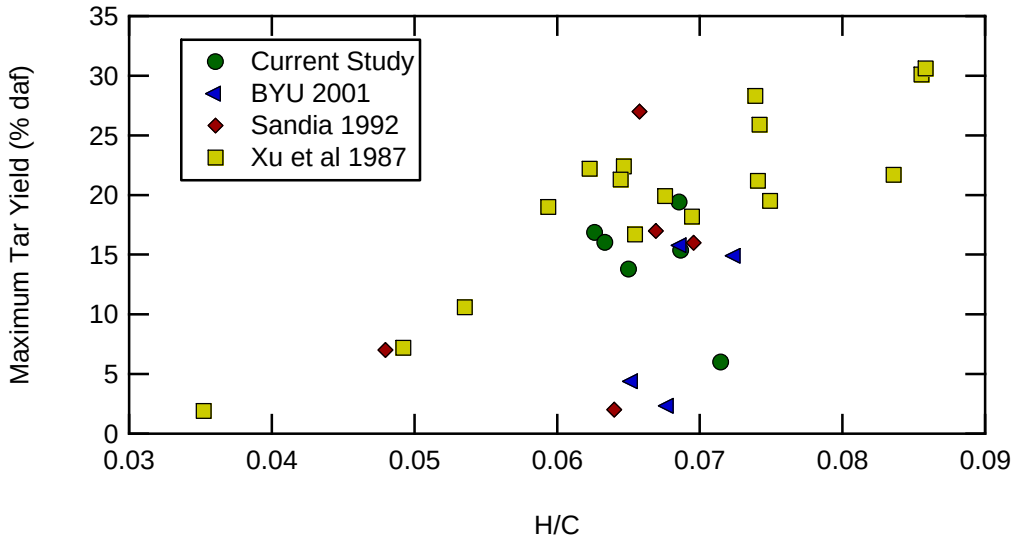

Figure 7-5 Database of tar yield as a function of rank

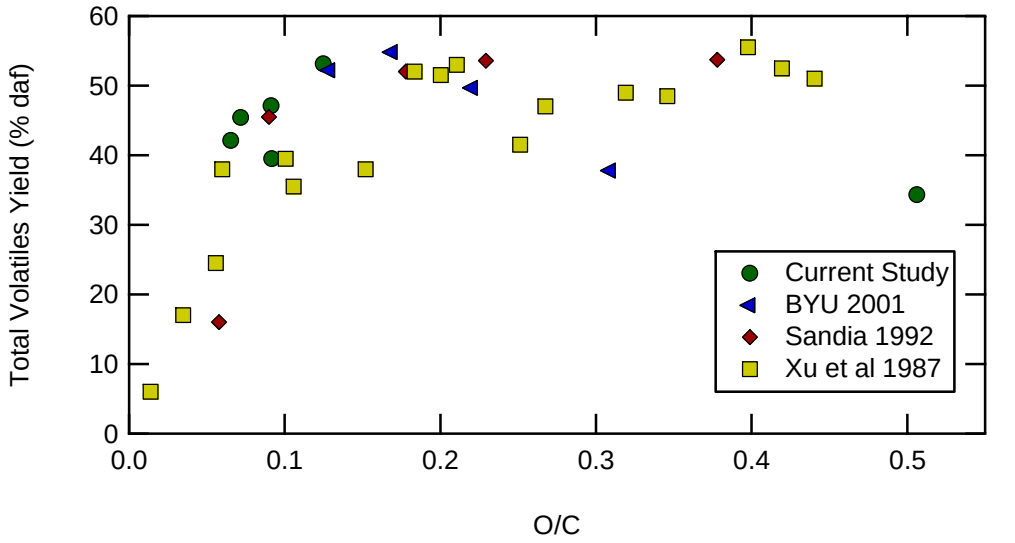

Figure 7-6 Database of mass release as a function of O to C ratio

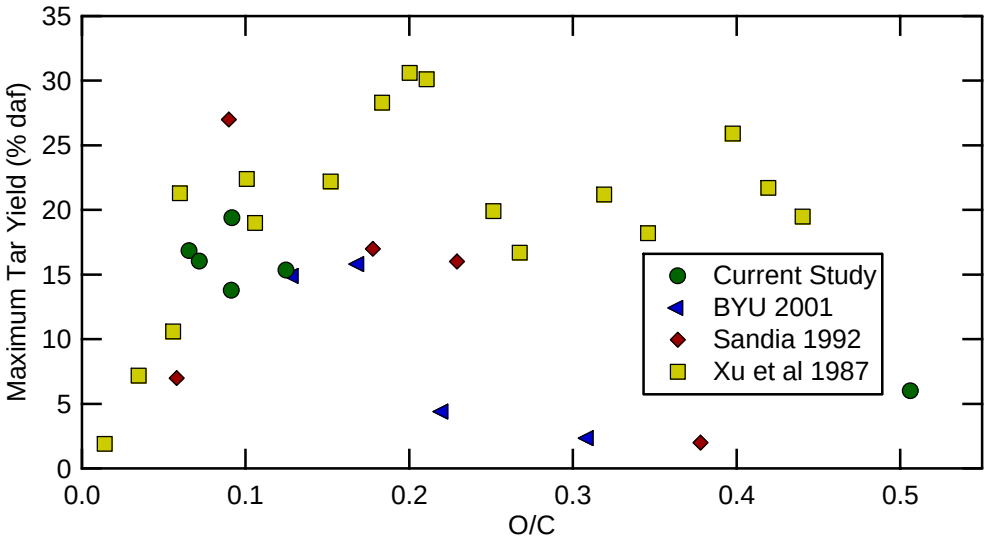

Figure 7-7 Database of tar yield as a function of O to C ratio

7.2.3 Discussion of Pyrolysis Results

The pyrolysis results showed several irregularities that will be discussed in this section. First, the nitrogen conversion into HCN and NH_3 was greater than 10% for all of the six coals studied, which was higher than in the Zhang study at a similar temperature (Zhang, 2001). Table 7-5 shows the coal nitrogen conversions reported by Zhang at 1 and 3 inch probe sampling heights with a peak temperature of 1281 K. Zhang's study was designed to cover coal ranks from bituminous to lignite, and therefore give a spectrum of results. The previous study reported that between 2.73 and 7.18 % of the coal nitrogen was converted to HCN, while 26.7% was measured in the current study. The reason for this discrepancy is not clear. The molar gas flow rate through the collection probe is currently read from flow meters and corrected for pressure and temperature, which was not done in previous experiments. Also, the tubing leading to the

FT-IR was shortened in the present experiments, which could explain some of the different results.

The measured HCN yield was higher than the NH_3 yield for all coals tested except for coal B. Coal B had a high ash content (17.8%) and a high carbon content (84.4% daf C), and was expected to behave in a manner similar to Coal A. One difference is that Coal B had the smallest mass mean diameter of all the coals tested. The smaller mass mean diameter means a higher particle heating rate and hence faster mass release. However, the faster heating rate and mass release rate should not have much bearing on the HCN to NH_3 ratio.

7.2.4 CPD Model Results

CPD calculations of mass release during pyrolysis are presented below. Figure 7-8 and Figure 7-9 shows a plot of nitrogen release versus distance, showing the coal was fully pyrolyzed in the second year experiment, but not the first. Table 7-5 shows the mass fractions of char (f_{char}), soot (f_{soot}), light gas (f_{gas}) calculated by the CPD model, as well as the nitrogen fractions ($f_{N,char}$, $f_{N,tar}$, $f_{N,gas}$). The CPD model does not yet

Table 7-5 Nitrogen gas species results from Zhang (2001)

	% conversion (N in coal basis)					
	1 inch			3 inch		
Coal	HCN	NH_3	HCN/NH_3	HCN	NH_3	HCN/NH_3
Ill #6	2.14	1.9	1.13	7.69	3.91	1.97
Utah	2.73	3.71	0.74	7.18	5.51	1.30
BT	2.14	3.84	0.56	9.11	6.28	1.45
Knife River	0	5.09	n/a	7.89	11.34	0.70

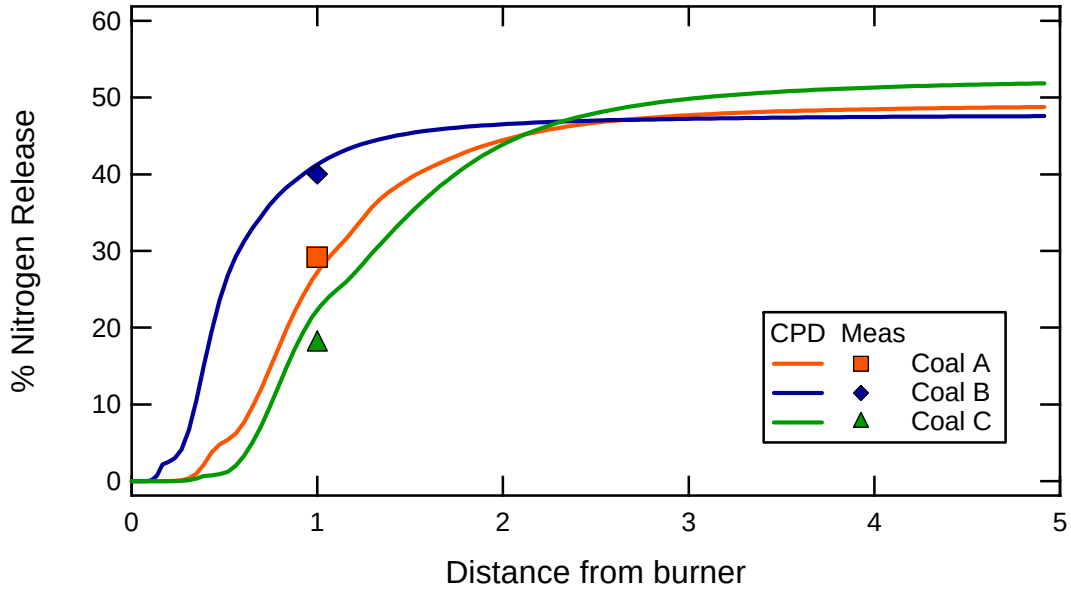

Figure 7-8 Nitrogen release as a function of time for the first year coals (A, B, C)

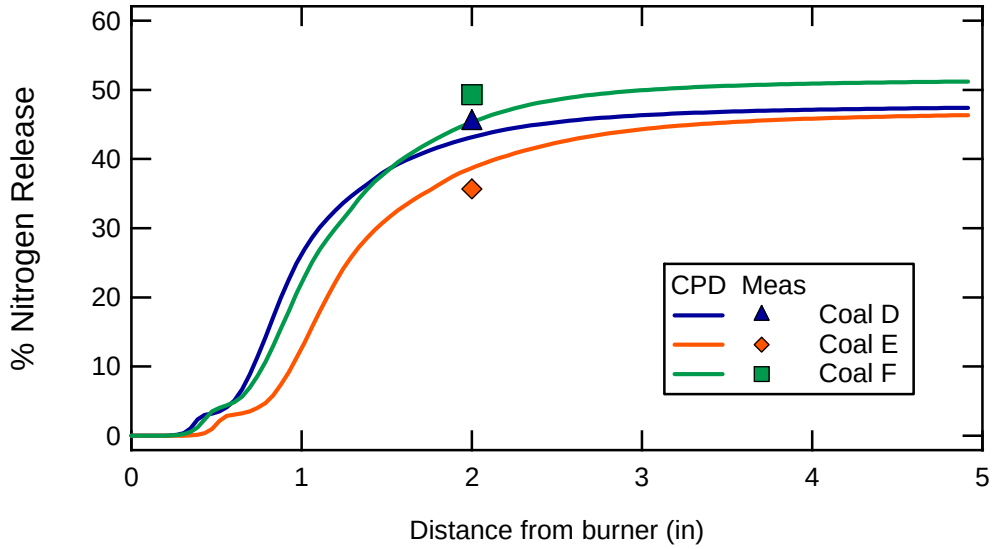

Figure 7-9 Nitrogen release as a function of time for the second year suite of coals (D, E, F)

Table 7-6 CPD calculations of coal pyrolysis in the 1300 K FFB condition

Coal	wt% (daf) Volatiles	f_{char}	f_{soot}	f_{gas}	$f_{N,char}$	$f_{N,tar}$	$f_{N,gas}$
Coal B	45.6	0.544	0.3	0.156	0.588	0.314	0.097
Coal A	38.8	0.611	0.28	0.109	0.664	0.294	0.04
Coal C	35.6	0.644	0.16	0.094	0.765	0.167	0.068
Coal D	43.8	0.562	0.310	0.123	0.615	0.332	0.053
Coal E	47.3	0.527	0.320	0.153	0.569	0.338	0.092
Coal F	50.3	.497	0.32	0.183	0.549	0.336	0.115

distinguish between HCN and NH_3 release. The agreement between the model predictions and the data is quite good as far as the overall volatiles yield, but not as good as expected for the tar yield (see figures 7-10 and 7-11). Predicted tar yields are greater than the measured tar yields, which is surprising based on past history with the CPD model. At 1300 K, there is some degree of secondary pyrolysis; hence the tar fraction in particular will have decreased from the primary pyrolysis value.

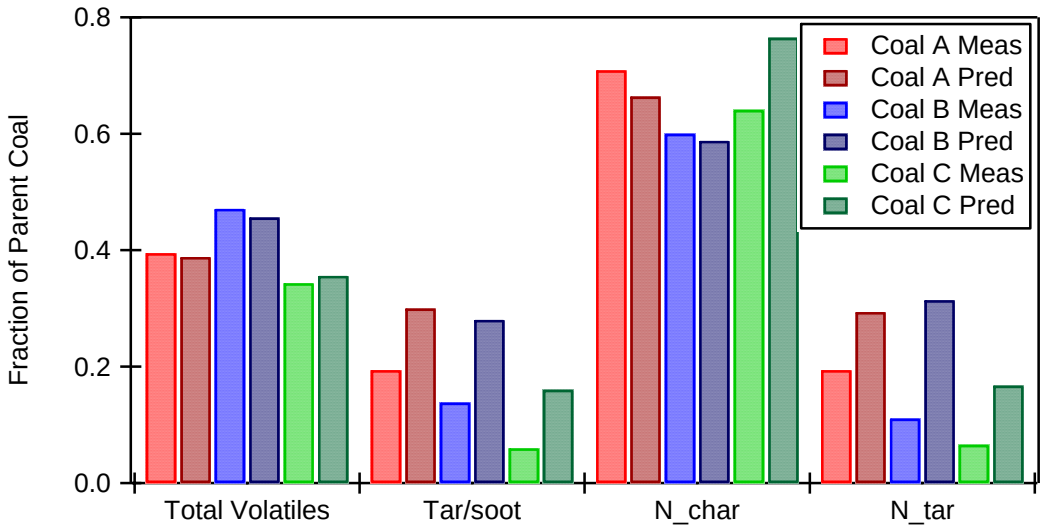

Figure 7-10 Comparison of CPD model predictions with measured values of total volatiles, tar/soot formed, fraction of nitrogen remaining in the char, and fraction of nitrogen in the tar/soot for the three coals

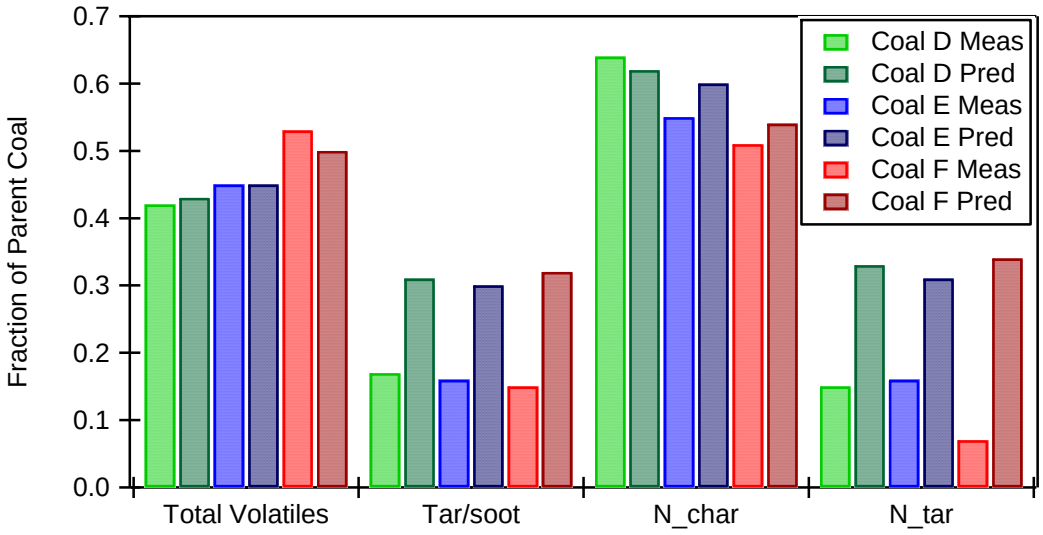

Figure 7-11 Comparison of CPD model predictions with measured values of total volatiles, tar/soot formed, fraction of nitrogen remaining in the char, and fraction of nitrogen in the tar/soot for the three coals

7.3 Char Oxidation Results

Char samples were collected from each coal at four vertical locations above the burner surface in the two different oxidizing conditions in the FFB. The char samples were analyzed as explained in chapter 4. The results in are summarized in Figure 7-12 and Figure 7-13 with the complete set of data presented in Appendix G. In general, the sub-bituminous coal had the highest mass and nitrogen release and Coal A had near the lowest. The mass release in the 1500 K experiments increased with residence time for all coals except Coal A. Lower mass and nitrogen release were observed in the 1700 K condition than in the 1500 K condition. This was partially due to the lower O_2 content in the 1700 K condition, but may also suggest another factor such as smoldering combustion occurring.

7.3.1 Char Combustion Model

The char combustion model used for these experiments is the same model presented in chapter 5. A value of 95 kJ/mol was chosen as a representative global activation energy for the year 1 coals, while a value of 100 kJ/mol was chosen for the year 2 coals. The resulting curve fits are shown in Appendix G.2. Model agreement was generally within 5% absolute of the experimental values for the 6 inch conditions. Table 7-7 shows the values obtained for reactivity (A) and activation energy (E) from the experiments. Coal C was fit with E = 95 kJ/mol for comparison, though the fit obtained with this value of E appeared low. Data obtained for Coals C-E had high error when reactivity was assumed temperature independent. Each condition was fit separately for these coals assuming temperature independence. Coal F had the best fit but had a lower reactivity (111 g cm^{-2} s^{-1} atm_{O2}^{-1}) for the second group of coals. It is possible that an n^{th} order model could better explain why a higher temperature but lower O_2 content causes less char oxidation. The 1700 K experiments had a lower reactivity in general. It is possible that there is smoldering regime reached when there are lower oxygen concentrations (< ~ 3%) (Hurt and Mitchell, 1992; Yi et al., 2001; Fang et al., 2009).

Table 7-7 Pre-exponential factors determined for the 1st-order model

Coal	**E* (kJ/mol)**	**A (g cm^{-2} s^{-1} atm_{O2}^{-1})** (2 conditions)	**A (g cm^{-2} s^{-1} atm_{O2}^{-1})** (1500 K data)	**A (g cm^{-2} s^{-1} atm_{O2}^{-1})** (1700 K data)
Coal D	100	284	319	85
Coal E	100	189	215	100
Coal F	100	111		
Coal A	95	89		
Coal B	95	100		
Coal C	95	64		

*Assumed from correlation by Hurt and Mitchell (1992)

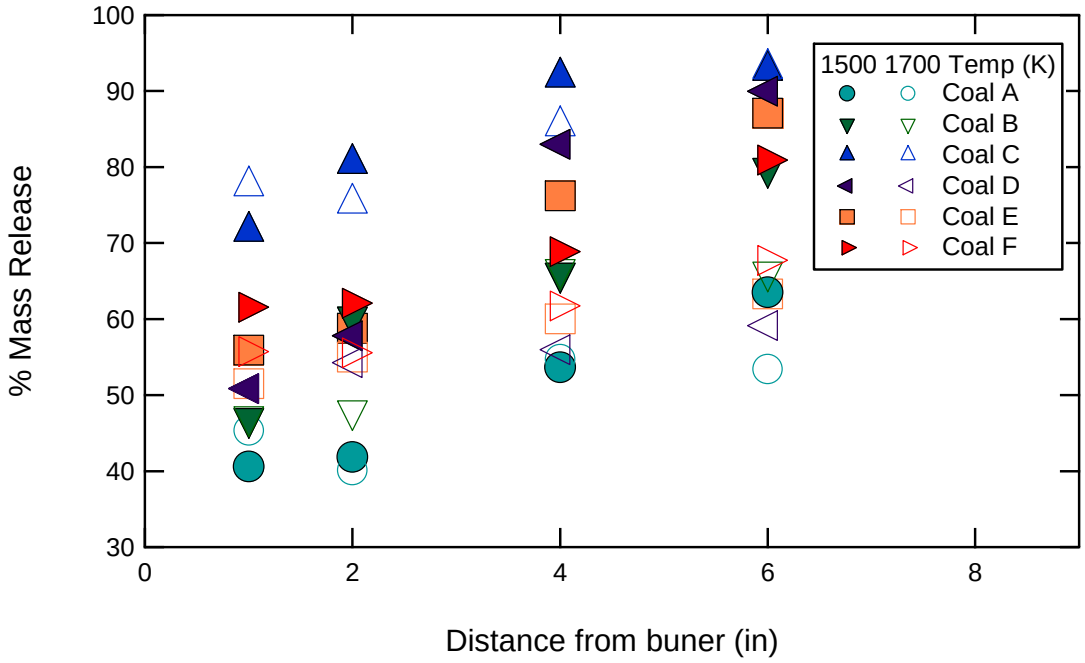

Figure 7-12 Mass release during char oxidation experiments for the suite of coals

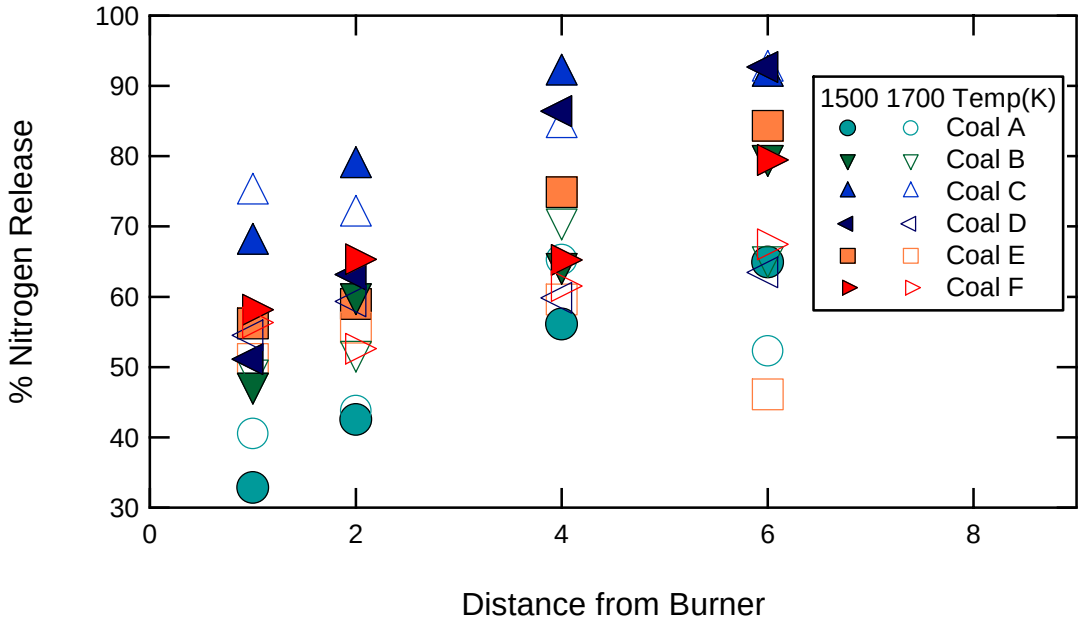

Figure 7-13 Nitrogen release during char oxidation experiments for the suite of coals

7.3.2 C/H and C/N Ratios From Char Oxidation Experiments

The carbon to nitrogen and carbon to hydrogen ratios for the coal combustion experiments are shown in Figure 7-14 and Figure 7-15, and the complete data set is tabulated in Appendix G. The values in these figures were normalized by the C/N or C/H ratios in the parent coal. These data clearly show that the C/N ratios stay roughly constant during char oxidation in the FFB, while the C/H ratio increases steadily. This means that the hydrogen is preferentially burned during char oxidation, leaving the more unreactive carbon in the char. Another way of thinking of this is that the char is becoming more graphitic as it burns, with less peripheral hydrogen (but the same ratio of nitrogen in the aromatic ring structures). The fact that the C/H data in the 1700 K condition shows increased hydrogen release than in the 1500 K case seems to confirm that the temperature was indeed higher in the 1700 K condition. This seems to rule out errors in temperature measurement as an explanation is sought for why the char burnout is less in the 1700 K condition than in the 1500 K condition. This same phenomenon was seen in the char oxidation experiments discussed in Chapter 6.

The 1700 K char oxidation data have lower burnouts than the 1500 K char oxidation data, albeit with a smaller mole fraction of O_2. The first-order model cannot explain a lower burnout level at the 1700 K gas condition. The method chosen to determine kinetic coefficients was to use the data from the 1500 K gas condition with an activation energy taken from the literature.

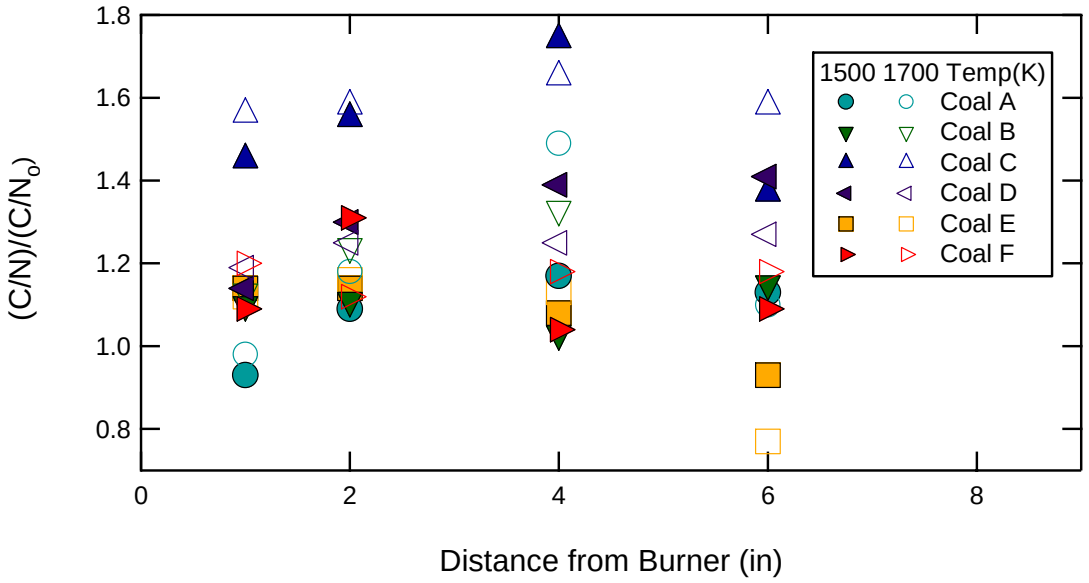

Figure 7-14 C/N ratios for char oxidation experiments

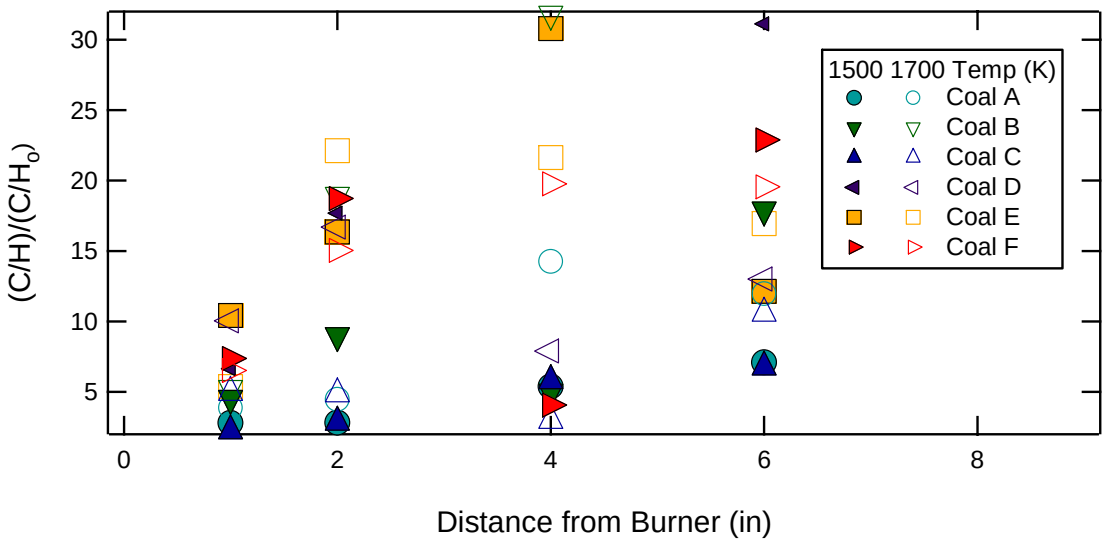

Figure 7-15 C/H ratios for char oxidation experiments

7.3.3 Changes in Diameter and Density During Char Oxidation

The density ratios and resulting diameter ratios for the char oxidation experiments are shown in Figure 7-16 and Figure 7-17 and tabulated in Appendix G. A few points like the ρ/ρ_0 for Coal E at 6 inches may be errant data. Overall, the diameter and density

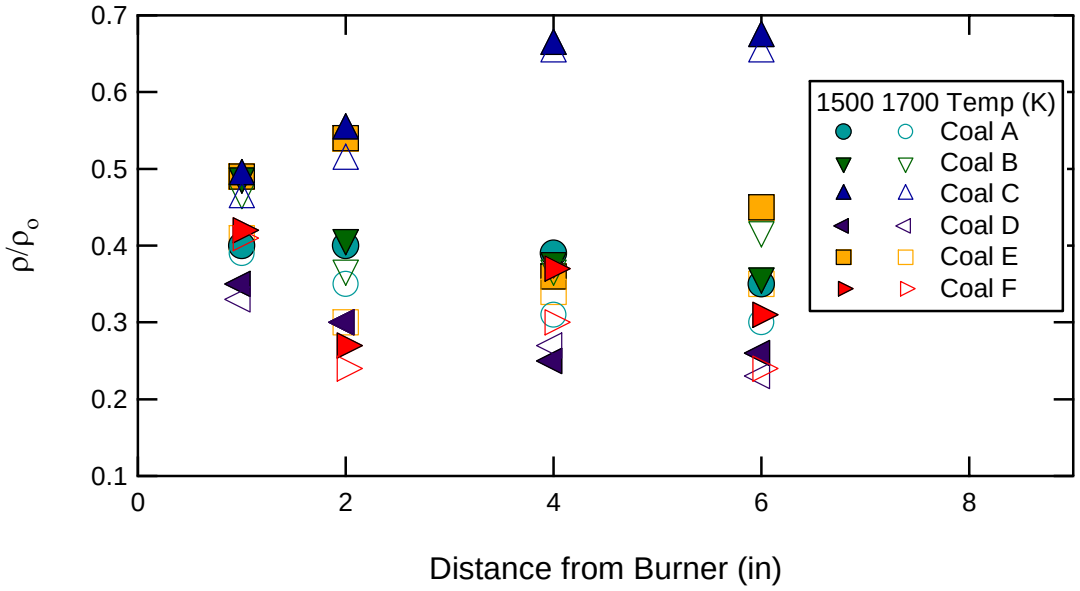

Figure 7-16 Char to coal density ratios for char oxidation experiments

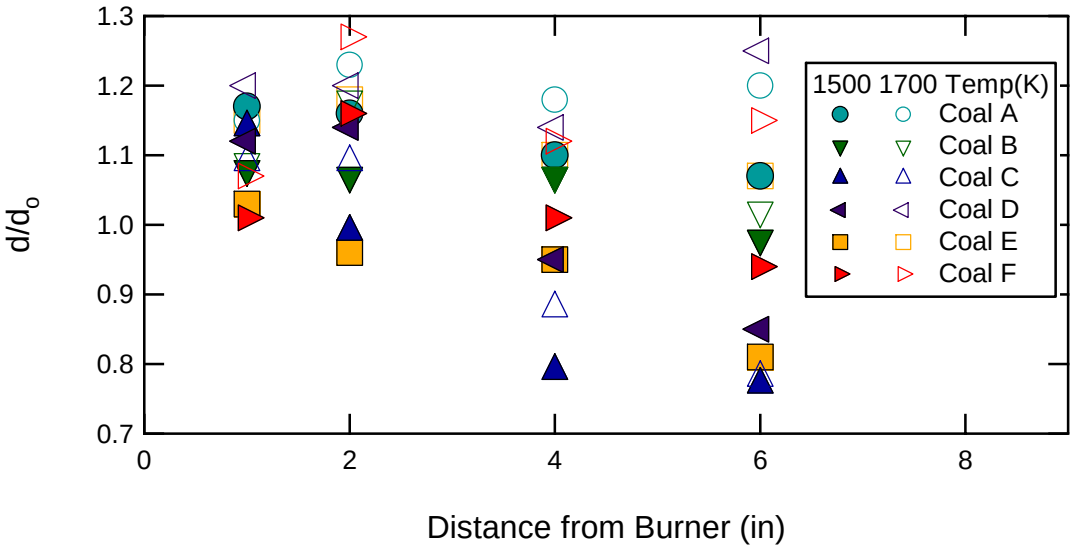

Figure 7-17 Char to coal diameter ratios for char oxidation experiments

ratios decreased during combustion for both bituminous coals, as expected. This means that the char is burning in neither constant diameter nor constant density mode, but a

combination mode where both diameter and density are changing. The diameter also decreases for Coal C, but the density ratio increases slightly. This is because of the high degree of burnout, so that the ash content becomes appreciable and contributes to the density increase when less organic material is present.

7.3.4 Conclusions

Pyrolysis FFB burner experiments conducted at a peak gas temperature of 1300 K indicated that both HCN and NH_3 were released from all coals tested except coal D, which had no measured NH_3 release. All coals had a ratio of HCN to NH_3 greater than 1 except for the coal B, which had a ratio of 0.15. Measured HCN and NH_3 concentrations were higher than previous experiments conducted by Zhang (2001) which could be due to a modified FT-IR setup. All pyrolysis data showed reasonable agreement with predictions from the CPD code. More work is needed to determine how nitrogen evolves from coal during pyrolysis, especially at industrially applicable high heating rates like in the present experiments. Char oxidation experiments were fit to a first-order model. Reactivities of Coals D & E were higher than the other coals tested. Post flame oxygen content differences between the two experiments caused higher temperature runs to exhibit less mass release. This can be explained by a smoldering combustion with the O_2 content present in the 1700 K temperature conditions. More advanced models such as the CBK may obtain more rigorous results.

8 Conclusions

8.1 Oxyfuel Combustion

Pyrolysis experiments were performed in a flat-flame burner using either N_2 (air-fired) or CO_2 (oxy-fired) as the background gas. Conclusions from these experiments are as follows:

1. Mass and nitrogen release of bituminous coals showed no statistical difference between air-fired and oxy-fired conditions during pyrolysis between 1600 and 1900 K.
2. A sub-bituminous coal showed an increase in both mass and nitrogen release in the oxy-fired condition for the same temperature range. However, with increased residence time in the air-fired condition the mass and nitrogen release become roughly equivalent to oxy-fuel conditions. Early char gasification or gas property differences are likely causes of the difference in mass release between the oxy-fired and air-fired condition.
3. Three versions of the CPD code were used to model the experiments (the traditional CPD in a nitrogen environment, a version modified to be in a CO_2 environment and a version previously modified for CO_2 to run in Matlab). The agreement of final volatiles yield was good between the codes and the

experimental results for the bituminous coals. For the sub-bituminous coal, the effect of the Oxy-fuel environments was not captured by any version of the code, which could be an indication of some early char gasification.

8.2 Combustion Enhance Through a Chemical Additive

A series of pyrolysis and combustion experiments were conducted in a flat-flame burner with three coals: (1) untreated Kentucky #9 coal, (2) a moderately treated coal (CC2), and a highly treated coal (CF2). Conclusions from these experiments are as follows:

1. The chemical additive increased pyrolysis yield between 35 and 49% on a relative basis.
2. Both the tar and light gas yields were higher for the treated coals in this set of experiments. The nitrogen release followed the same trend with treatment severity as the volatiles release.
3. Some of the increased yield in volatiles was modeled by the CPD model based on the changes in the composition of the parent treated coals.
4. There was evidence for decreased particle swelling during pyrolysis of the treated coals as well.
5. Char oxidation data from two temperature conditions were fit with a first-order oxidation model to show differences in reactivity. Reactivity decreased for the lighter treatment by 5%, but increased by 34 % for the heavier treatment of the additive.

8.3 Coal Nitrogen Release Data

A suite of 5 bituminous coals and 1 sub-bituminous coal was tested for nitrogen release in the Flat Flame Burner (FFB). Gas phase nitrogen species were measured using an FT-IR. Conclusions from these experiments are as follows:

1. Measured nitrogen balances for three coals at a 1300 K peak temperature condition showed balances above 85% which is good for an entrained flow reactor.
2. Ratios of HCN to NH_3 observed during pyrolysis of all coals were greater than 1, except for one bituminous coal, indicating that HCN is the dominant product of pyrolysis at 1300 K. Measured HCN and NH_3 concentrations were higher than in Zhang's study in the same system at a similar peak temperature. Zhang's data showed a sharp rise in HCN concentration above 1450 K. This study shows greater HCN release at a lower temperature (1300 K).
3. Char oxidation experiments were conducted and coals were fit to a first order model. The three of the coals were fit using an activation energy of 95 kJ/mol, while the other three were fit using an activation energy of 100 kJ/mol. Reactivities in general were higher for the second year coals.

9 Recommendations

1. More experiments are needed with the Oxy-fuel settings to determine whether there would be more mass and nitrogen release with more residence time for sub-bituminous coals.
2. Characterize the radial temperature gradients and feeding system preheating in flat flame burner to have a more precise temperature profile input in the CPD code. This would negate the need to use an apparent density 0.7 gm/cm^3 as a correction factor, instead inputting the measured apparent density.
3. Study the additive effects by having a 1700 K case that has 6 mole% post flame O_2 content. Run another coal to verify the effects.
4. Collect more HCN to NH_3 ratios at different temperatures to determine a more detailed explanation of secondary pyrolysis products, which could be included in a model.
5. Use an nth order model such as the CBK-8 or a more complex model such as the CBK-E to quantify the effects of char oxidation experiments.

10 References

Aarna, I. and E. M. Suuberg, "A Review of the Kinetics of the Nitric Oxide-Carbon Reaction," *Fuel,*(76), 475-491 (1997).

Bahlawane, N., U. Struckmeier, T. S. Kasper, and P. Oßwald, "Noncatalytic thermocouple coatings produced with chemical vapor deposition for flame temperature measurements," *Review of Scientific Instruments,* **78** (2007).

Blair, D. W., J. O. L. Wendt and W. Bartok, "Evolution of Nitrogen and Other Species during Controlled Pyrolysis of Coal," *16th International Symposium on Combustion*, 475-489 (1976).

Borrego, A. G. and D. Alvarez, "Comparison of Chars Obtained under Oxy-Fuel and Conventional Pulverized Coal Combustion Atmospheres," *Energy and Fuels,* **21**(6), 3171-3179 (2007).

Buhre, B. J. P., L. K. Elliot, C. D. Sheng, R. P. Gupta and T. F. Wall, "Oxy-fuel Combustion Technology for Coal-Fired Power Generation," *Progress in Energy and Combustion Science,* **31**, 283-307 (2005).

Châtel-Pélage, F., P. Pranda, N. Perrin, H. Farzan and S. T. Vecci, "Oxygen-Enrichment for NO_x Control in Coal-fired Utility Boilers," The 29th Technical Conference on Coal Utilization & Fuel Systems, Clearwater, FL(2004).

Claus, R. W., "Chemical Equilibrium with Applications," NASA, **2009** (2008).

Fang, H., N. Zobel, W. Zha and F. Behrendt, "Effects of physical properties on one-dimensional downward smoldering of char: Numerical analysis.," *Biomass and Bioenergy,* **33**, 1019-1029 (2009).

Fletcher, T., "Burner Centerline Velocity Profile," http://www.et.byu.edu/~tom/cpd/cpdcpnlg/cpdcp_velocity.dat (1988).

Fletcher, T., "Time-Resolved Temperature Measurements of Individual Coal Particles During Devolatilization " *Combustion Science and Technology,* **63**, 89-105 (1989).

Fletcher, T. H., A. R. Kerstein, R. J. Pugmire and D. M. Grant, "Chemical Percolation Model for Devolatilization: II. Temperature and Heating Rate Effects on Product Yields," *Energy and Fuels,* **4**(54) (1990).

Fletcher, T. H. and D. R. Hardesty, "Compilation of Sandia coal devolatilization data: Milestone report," Medium: X; Size: Pages: (346 p) (1992).

Fletcher, T. H., A. R. Kerstein, R. J. Pugmire, M. S. Solum, and D. M. Grant, "A Chemical Percolation Model for Devolatilization: 3. Chemical Structure as a Function of Coal Type," *Energy and Fuels,* **6** (1992).

Fristrom, R. M., Flame Structure and Processes, New York, Oxford University Press (1995).

Gale, T. K., C. H. Bartholomew and T. H. Fletcher, "Decreases in the Swelling and Porosity of Bituminous Coals During Devolatilization at High Heating Rates," *Combustion and Flame,* **100**, 94-100 (1995).

Genetti, D., "An Advanced Model of Coal Devolatilization Based on Chemical Structure," Masters, Chemical Engineering, Brigham Young University (1999).

Glarborg, P., A. D. Jensen and J. E. Johnsson, "Fuel Nitrogen Conversion in Solid Fuel Fired Systems," *Progress in Energy and Combustion Science,* **29**(2), 89-113 (2003).

Himmelblau, D. M., Basic principles and calculations in chemical engineering Upper Saddle River, NJ, Prentice-Hall (2004).

Holman, J. P., Heat Transfer, San Francisco, McGraw-Hill (1976).

Hurt, R., J. K. Sun and M. Lunden, "A Kinetic Model of Carbon Burnout in Pulverized Coal Combustion," *Combustion and Flame,* **113**, 181-197 (1998).

Hurt, R. H. and R. E. Mitchell, "Unified High Temperature Char Combustion Kinetics for a Suite of Coals of Various Rank," *24th Symposium (International) on Combustion*, 1243-1250 (1992).

Kelemen, S. R., M. L. Gorbaty and P. J. Kwiatek, "Quantification of Nitrogen Forms in Argonne Premium Coals," *Energy and Fuels,* **8**(4), 896-906 (1994).

Ledesma, E. B., C. Z. Li, P. F. Nelson and J. C. Mackie, "Release of HCN, NH3, and HNCO from the thermal gas-phase cracking of coal pyrolysis tars," *Energy and Fuels,* **12**, 536-541 (1998).

Ma, J., "Soot Formation during Coal Pyrolysis," PhD Dissertation, Chemical Engineering, Brigham Young University (1996).

Mackrory, A., "A Mechanistic Investigation of Nitrogen Evolution in Pulverized Coal Oxy-fuel Combustion," PhD Dissertation, Mechanical Engineering, Brigham Young University (2008).

Madsen, M., Theby, E.A., "SiO2 Coated Thermocouples," *Combustion Science and Technology,* **36**, 205-209 (1984).

Molina, A. and C. R. Shaddix, "Ignition and devolatilization of pulverized bituminous coal particles during oxygen/carbon dioxide coal combustion," *Proceedings of the Combustion Institute,* **31**, 1905-1912 (2007).

Murphy, J. J. and C. R. Shaddix, "Combustion Kinetics of Coal Chars in Oxygen-Enriched Environments," *Combustion and Flame,* **144**, 710-729 (2006).

Niksa, S. and A. R. Kerstein, "FLASHCHAIN theory for rapid coal devolatilization kinetics. 1. Formulation," *Energy and Fuels,* **5**(5), 647-665 (1991).

Ninomiya, Y., Q. Wang, S. Xu, K. Mizuno and I. Awaya, "Effect of Additives on the Reduction of PM2.5 Emissions during Pulverized Coal Combustion," *Energy and Fuels,* **23**, 3412-3417 (2009).

Oehr, K. H. and F. Z. Yao, "Method and Product for Improved Fossil Fuel Combustion," United States (2000).

Ohtsuka, Y., T. Watanabe, K. Asami and H. Mori, "Char-Nitrogen Functionality and Interactions between the Nitrogen and Iron-Catalyzed Conversion Process of Coal Nitrogen to N2," *Energy and Fuels,* **12**, 1356-1362 (1998).

Perry, S., "A Global Free-Radical Mechanism for Nitrogen Release during Coal Devolatilization Based on Chemical Structure," PhD Dissertation, Chemical Engineering, Brigham Young University (1999).

Pickett, B., "Effects of Moisture on Combustion of Live Wildland Forest Fuels," PhD Dissertation, Chemical Engineering, Brigham Young University (2008).

Pohl, J. H. and A. F. Sarofim, "Devolatilization and Oxidation of Coal Nitrogen," *16th International Symposium on Combustion*, 491-501 (1976).

Put, B., "Gold in Fly Ash," Energy**:** 25-28 (2000).

Smith, K. L., L. D. Smoot, T. H. Fletcher and R. J. Pugmire, The Structure and Reaction Processes of Coal, New York, Plenum Press (1994).

Solomon, P. R. and M. B. Colket, "Evolution of Fuel Nitrogen in Coal Devolatilization," *Fuel,* **57**(12) (1978).

Solomon, P. R., D. G. Hamblen, M. A. Serio, Z.-Z. Yu and S. Charpenay, "A characterization method and model for predicting coal conversion behaviour," *Fuel,* **72**(4), 469-488 (1993).

Spinti, J. P. and D. W. Pershing, "The Fate of Char-N at Pulverized Coal Conditions," *Combustion and Flame,* **135**(3), 299-313 (2003).

Tsubouchi, N., Y. Oshima, C. Xu and Y. Ohtsuka, "Enhancement of N2 formation from the nitrogen in carbon and coal by calcium," *Energy and Fuels,* **15**, 158-162 (2000).

Tsubouchi, N. and Y. Ohtsuka, "Nitrogen Release during High Temperature Pyrolysis of Coals and Catalytic Role of Calcium in N_2 Formation," *Fuel,* **81**, 2335-2342 (2002).

Tsubouchi, N. and Y. Ohtsuka, "Nitrogen Chemistry in Coal Pyrolysis: Catalytic Roles of Metal Cations in Secondary Reactions of Volatile Nitrogen and Char Nitrogen," *Fuel Processing Technology,* **89**, 379-390 (2008).

Wakai, K., Shimizu,S., Takahashi, H., Ohta, Y., Tahiguchi, H., "Correction of Radiation Heat Loss from Thermocouple," *Journal of Gas Turbine Society,* **7**(27), 33-38 (1979).

Weijuan, Y. Z. J., L. Maosheng, Z. Zhijun, L. Jianzhong and C. Kefa, "Combustion Process and Nitrogen Oxides Emission of Shenmu Coal Added with Sodium Acetate," *Energy and Fuels,* **21**(5), 2548-2554 (2007).

Williams, T. C. and C. R. Shaddix, "Contamination of Carbon Monoxide with Metal Carbonyls: Implications for Combustion Research," *Combustion Science and Technology,* **179**, 1225-1230 (2007).

Wu, Z., Y. Sugimoto and H. Kawashima, "Catalytic nitrogen release during a fixed-bed pyrolysis of model coals containing pyrrolic or pyridinic nitrogen," *Fuel,* **80**, 251-254 (2001).

Xu, W. C. and A. Tomita, "Effect of coal type on coal flash pyrolysis products," *Fuel,* **66**, 626-632 (1987).

Yi, S.-C., E.-S. Song and M. R. Hajaligol, "Mathematical model of smoldering combustion in a carbonaceous porous medium. Part 1 - Development of pyrolysis and combustion models for a cylindrical geometry.," *Journal of Fire Sciences,* **19**(6), 429-448 (2001).

Zeng, D., "Effects of Pressure on Coal Pyrolysis at High Heating Rate and Char Combustion," PhD Dissertation, Chemical Engineering, Brigham Young University (2005).

Zhang, H., "Nitrogen Evolution and Soot Formation during Secondary Pyrolysis," PhD Dissertation, Chemical Engineering, Brigham Young University (2001).

Zhang, H. and T. Fletcher, "Nitrogen Transformations during Secondary Coal Pyrolysis," *Energy and Fuels*, **15**, 1512-1522 (2001).

Appendix A. Gas Temperature Correction for Radiation

A spreadsheet was developed by Randy Shurtz to correct the measured gas temperature for radiation. This appendix summarizes the theory behind the equations used in the spreadsheet. The underlying assumption has to do with an energy balance around the bead where:

$$q_{radiation} = q_{convection} \tag{A-1}$$

$$A_b\sigma\varepsilon(T_b^4 - T_w^4) = hA_b(T_g - T_b) \tag{A-2}$$

$$T_g = T_b + \frac{\sigma\varepsilon(T_b^4 - T_w^4)}{h} \tag{A-3}$$

where h is the convective heat transfer coefficient, σ is the Stefan-Boltzmann constant, ε is the thermocouple bead emissivity, T_w is the wall temperature which is assumed to be 500 K for the Flat Flame Burner (FFB) system, T_b is the measured thermocouple bead temperature, and T_g is the actual gas temperature. The convective heating coefficient can be calculated the Nusselt number:

$$h = Nu(T_f)\frac{k_f(T_f)}{D_b} \tag{A-4}$$

where Nu is the Nusselt number, T_f is the film temperature in the boundary layer, k_f is the thermal conductivity of the gas evaluated at the film temperature, and D_b is the bead diameter. The thermal conductivity was found using the mole fractions of each gas

species and thermal conductivity as a function of film temperature from JANAF data using the Gordon-McBride database of curve fits. A value of 0.6 mm was measured bead diameter for the thermocouple used in these experiments. There are no Nusselt number correlations that accurately describe the physical parameters of the FFB, but two are close. These are the falling drop in a quiescent fluid and a general sphere correlation which were used by previous BYU researchers (Perry, 1999; Zhang, 2001; Zeng, 2005). The sphere correlation has a lower limit for Reynolds number of 3.5 while the falling drop is not entirely realistic for a thermocouple bead. However, the difference found between them is small, usually within 20 K for the temperatures used in this study. For this study, the drop correlation was used. Both equations are shown below in addition to equations for the Reynolds and Prandtl numbers:

$$Nu(T_f) = 2.0 + 0.6 \cdot Re(T_f)^{1/2} \cdot \mathrm{Pr}(T_f)^{1/3} \tag{A-5}$$

$$Nu(T_f) = 2 + \left(0.4Re(T_f)^{1/2} + 0.6Re(T_f)^{2/3}\right)\left(\mathrm{Pr}(T_f)^{0.4}\right)\left(\frac{\mu(T_f)}{\Phi(T_f)}\right)^{0.25} \tag{A-6}$$

$$Re(T_f) = \frac{D_b \cdot v_\infty \cdot \rho_f(T_f)}{\mu_f(T_f)} \tag{A-7}$$

$$\mathrm{Pr}(T_f) = \frac{C_p(T_f) \cdot \mu_f(T_f)}{k_f(T_f)} \tag{A-7}$$

where υ_∞ is the terminal velocity of the flowing gas, ρ is the density, C_p is heat capacity and μ is the viscosity. Terminal velocity was calculated using conservation of mass and measured gas temperature, while density was estimated assuming ideal gas behavior. Viscosities and heat capacities are calculated using calculated gas mole fractions and correlations from the DIPPR database. The gas temperature is calculated iteratively

using the secant method for the energy balance to converge on a T_g. Corrected profiles can be found in Appendix B and Appendix D.

Appendix B. Gas Temperature Profiles

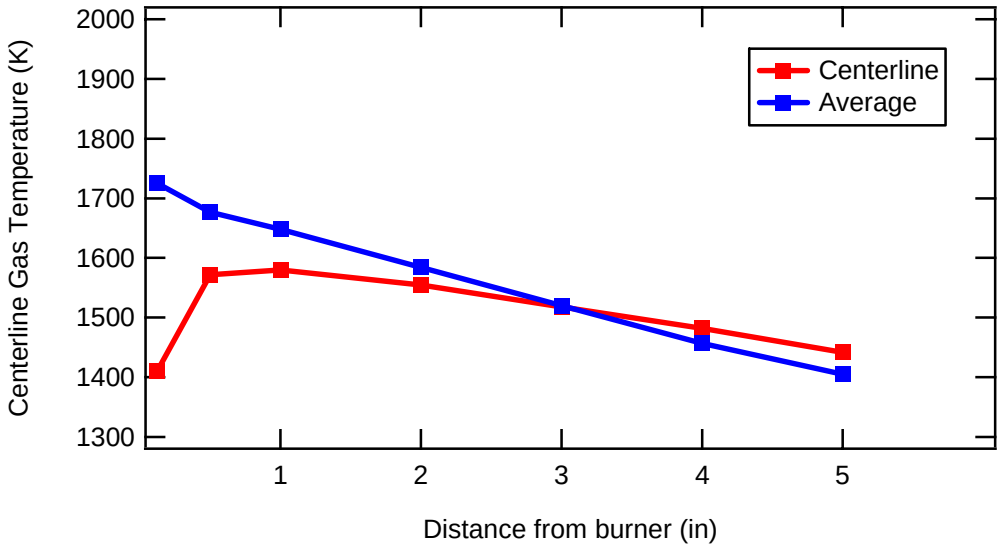

Figure B-1 Vertical gas temperature profiles for the 1600 K Oxy-fuel conditions in the FFB

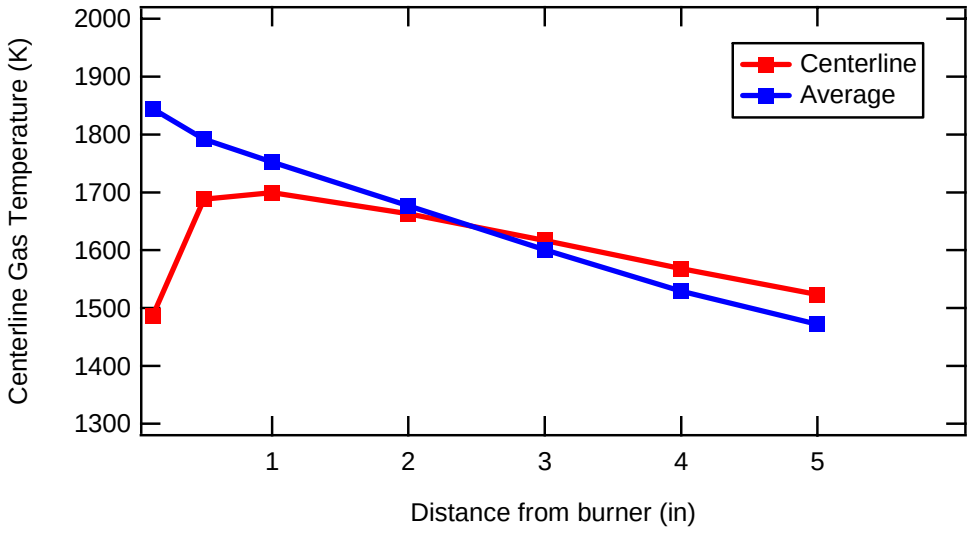

Figure B-2 Vertical gas temperature profiles for the 1700 K Oxy-fuel conditions in the FFB

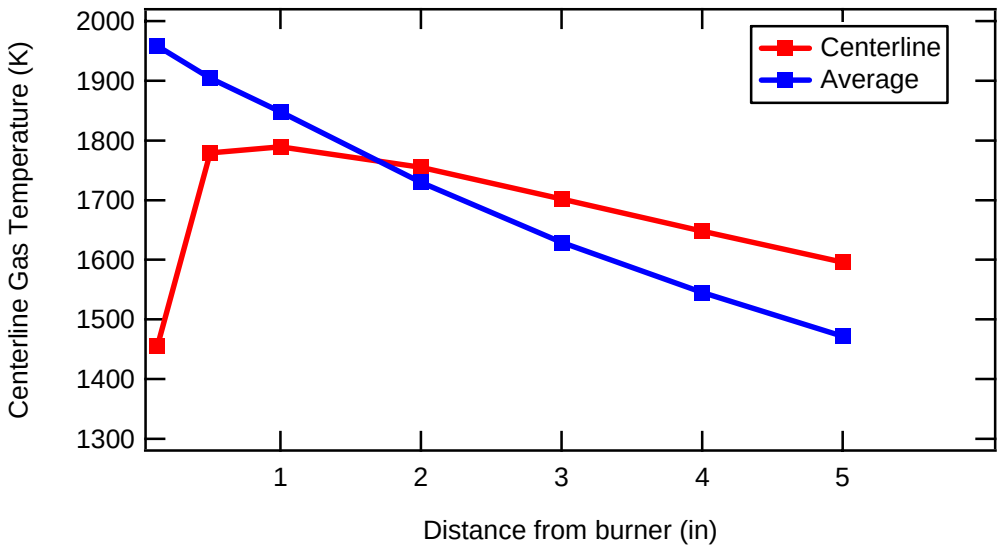

Figure B-3 Vertical gas temperature profiles for the 1800 K Oxy-fuel pyrolysis condition in the FFB

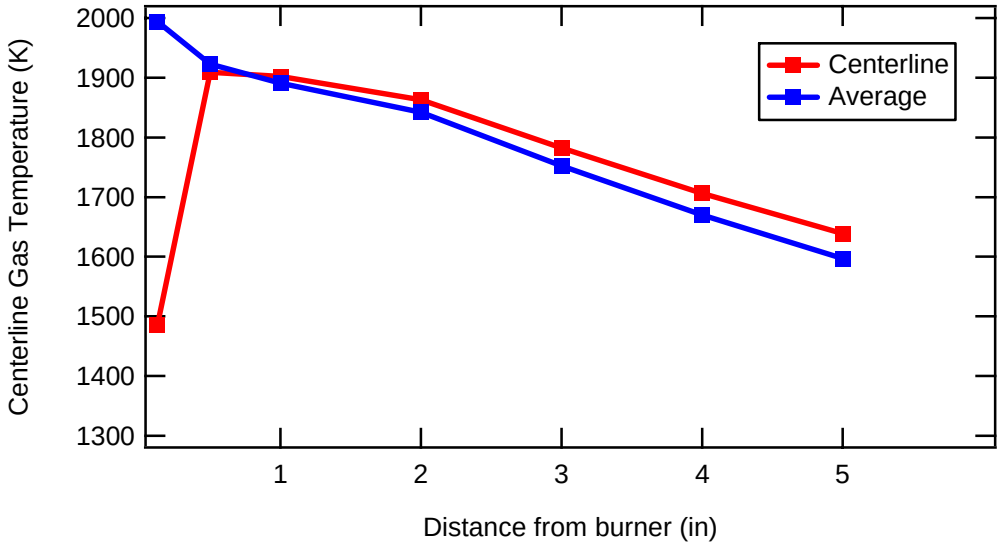

Figure B-4 Vertical gas temperature profiles for the 1900 K Oxy-fuel pyrolysis condition in the FFB

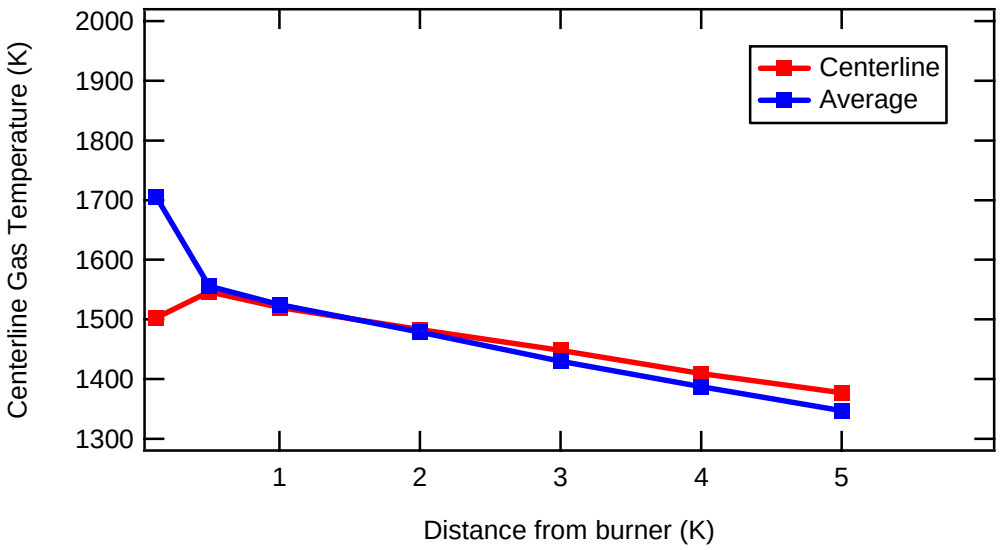

Figure B-5 Vertical gas temperature profiles for the 1600 K air simulated pyrolysis condition in the FFB

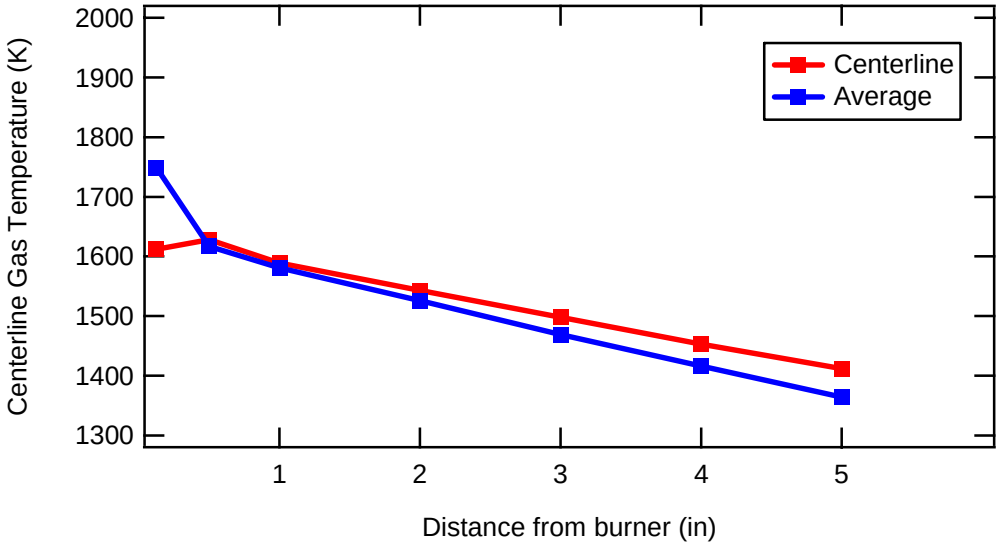

Figure B-6 Vertical gas temperature profiles for the 1700 K air simulated pyrolysis condition in the FFB

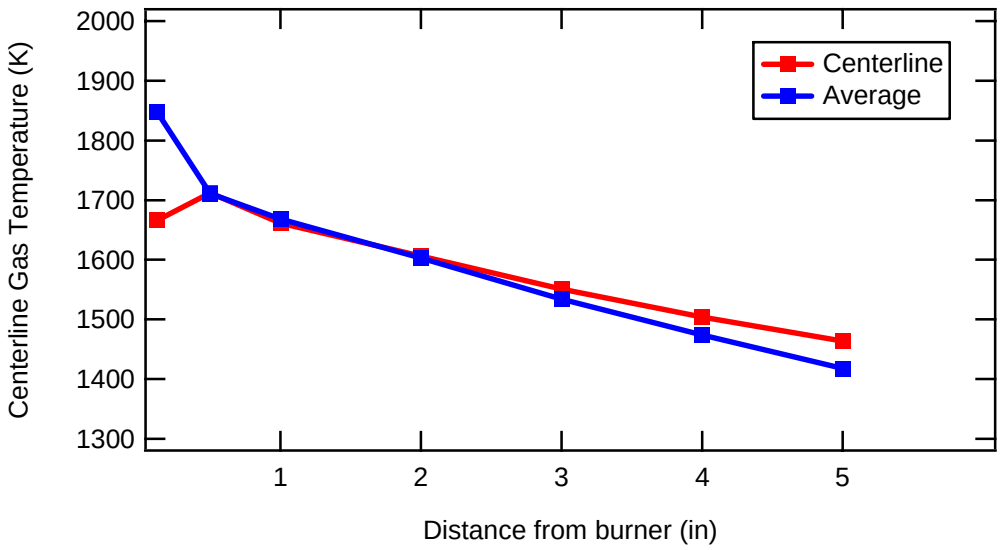

Figure B-7 Vertical gas temperature profiles for the 1800 K air simulated pyrolysis condition in the FFB

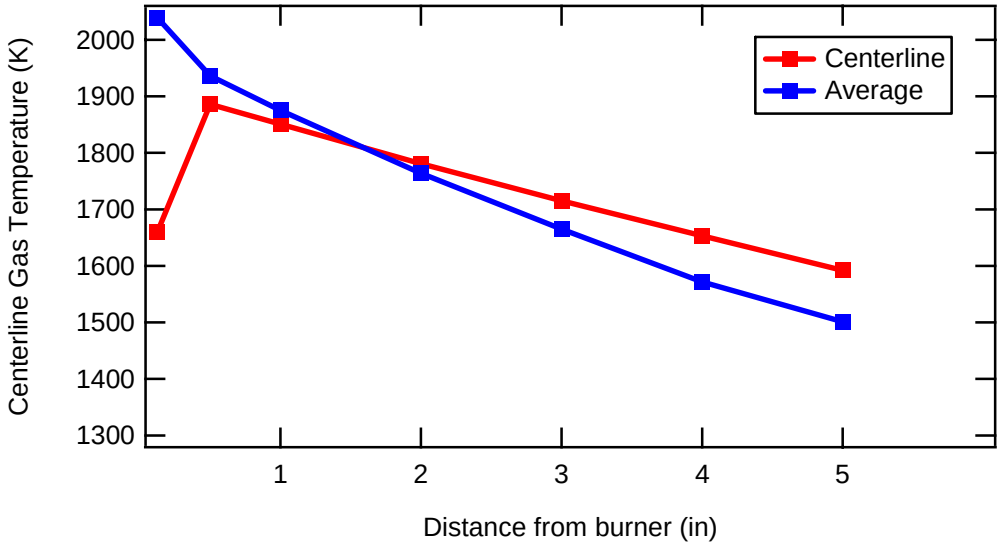

Figure B-8 Vertical gas temperature profiles for the 1900 K air simulated pyrolysis condition in the FFB

Appendix C. Oxyfuel Coal and Char Data

Table C-1 Ultimate analysis for Ill #6 coal and chars in CO_2 at 1 inch on a dry ash-free (daf) basis

	wt% daf	C	H	N	O (diff)	S
Ill. #6	**Coal**	75.08	5.55	1.28	15.33	2.77
	1600 K	88.61	2.52	1.38	5.87	1.61
	1700 K	91.41	1.74	1.39	3.84	1.62
	1800 K	87.77	2.51	1.43	6.83	1.46
	1800b K	82.12	3.39	1.3	11.74	1.45
	1900 K	94.17	1.31	1.3	1.57	1.66
Pitt. #8	**Coal**	81.6	5.79	1.33	7.23	4.05
	1600 K	91.94	2.21	1.37	0.9	3.59
	1700 K	87.68	1.97	1.37	5.02	3.96
	1800 K	87.91	5.24	1.3	2.72	2.83
	1900 K	95.15	0.93	1.31	-0.17	2.78
BT CO_2	**Coal**	71.19	5.3	1.02	21.91	0.58
	1600 K	88.96	1.54	1.13	8.06	0.31
	1700 K	92.34	1.4	1.2	4.74	0.33
	1800 K	86.93	2.16	1.19	9.34	0.39
	1900 K	86.75	2	1.2	9.69	0.36
	1900b K	90.85	1.6	1.26	5.83	0.46
BT N_2-1	**Coal**	71.19	5.3	1.02	21.91	0.58
	1600 K	88.96	1.54	1.13	8.06	0.31
	1700 K	92.34	1.4	1.2	4.74	0.33
	1800 K	86.93	2.16	1.19	9.34	0.39
	1900 K	86.75	2	1.2	9.69	0.36
BT N_2-2	**Coal**	71.19	5.3	1.02	21.91	0.58
	1600 K	83.3	2.7	1.46	12.12	0.42
	1700 K	85.38	2.43	1.7	10.01	0.47
	1800 K	88.53	1.67	1.4	7.93	0.46
	1900 K	89.99	1.24	1.62	6.72	0.43

Table C-2 Mass release and nitrogen release data from Oxy-fuel experiments

		Mass Release (dry-ash free)						
	Temp (K)	Ash Tracer	Ti Tracer	Si Tracer	Al Tracer	MR Average	St. Dev.	Nitrogen Release
Ill. # 6	1600	49.65%	55.57%	54.99%	59.43%	56.66%	2.40%	53.00%
	1700	53.30%	61.13%	60.57%	63.43%	61.71%	1.50%	58.32%
	1800	50.37%	56.59%	56.21%	59.43%	57.41%	1.80%	52.32%
	1800b	47.13%	56.59%	56.21%	59.43%	57.41%	1.80%	56.70%
	1900	58.59%	64.23%	61.17%	66.82%	64.07%	2.80%	63.49%
Pitt. # 8	1600	60.94%	61.56%	60.58%	61.72%	61.29%	0.60%	60.20%
	1700	58.54%	60.22%	60.05%	60.08%	60.12%	0.10%	59.03%
	1800	48.51%	59.05%	57.28%	59.22%	58.51%	1.10%	59.50%
	1900	53.20%	61.78%	61.21%	62.50%	61.83%	0.60%	62.41%
BT CO_2	1600	43.23%	61.68%	63.65%	56.83%	60.72%	3.50%	56.59%
	1700	49.64%	61.16%	62.00%	58.53%	60.56%	1.80%	53.75%
	1800	42.03%	71.68%	73.60%	63.87%	69.72%	5.20%	64.84%
	1900	43.28%	61.68%	55.04%	60.62%	61.15%	3.60%	54.31%
	1900b	53.30%	67.12%	66.84%	64.72%	65.92%	1.30%	58.05%
BT N_2-1	1600	51.80%	65.89%	65.68%	64.72%	65.43%	0.60%	55.56%
	1700	49.21%	62.69%	62.00%	64.72%	63.14%	1.40%	54.09%
	1800	51.75%	61.16%	61.13%	60.12%	60.80%	0.60%	54.48%
	1900	60.01%	67.12%	64.69%	64.72%	65.92%	1.40%	59.91%
BT N_2-2	1600	38.23%	50.82%	37.59%	48.76%	49.79%	1.50%	27.18%
	1700	45.98%	55.80%	56.71%	51.95%	53.88%	2.50%	22.19%
	1800	51.10%	57.19%	59.40%	55.91%	56.55%	1.80%	39.59%
	1900	45.57%	56.73%	43.33%	57.82%	57.28%	0.80%	31.56%

Appendix D. Chemical Additive Temperature Profiles

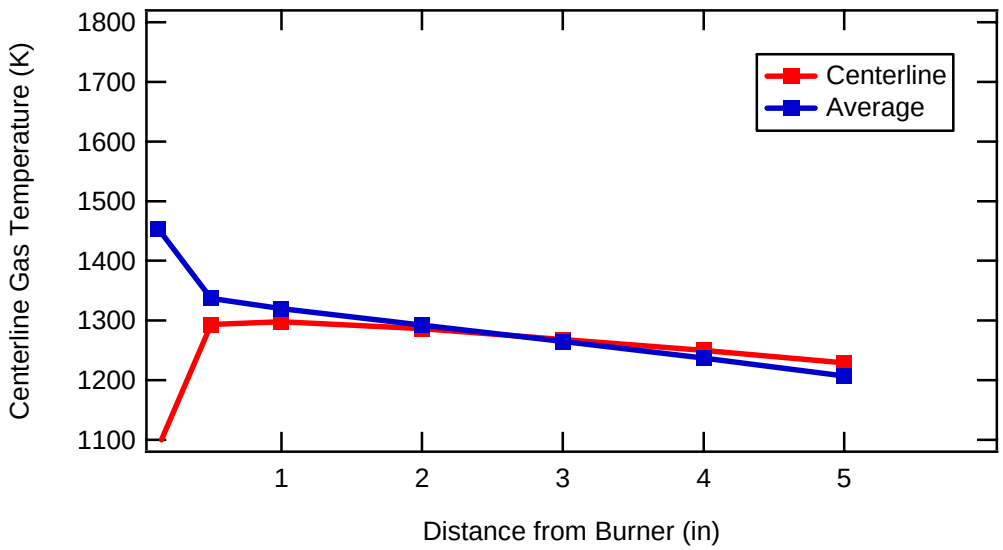

Figure D-1 Vertical gas temperature profile of the 1300 K pyrolysis condition in the FFB

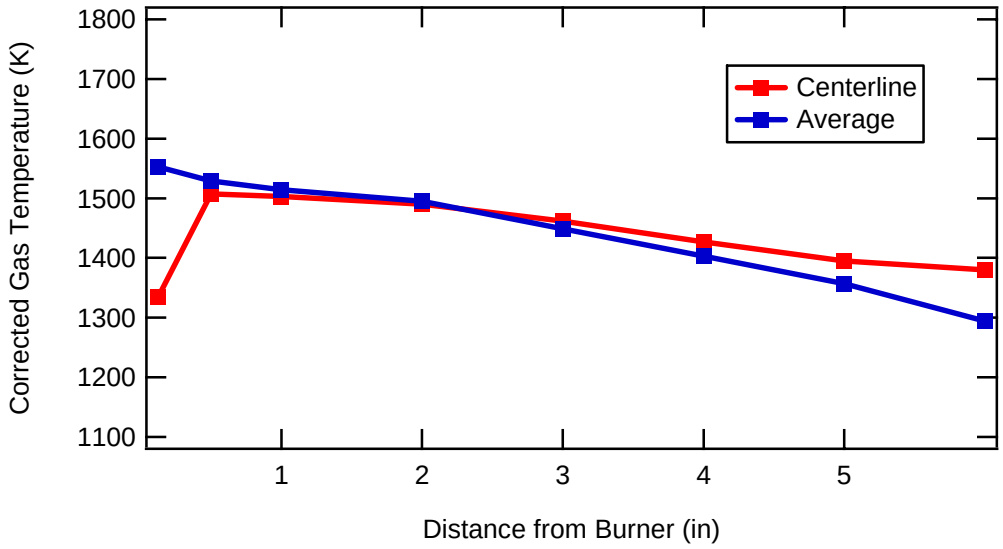

Figure D-2 Vertical gas temperature profile of the 1500 K char oxidation condition in the FFB

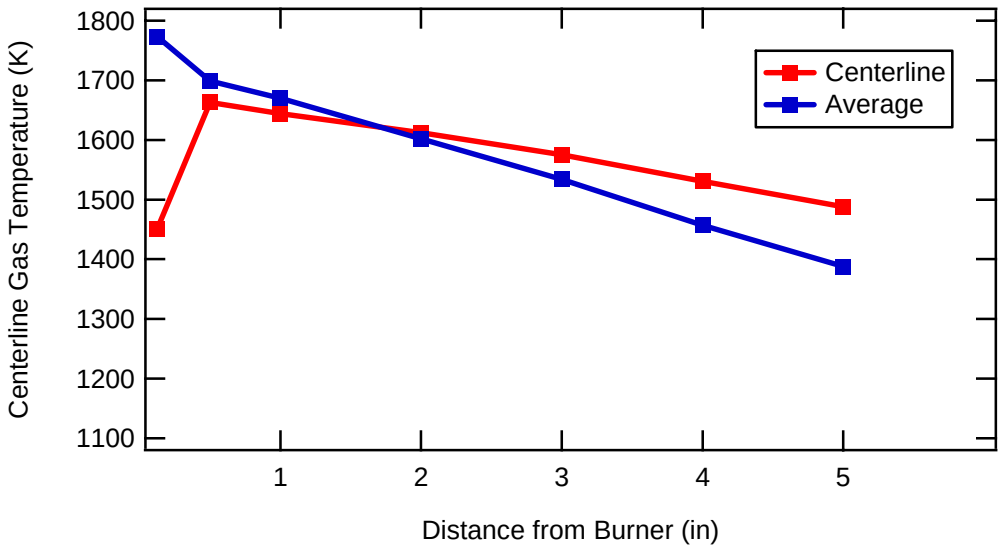

Figure D-3 Vertical gas temperature profile of the 1700 K char oxidation condition in the FFB

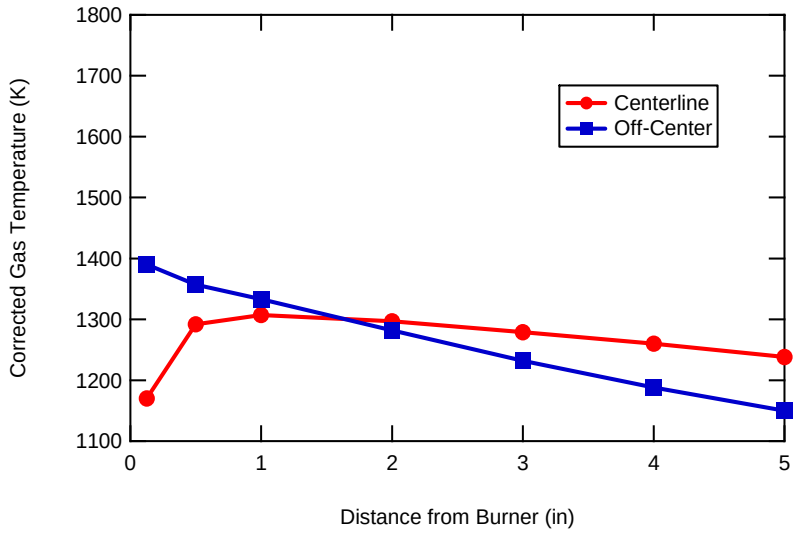

Figure D-4 Vertical gas temperature profiles for the 1300 K pyrolysis condition in the FFB

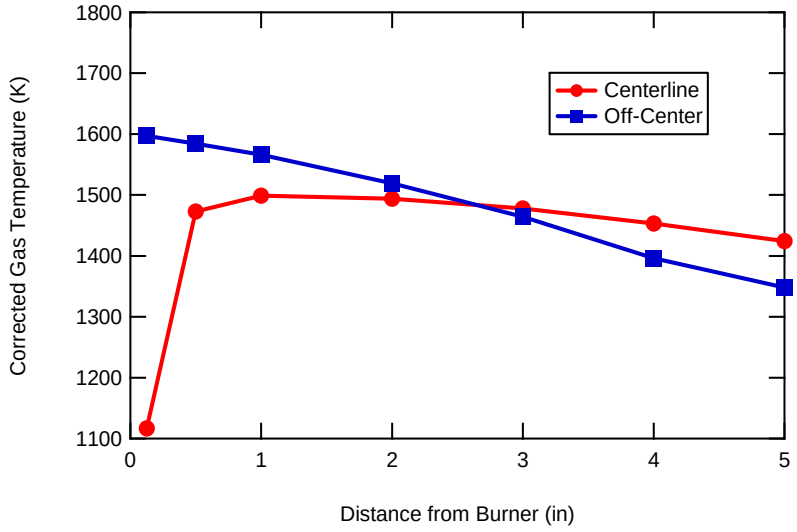

Figure D-5 Vertical gas temperature profile of the 1500 K char oxidation condition in the FFB

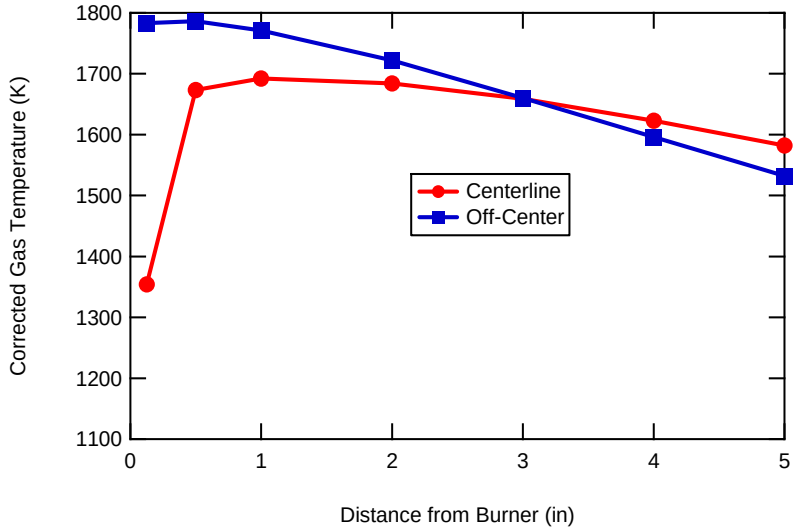

Figure D-6 Vertical gas temperature profile of the 1700 K char oxidation condition in the FFB

Appendix E. Chemical Additive Pyrolysis Results

Table E-1 Ultimate analysis for coal, tar/PAH, and char samples

	Sample	C *	H	N	O (diff)	S
KY	Tar/PAH	90.8	3	1.4	3.4	1.5
	Char	84.48	3.87	1.88	5.81	3.96
	Coal	87.93	5.7	1.68	0.11	4.58
CC2	Tar/PAH	90.6	3.5	1.6	2.6	1.7
	Char	87.53	2.64	2.3	4.91	2.62
	Coal	87.12	5.73	1.66	0.97	4.52
CF2	Tar/PAH	90.5	3.3	1.6	3.1	1.6
	Char	87.05	2.42	2.05	5.98	2.51
	Coal	85.91	5.74	1.64	2.16	4.55

*** All data reported on a dry-ash free basis**

Table E-2 Ash and elemental tracer analysis results

	Kentucky	CC2	CF2
Ash Tracer	40.8%	42.7%	48.4%
Ti Tracer	35.0%	48.1%	51.2%
Si Tracer	33.4%	46.5%	54.3%
Al Tracer	37.7%	51.2%	52.1%
MR Average (not ash)	35.4%	48.6%	52.5%
St. Dev. (not ash)	2.2%	2.4%	1.6%
Nitrogen Release	27.8%	28.8%	40.8%

Appendix F. Coal Additive Char Oxidation Results

Table F-1 Ultimate analyses from char oxidation experiments

Coal	Temp (K)	Height / Sample	C *	H	N	O (by diff)	S	Ash **
KY	1500	1	91.7	1	1.98	2.6	2.7	22.84
		2	94	0.97	1.42	0	3.61	27.1
		4	93.31	0.29	1.26	2.91	2.23	32
		6	91.8	1.3	1.5	2.5	2.9	37.23
	1700	1	91.4	2.2	2.02	1.4	3	21.58
		2	89.78	1.88	1.62	3.76	2.96	20.39
		4	95.69	0.46	1.46	0.04	2.34	22.69
		6	95.4	0.6	1.4	0	2.7	24
		Coal	87.93	5.7	1.68	0.11	4.58	12
CC2	1500	2	95.56	0.65	1.55	0	2.25	23.99
		4	93.99	0.99	1.39	0.02	3.62	31.4
		6	95.6	0.3	1.3	0	2.7	33.3
	1700	2	94.86	0.64	1.55	0.89	2.06	18.48
		4	92.18	0.43	1.45	3.5	2.43	27.26
		6	95.8	0.5	1.3	0	2.4	29.24
		Coal	87.12	5.73	1.66	0.97	4.52	11.4
CF2	1500	2	95.94	0.51	1.39	0	2.17	24.1
		4	94.15	0.42	1.48	1.09	2.86	36.8
		6	96.1	0.4	1.3	0	2.2	45.24
	1700	2	95.02	0.55	1.76	0.9	1.77	16.42
		4	94.83	0.5	1.55	0.75	2.37	27.48
		6	91.2	0.3	1.4	5.1	1.9	22.53
		Coal	85.91	5.74	1.64	2.16	4.55	11.66

* on a dry-ash free basis
** on a dry basis

Table F-2 Sample analysis from 1500 K char oxidation experiments

	Temp (K)	Mass Release (dry-ash free)						
	Height (in)	Ash Tracer	Ti Tracer	Si Tracer	Al Tracer	MR Ave	St. Dev.	Nitrogen Release
KY	1500 - 1	54.99%	56.88%	58.44%	56.61%	57.31%	1.00%	49.71%
	2	64.60%	65.86%	64.79%	64.70%	65.12%	0.60%	70.32%
	4	71.65%	78.86%	79.75%	77.47%	78.69%	1.10%	84.07%
	6	77.27%	83.35%	85.44%	82.35%	83.71%	1.60%	85.79%
	1700 - 1	50.76%	58.94%	60.37%	60.97%	60.09%	1.00%	52.17%
	2	47.46%	58.44%	61.23%	56.61%	58.76%	2.30%	60.32%
	4	54.89%	63.69%	66.65%	64.70%	65.01%	1.50%	69.57%
	6	60.16%	71.36%	72.92%	70.77%	71.68%	1.10%	76.43%
CC2	1500 - 2	60.06%	63.65%	64.15%	64.31%	64.04%	0.30%	66.48%
	4	73.08%	78.65%	78.79%	78.78%	78.74%	0.10%	82.17%
	6	78.52%	82.79%	83.47%	83.18%	83.15%	0.30%	86.95%
	1700 - 2	43.82%	53.48%	57.72%	56.27%	55.82%	2.20%	58.62%
	4	66.26%	69.78%	70.73%	67.52%	69.34%	1.60%	73.15%
	6	70.15%	70.53%	71.40%	67.52%	69.82%	2.00%	75.50%
CF2	1500 - 2	58.42%	60.12%	60.83%	60.23%	60.39%	0.40%	66.38%
	4	77.60%	76.95%	78.61%	75.29%	76.95%	1.70%	79.20%
	6	84.34%	83.88%	83.30%	83.66%	83.61%	0.30%	86.07%
	1700 - 2	33.52%	32.17%	33.82%	41.07%	35.69%	4.70%	30.92%
	4	65.67%	65.20%	64.25%	63.53%	64.33%	0.80%	66.24%
	6	55.52%	58.89%	59.92%	56.47%	58.42%	1.80%	63.77%

*Average of the mass release from the Al, Si, and Ti tracers

Appendix G. Coal Nitrogen Release Data

G.1 Pyrolysis Results

Table G-1 CHNS analysis for coal, tar/PAH, and char

	(wt% daf)	C	H	N	O (diff)	S
Coal A	**Tar/PAH**	89.58	4.37	1.72	3.69	0.64
	Char	82.49	3.75	1.89	10.75	1.13
	Coal	83.59	5.73	1.72	7.66	1.3
Coal B	**Tar/PAH**	92.54	3.17	1.11	2.77	0.41
	Char	89.23	3.48	1.57	4.77	0.96
	Coal	84.44	5.49	1.38	7.71	0.98
Coal C	**Tar/PAH**	87.25	4.53	1.52	6.09	0.61
	Char	85.56	3.23	1.35	9.23	0.63
	Coal	62.26	4.45	1.08	31.52	0.69
Coal D	**Tar/PAH**	91.79	3.22	1.57	2.83	0.59
	Char	95.15	2.09	1.94	0	0.82
	Coal	85.11	5.33	1.75	5.57	2.24
Coal E	**Tar/PAH**	94.79	2.96	1.57	0	0.68
	Char	94.9	2.46	1.55	0	1.09
	Coal	85.54	5.42	1.54	6.13	1.37
Coal F	**Tar/PAH**	95.23	1.51	0.73	2.22	0.3
	Char	92.67	2.33	1.66	2.84	0.5
	Coal	81.99	5.63	1.53	10.23	0.61

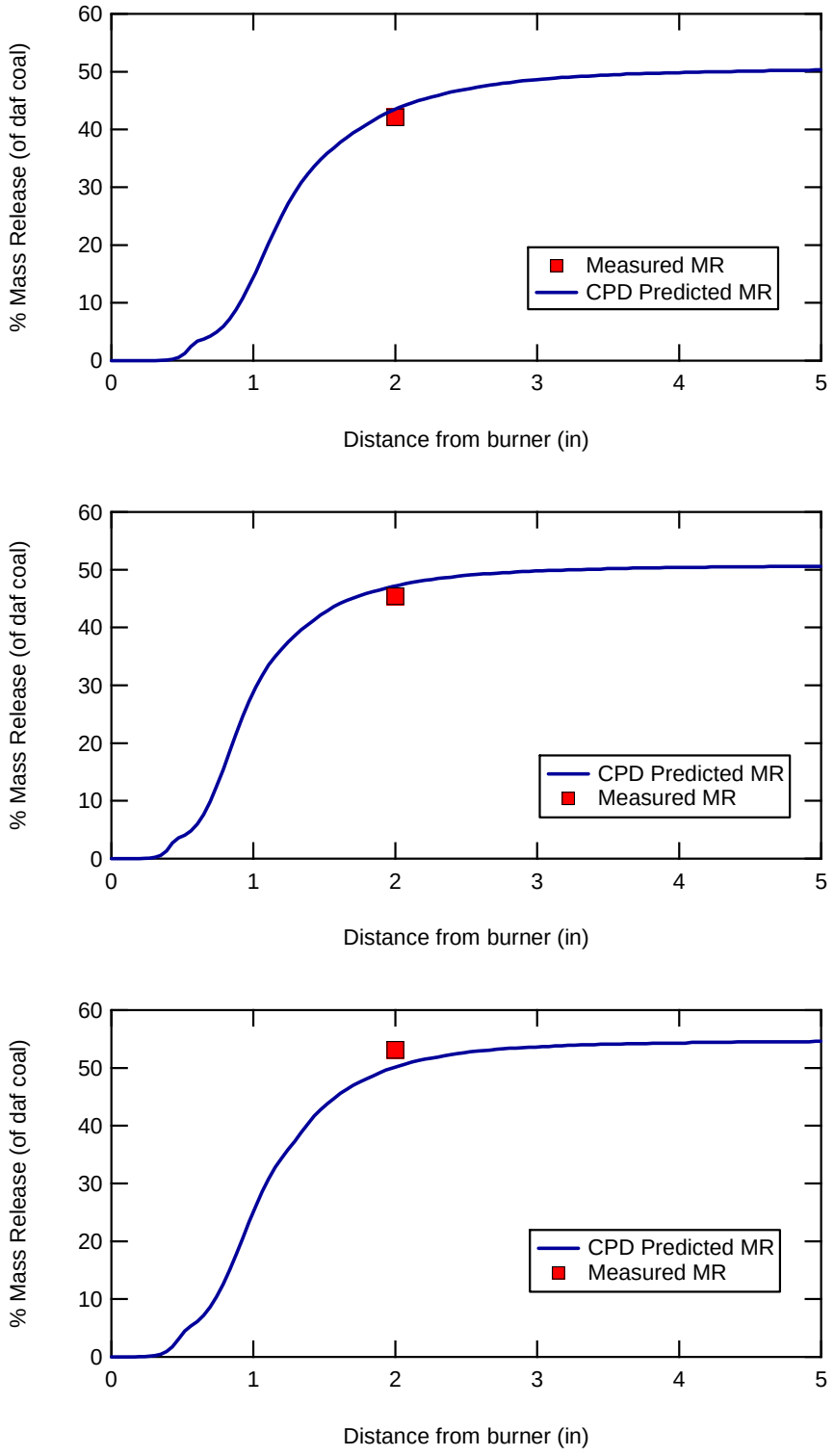

Figure G-1 CPD model predictions of volatiles release during pyrolysis of Coals D, E, & F in the 1300 K FFB condition

Table G-2 Ash and elemental tracer analysis results

	Coal A	Coal B	Coal C	Coal D	Coal E	Coal F
Ash Tracer	35.4%	43.2%	41.4%	10.0%	39%	38.4%
Ti Tracer	47.9%	47.1%	35.8%	35.3%	46.8%	54.1%
Si Tracer	33.4%	49.9%	36.0%	10.1%	35.8%	50.2%
Al Tracer	37.3%	44.2%	31.0%	48.9%	44.0%	55.0%
MR Average (not ash)	39.5%	47.1%	34.3%	42.1%	45.4%	53.1%
St. Dev. (not ash)	2.7%	2.8%	2.8%	9.6%	2.0%	2.6%
Nitrogen Release	29.2%	40.0%	17.8%	35.7%	45.0%	49.3%

G.2 Oxidation Results

Table G-3 Ultimate analyses from char oxidation experiments on Coals A, B & C

Coal	Temp (K)	Height/ Sample	C *	H	N	O (by diff)	S	Ash**
A	**1500**	**1**	88.01	2.15	1.95	6.91	0.98	17.49
		2	89.83	2.18	1.7	5.17	1.12	18.29
		4	92.76	1.18	1.63	3.41	1.03	21.45
		6	93.3	0.9	1.7	3.2	1	25.14
	1700	**1**	89.15	1.57	1.87	6.35	1.05	19.01
		2	92.02	1.41	1.61	3.98	0.97	17.32
		4	95.7	0.46	1.32	1.58	0.95	22.1
		6	94.34	0.54	1.76	2.47	0.88	21.89
		Coal	83.59	5.73	1.72	7.66	1.3	10.55
B	**1500**	**1**	91.77	1.31	1.36	5.03	0.53	25.62
		2	94.13	0.68	1.38	3.22	0.59	33.95
		4	91.13	1.19	1.44	4.14	2.11	40.16
		6	96.45	0.35	1.37	1.43	0.4	47.51
	1700	**1**	91.24	1.13	1.32	5.65	0.66	29.24
		2	96.12	0.33	1.27	1.84	0.44	25.22
		4	97.81	0.2	1.2	0.39	0.4	34.26
		6	88.76	2.15	1.41	5.69	2	41.27
		Coal	84.44	5.49	1.38	7.71	0.98	17.41
C	**1500**	**1**	86.4	1.9	1.23	9.9	0.5	19.32
		2	89.53	1.55	1.19	7.15	0.58	23.55
		4	94.32	0.8	1.12	3.05	0.71	42.1
		6	85.24	0.62	1.28	12.05	0.81	43.88
	1700	**1**	92.02	0.91	1.22	5.22	0.63	23.38
		2	94.75	0.96	1.24	2.45	0.59	20.15
		4	94.05	1.55	1.18	2.44	0.78	31.37
		6	92.52	0.43	1.21	5.27	0.58	43.92
		Coal	69.77	3.43	1.44	24.27	1.09	10.55

Note: On a dry-ash free (*) or dry (**) basis

Table G-4 Sample analysis from 1700 K char oxidation experiments on Coals A, B & C

	Temp (K)	Mass Release (dry-ash free)						
	Height (in)	Ash Tracer	Ti Tracer	Si Tracer	Al Tracer	MR Ave*	St. Dev.	Nitrogen Release
Coal A	1500 - 1	44.36%	47.91%	33.43%	40.49%	40.61%	7.2%	32.88%
	2	47.31%	47.91%	36.82%	40.77%	41.83%	5.6%	42.53%
	4	56.81%	59.19%	48.78%	52.99%	53.65%	5.2%	56.12%
	6	64.88%	69.21%	58.75%	62.58%	63.51%	5.3%	64.94%
	1700 - 1	49.75%	52.17%	39.59%	44.22%	45.33%	6.4%	40.54%
	2	43.70%	47.91%	32.43%	39.93%	40.09%	7.7%	43.80%
	4	58.43%	59.19%	50.99%	54.66%	54.71%	4.1%	65.29%
	6	57.91%	59.19%	46.81%	54.30%	53.43%	6.2%	52.29%
Coal B	1500 - 1	38.80%	48.31%	41.46%	50.98%	46.92%	4.9%	47.65%
	2	58.99%	59.77%	60.54%	60.54%	60.28%	0.4%	60.37%
	4	68.59%	65.45%	67.05%	65.59%	66.03%	0.9%	64.72%
	6	76.71%	79.85%	78.87%	80.72%	79.82%	0.9%	80.04%
	1700 - 1	48.99%	47.09%	47.46%	47.00%	47.18%	0.2%	49.55%
	2	37.50%	54.49%	39.10%	50.28%	47.95%	8.0%	52.23%
	4	59.55%	69.85%	61.34%	68.40%	66.53%	4.6%	71.04%
	6	70.00%	65.59%	68.25%	64.80%	66.21%	1.8%	65.65%
Coal C	1500 - 1	64.28%	74.63%	66.67%	73.27%	71.53%	4.3%	67.48%
	2	72.23%	79.99%	80.52%	80.77%	80.43%	0.4%	78.37%
	4	88.24%	91.05%	92.38%	92.03%	91.82%	0.7%	91.54%
	6	89.06%	92.11%	92.92%	93.05%	92.69%	0.5%	91.36%
	1700 - 1	71.97%	76.63%	78.06%	77.74%	77.48%	0.8%	74.61%
	2	66.10%	78.40%	70.33%	76.91%	75.21%	4.3%	71.47%
	4	81.29%	84.96%	85.32%	85.87%	85.38%	0.5%	84.05%
	6	89.08%	92.59%	92.96%	93.21%	92.92%	0.3%	92.10%

*Average of Al, Ti, and Si Tracers

Table G-5 Sample analysis from char oxidation experiments on Coals D, E, & F

Coal	Temp (K)	Sample	C *	H	N	O (diff)	S	Ash**
D	**1500**	**1**	96.3	0.9	1.74	0	1.1	11.31
		2	96.39	0.34	1.53	0	1.74	17.54
		4	94.29	0	1.39	2.37	1.95	29.17
		6	88	0.2	1.3	8	2.5	43.92
	1700	**1**	94	0.6	1.62	2.8	1	10.4
		2	94.88	0.36	1.55	1.96	1.25	14.42
		4	96.57	0.76	1.58	0	1.09	15.87
		6	96.6	0.5	1.6	0	1.4	17.07
		Coal	85.11	5.33	1.75	5.57	2.24	9.33
E	**1500**	**1**	97.1	0.6	1.53	0	0.8	22.99
		2	97.42	0.38	1.54	0	0.67	21.45
		4	97.66	0.2	1.63	0	0.51	24.49
		6	96.4	0.5	1.9	0	1.2	28.5
	1700	**1**	96.4	1.1	1.55	0	1	29.24
		2	97.46	0.28	1.52	0	0.74	25.22
		4	97.46	0.29	1.56	0	0.7	34.26
		6	96.7	0.4	2.3	0	0.7	41.27
		Coal	85.54	5.42	1.54	6.13	1.37	15.1
F	**1500**	**1**	97	0.9	1.67	0	0.4	19.04
		2	97.98	0.36	1.4	0	0.26	18.84
		4	95.13	1.6	1.71	1.21	0.35	25.52
		6	96.3	0.3	1.6	1.4	0.3	34.04
	1700	**1**	96.7	1	1.51	0.4	0.4	19.04
		2	97.53	0.45	1.63	0	0.4	17.69
		4	97.75	0.34	1.54	0	0.37	17.8
		6	97.7	0.3	1.5	0	0.4	18.41
		Coal	81.99	5.63	1.53	10.23	0.61	9.21

* On a dry-ash free basis

** On a dry basis

Table G-6 Mass and nitrogen release during char oxidation experiments on Coals D, E, & F

	Temp (K)	Mass Release (dry-ash free)						
	Height (in)	Ash Tracer	Ti Tracer	Si Tracer	Al Tracer	MR Ave	St. Dev.	Nitrogen Release
D	1500 - 1	21.28%	46.67%	25.87%	55.03%	50.85%	5.9%	51.11%
	2	53.84%	60.54%	52.79%	60.04%	57.79%	4.3%	63.14%
	4	74.83%	83.02%	83.37%	82.55%	82.98%	0.4%	86.44%
	6	87.00%	89.32%	90.96%	89.68%	89.99%	0.9%	92.68%
	1700 - 1	12.61%	46.67%	24.78%	55.03%	50.85%	5.9%	54.53%
	2	39.93%	53.46%	43.51%	55.03%	54.25%	1.1%	59.33%
	4	46.37%	56.88%	74.63%	55.03%	55.96%	1.3%	59.86%
	6	50.69%	58.27%	53.94%	60.04%	59.15%	1.2%	63.50%
E	1500 - 1	45.75%	56.35%	44.79%	55.55%	55.95%	0.6%	56.19%
	2	49.02%	58.98%	53.01%	58.64%	58.81%	0.2%	58.96%
	4	70.01%	77.10%	74.77%	76.84%	76.24%	1.3%	74.89%
	6	83.60%	85.63%	90.11%	85.58%	87.11%	2.6%	84.31%
	1700 - 1	44.27%	53.48%	52.13%	48.92%	51.51%	2.3%	51.19%
	2	40.20%	56.35%	55.55%	53.11%	55.00%	1.7%	55.63%
	4	50.18%	60.61%	61.43%	58.04%	60.03%	1.8%	59.63%
	6	59.90%	63.75%	63.97%	62.28%	63.33%	0.9%	46.11%
F	1500 - 1	56.86%	63.68%	59.92%	61.14%	61.58%	1.9%	58.18%
	2	56.35%	63.34%	61.85%	61.14%	62.11%	1.1%	65.34%
	4	70.22%	70.46%	70.13%	66.04%	68.88%	2.5%	65.23%
	6	80.04%	82.89%	81.32%	78.61%	80.94%	2.2%	79.49%
	1700 - 1	56.27%	58.11%	55.03%	54.07%	55.74%	2.1%	56.36%
	2	52.18%	57.27%	55.03%	54.35%	55.55%	1.5%	52.63%
	4	52.81%	62.66%	61.14%	61.43%	61.75%	0.8%	61.51%
	6	55.00%	68.43%	66.04%	68.74%	67.74%	1.5%	67.47%

*Average of the mass release from the Al, Si, and Ti tracers

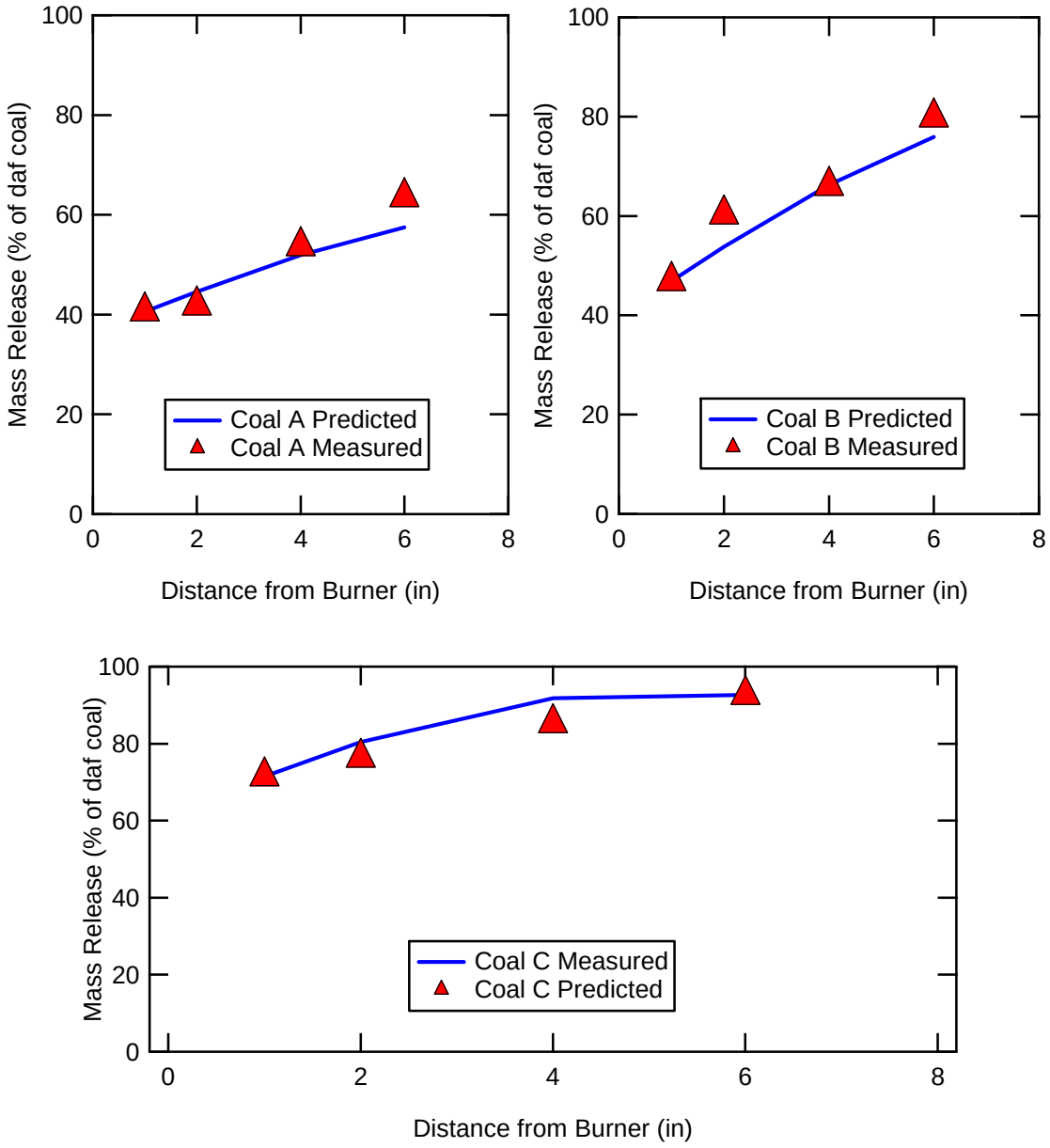

Figure G-2 Char oxidation predictions and measurements for Coals A, B, & C in the 1500 K FFB condition

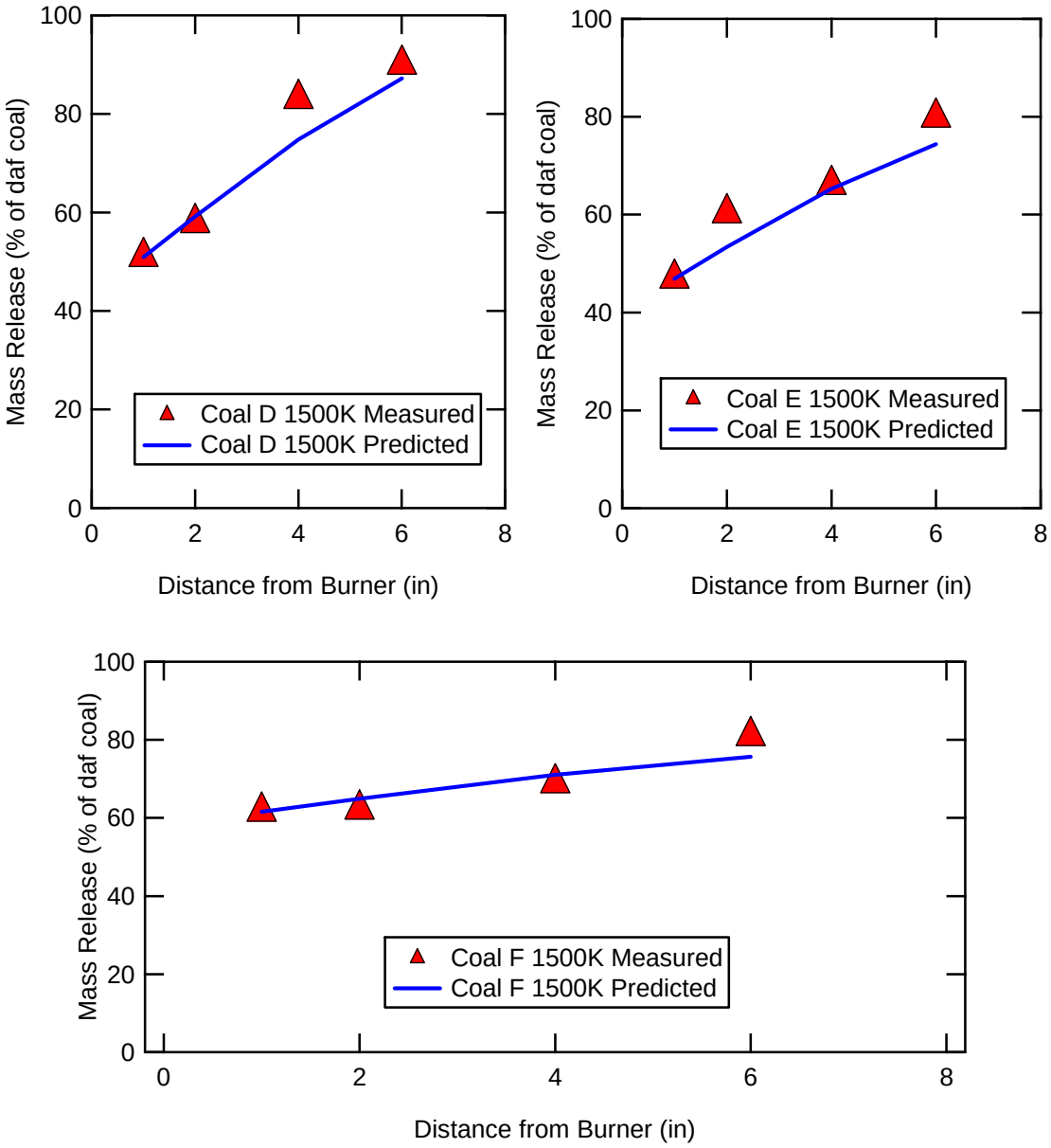

Figure G-3 Char oxidation predictions and measurements for Coals D, E & F in the 1500 K FFB condition. These results are from curve fits of both the 1500 and 1700 K data

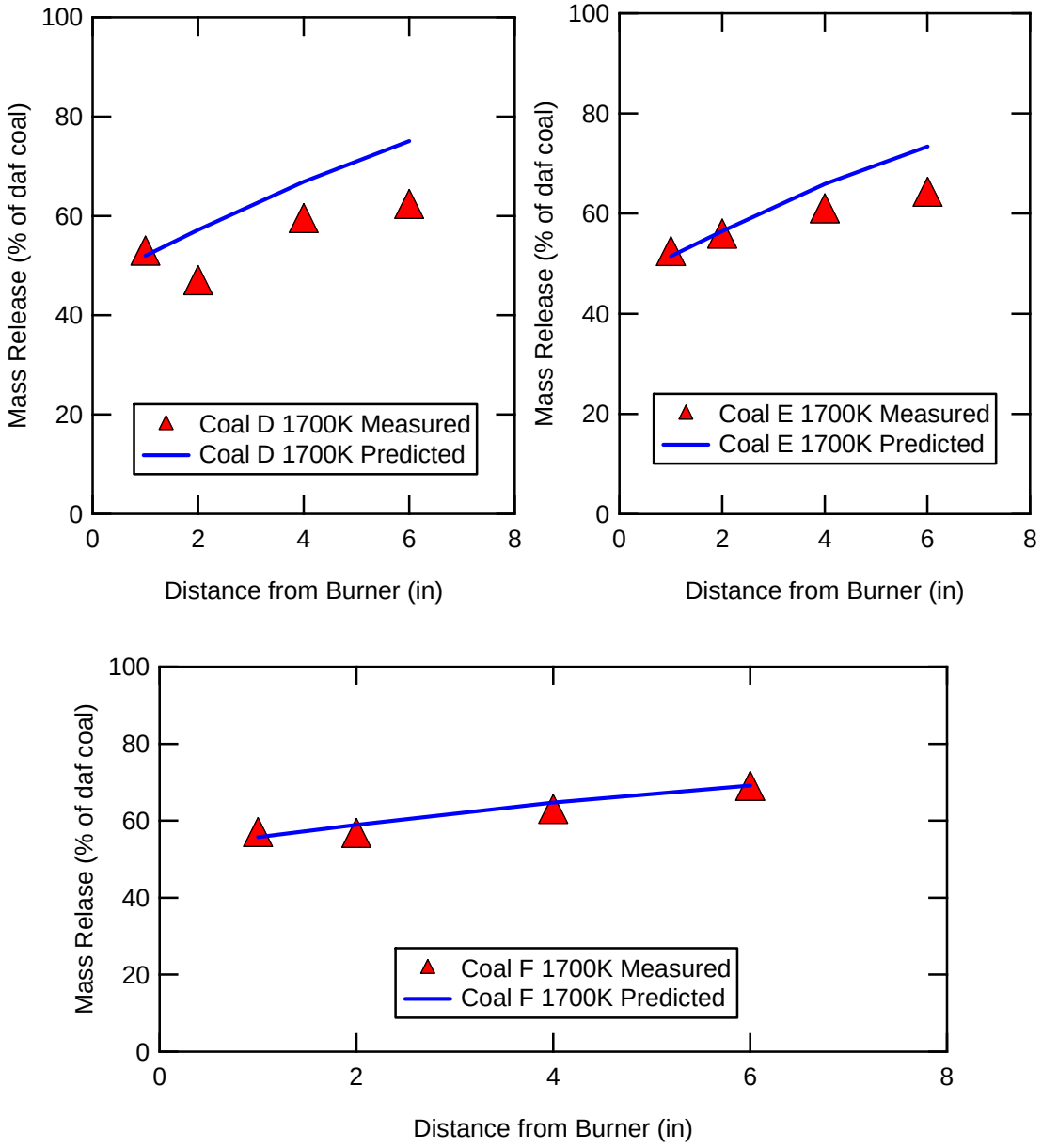

Figure G-4 Char oxidation predictions and measurements for Coals D, E, & F in the 1700 K FFB condition. These results are from curve fits of both the 1500 and 1700 K data

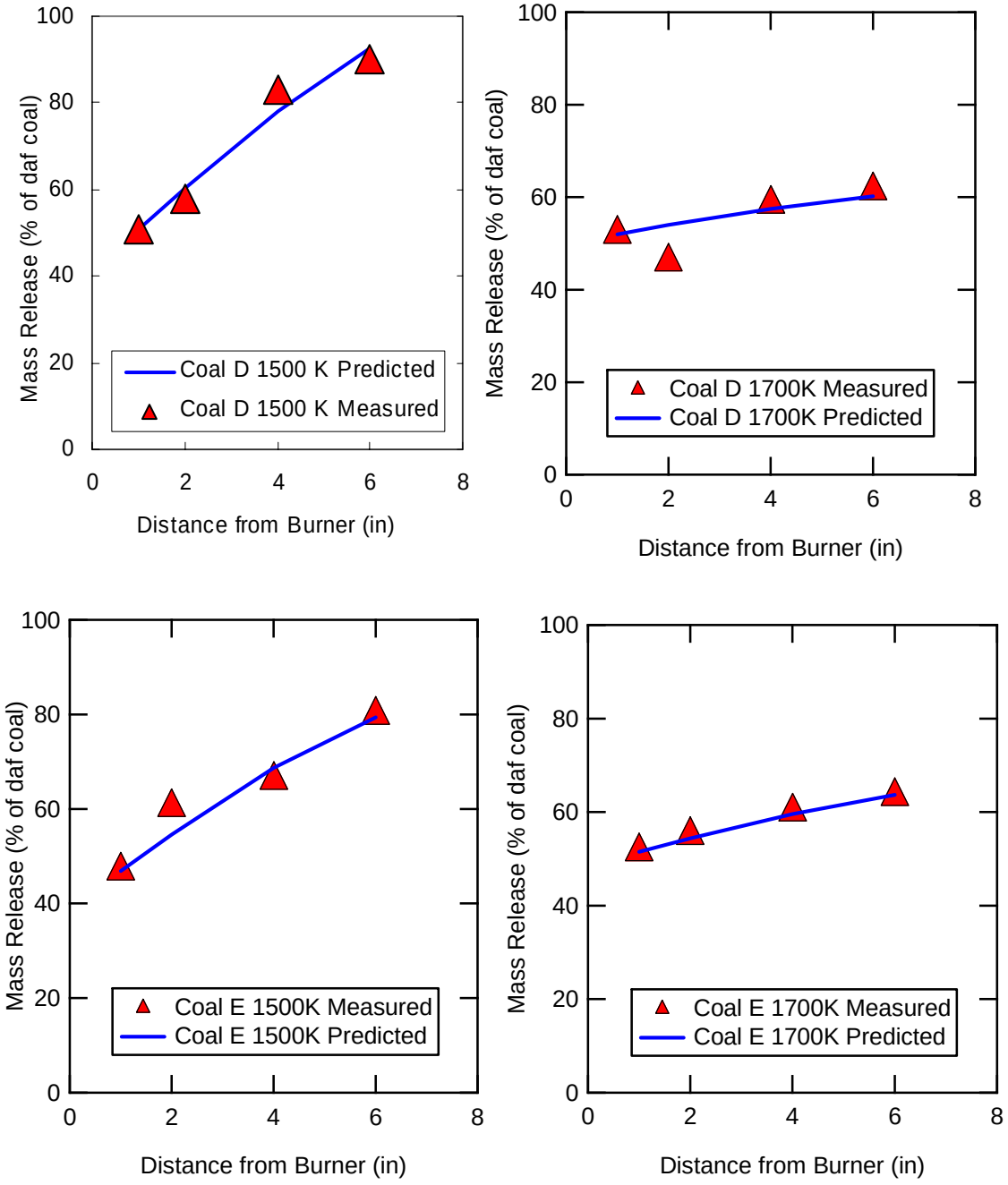

Figure G-5 Char oxidation predictions and measurements for Coals D & E in the 1500 and 1700 K FFB condition considered separately

G.3 C/H, C/N Ratios

Table G-7 C/N and C/H ratios for coal combustion experiments

Coal	Distance (inches)	$(C/N)/(C/N)_0$		$(C/H)/(C/H)_0$	
		1500 K	1700 K	1500 K	1700 K
A	1	0.93	0.98	2.81	3.89
	2	1.09	1.18	2.82	4.48
	4	1.17	1.49	5.39	14.27
	6	1.13	1.1	7.11	11.98
B	1	1.1	1.13	4.55	5.25
	2	1.11	1.24	9	18.94
	4	1.03	1.33	4.98	31.8
	6	1.15	-	17.92	-
C	1	1.45	1.56	2.24	4.97
	2	1.55	1.58	2.84	4.85
	4	1.74	1.65	5.8	2.98
	6	1.37	1.58	6.76	10.58
D	1	1.14	1.19	6.66	10.06
	2	1.3	1.25	17.69	16.71
	4	1.39	1.25	-	7.92
	6	1.41	1.27	31.13	13.01
E	1	1.14	1.12	10.43	5.4
	2	1.14	1.16	16.36	22.12
	4	1.08	1.13	30.79	21.64
	6	0.93	0.77	12.14	16.96
F	1	1.09	1.2	7.38	6.53
	2	1.31	1.12	18.73	15.06
	4	1.04	1.18	4.08	19.78
	6	1.09	1.18	22.89	19.57

G.4 Coal Density and Swelling

Table G-8 Density and diameter changes during combustion coals in FFB

		1500 K			1700 K		
	Distance (in)	m/m_0*	ρ/ρ_o*	d/d_o	m/m_0*	ρ/ρ_o*	d/d_o
A	1	0.64	0.4	1.17	0.60	0.39	1.15
	2	0.63	0.4	1.16	0.64	0.35	1.23
	4	0.52	0.39	1.1	0.51	0.31	1.18
	6	0.43	0.35	1.07	0.52	0.3	1.2
B	1	0.61	0.49	1.08	0.61	0.47	1.09
	2	0.50	0.41	1.07	0.60	0.37	1.18
	4	0.46	0.38	1.07	0.45	0.37	1.07
	6	0.34	0.36	0.98	0.45	0.42	1.02
C	1	0.72	0.49	1.14	0.60	0.46	1.09
	2	0.55	0.55	0.99	0.67	0.51	1.09
	4	0.32	0.66	0.79	0.45	0.65	0.88
	6	0.31	0.67	0.77	0.30	0.65	0.78
D	1	0.49	0.35	1.12	0.58	0.33	1.2
	2	0.45	0.3	1.14	0.52	0.3	1.2
	4	0.22	0.25	0.95	0.40	0.27	1.14
	6	0.16	0.26	0.85	0.46	0.23	1.25
E	1	0.54	0.49	1.03	0.63	0.41	1.15
	2	0.48	0.54	0.96	0.49	0.3	1.18
	4	0.31	0.36	0.95	0.45	0.34	1.1
	6	0.23	0.45	0.81	0.43	0.35	1.07
F	1	0.44	0.42	1.01	0.50	0.41	1.07
	2	0.43	0.27	1.16	0.50	0.24	1.27
	4	0.38	0.37	1.01	0.43	0.3	1.12
	6	0.26	0.31	0.94	0.36	0.24	1.15

* on an as received basis

Appendix H. CPD Input Parameters

Output files were stored as text files (rather than .out) and transferred to Excel where all could be put on one spreadsheet.

Table H-1 Oxyfuel CPD input parameters

Input Parameter	**Illnois 6**	**Pittsburgh 8**	**BT**
$\mathbf{p_o}$	0.494	0.437	0.61
$\mathbf{c_o}$	0.040	0.0	0.15
$\mathbf{\sigma + 1}$	4.97	5.22	4.52
MW	411.2	424.2	350.3
$\mathbf{M_{del}}$	42.9	33.7	47.6

Table H-2 Chemical additive CPD input parameters

Input Parameter	**Kentucky**	**CC2**	**CF2**
$\mathbf{p_o}$	0.454	0.445	0.438
$\mathbf{c_o}$	0.242	0.146	0.003
$\mathbf{\sigma + 1}$	5.05	5.10	5.19
MW	374.6	382.7	392.7
$\mathbf{M_{del}}$	22.3	23.8	25.8

Table H-3 Coal nitrogen database CPD chemical structure input parameters

Input Parameter	**Coal D**	**Coal E**	**Coal F**	**Coal A**	**Coal B**	**Coal C**
$\mathbf{p_o}$	0.51	0.522	0.488	0.473	0.546	0.758
$\mathbf{c_o}$	0.0	0.0	0.0	0.0	0.0	0.150
$\mathbf{\sigma + 1}$	4.97	4.79	4.93	4.91	4.78	3.66
MW	328.7	331.3	368.8	383.6	348.4	355.4
$\mathbf{M_{del}}$	27.4	27.8	33.7	31.7	29.1	54.2

Appendix I. Raw FT-IR Data

Table 3-4 shows the concentrations in ppm and the corresponding conversion to the percentage of fuel nitrogen. For the majority of the coals the concentration of HCN was greater than NH_3 at this condition. The first run on the Eastern Bituminous coal seemed have a bit of an anomaly with low concentrations in both gases. However, experiment replicates, shown below, agree with similar coals. The coal B showed more NH_3 than HCN. Coal D did not have any detectable NH_3 in the FTIR.

Table I-1 FTIR results from the 1300 K pyrolysis experiments

	Factors* from FTIR		Concentration (ppm)		Fraction coal N	% conversion of coal fuel N	
Coal	**HCN**	**NH_3**	**HCN**	**NH_3**		**HCN**	**NH_3**
F	0.128	0.00165	1.2786	0.0825	0.0153	26.69	1.72
C	0.072	0.00101	0.7201	0.0505	0.0108	23.57	1.65
B	0.016	0.022	0.1554	1.1	0.0138	3.96	28.04
A	0.071	0.0027	0.7054	0.138	0.0152	13.37	2.62
D	0.082	0	0.8248	0	0.0175	15.33	0.00
E	0.066	0.0037	0.6631	0.185	0.0154	14.92	4.16

*Ratio of the integrated peak areas for the sample divided by that of the calibration standard

Appendix J. Sample FT-IR Calculation

The process for obtaining a concentration of a sample gas in the FTIR starts by subtracting off the flame background using the GRAMS/AI spectral subtract feature. This is necessary because high CO_2 and CO concentrations create noise throughout the entire spectra. This CO_2 noise is eliminated from the scan when the flame background is removed.

The remainder of the subtraction in the 3400-3200 cm^{-1} is a double-hump that is both C_2H_2 and HCN. Since the HCN is in much lower concentrations than C_2H_2, it is necessary to first remove the part of the peak caused by C_2H_2. HCN is now visible in the spectra. The HCN peak is quantified by using the spectral subtract and a calibration gas scan. A factor is given by the GRAMS/AI software as to a fraction of the calibration scan was needed in order to remove the peak. The concentration of the HCN is given by multiplying the factor times the calibration gas concentration shown by Equation J-1.

A similar process is used for NH_3 except in a different region (1200-800 cm^{-1}). Also, instead of having to subtract out C_2H_2, C_2H_4 needs to be removed in order to get an accurate scan of NH_3. An example of scans from each step in this process is shown in Figure J-1. Examples of spectral subtracts are shown in Figure J-2 and Figure 2-1.

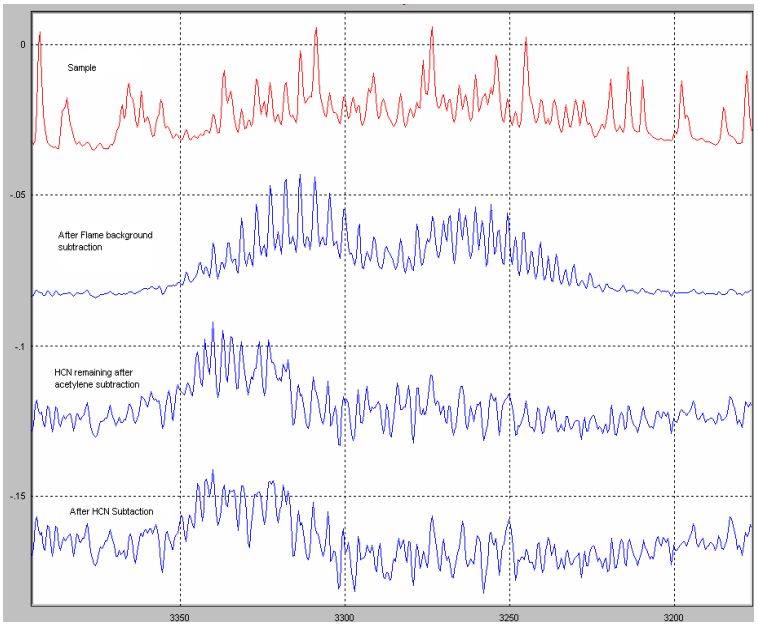

Figure J-1 The spectra for each step in the quantification process.

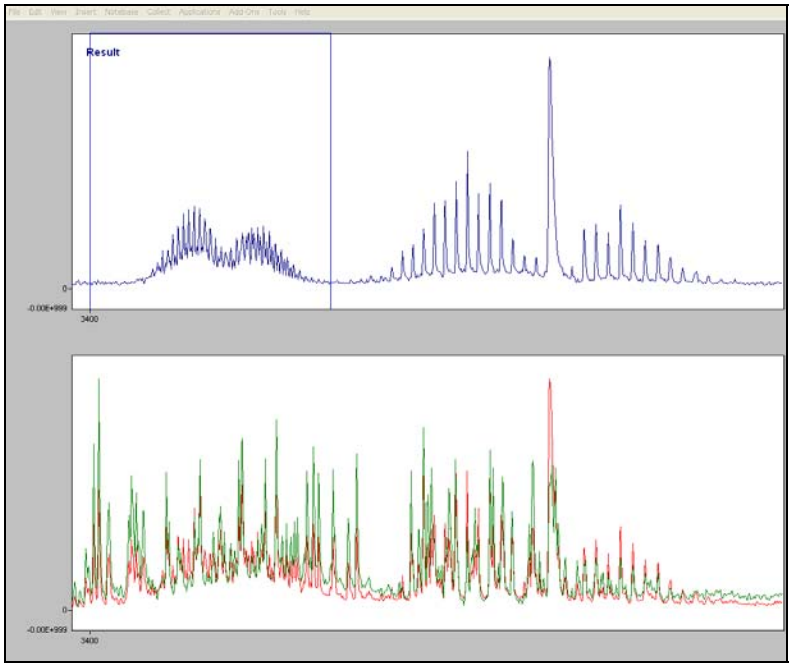

Figure J-2 A comparison of the flame background and the gas sample is on the bottom and the result of the subtraction is on top. The subtraction factor can be seen in the top box of the window in the upper left corner

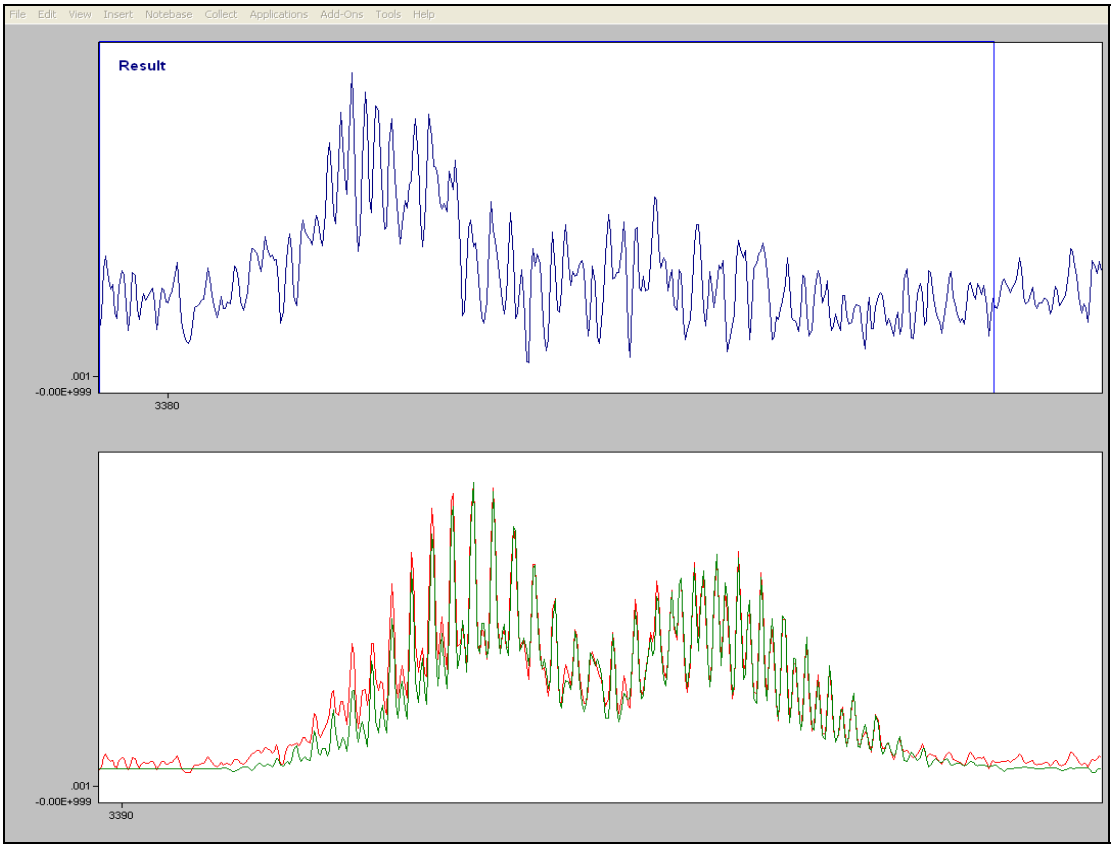

Figure J-3 A comparison of C_2H_2 calibration gas sample and the coal sample is on the bottom and the result of the subtraction is on top. The subtraction factor can be seen in the top box of the window in the upper left corner

$$y_{HCN} = f * y_{HCN,cali} \qquad \textbf{J-1}$$